

UC Riverside

UC Riverside Electronic Theses and Dissertations

Title

Division Plane Orientation in Maize

Permalink

<https://escholarship.org/uc/item/2x71q34p>

Author

Uyehara, Aimee Naomi

Publication Date

2024

Copyright Information

This work is made available under the terms of a Creative Commons Attribution License, available at <https://creativecommons.org/licenses/by/4.0/>

Peer reviewed|Thesis/dissertation

UNIVERSITY OF CALIFORNIA
RIVERSIDE

Division Plane Orientation in Maize

A Dissertation submitted in partial satisfaction
of the requirements for the degree of

Doctor of Philosophy

in

Plant Biology

by

Aimee Naomi Uyehara

June 2024

Dissertation Committee:

Dr. Carolyn G. Rasmussen, Chairperson

Dr. Daniel Koenig

Dr. Julia Bailey-Serres

Dr. Meng Chen

Copyright by
Aimee Naomi Uyehara
2024

The Dissertation of Aimee Naomi Uyehara is approved:

Committee Chairperson

University of California, Riverside

ACKNOWLEDGEMENTS

There are many people that I am deeply grateful to at UCR for their contributions to my growth as a scientist, teacher, and person.

I would like to acknowledge all the previous and current Rasmussen lab members for their training and friendship – Pablo Martinez, Marschal Bellinger, Alison Mills, and Hong Liang for their guidance when I first joined and Lindy Allsman, Stephanie Martinez, and Makayla Drew for all of the spontaneous science conversations as well the many lab adventures. Thank you Stephanie for all the troubleshooting discussions and brainstorming– I will miss our trips to the vending machine and to coffee spots to fuel your coffee addiction. Thank you Makayla for all the hot takes – I can't wait to see what other personality tests you come up with in addition to your research. All of the amazing undergraduate researchers in the Rasmussen lab including Shreya Agarwal, Ian Ceballos, Audrey Choi, Alondra Contreras, Mina Dalkiran, Beatrice Diep, Matthew Duong, Sarah Gayer, Cassetty Habib, Vivian Huang, Cassandra Irahola, Janice Kim, Joseph Nguyen, Alex Noriega, Jennifer Phan, and Gabriela Salazar Soriano shared their enthusiasm, creativity, and feedback with me. In particular, I am grateful to Beatrice who dedicated 3.5 years of her undergraduate career to working on the de novo TAN1 recruitment project. Not to be forgotten, I am grateful to my advisor Carolyn for gifting me her time and support as a mentor that generated a robust PhD project that truly lies at the nexus of plant-based cell biology. While we haven't yet created a complete division or another -ome, I can be satisfied that Carolyn is signing off on a document that contains all of her favorite words. I have truly learned so much from everyone in the lab and am excited for what the future holds.

There were also many experiences that shaped me as an instructor. The Dynamic Genome staff inspired my enthusiasm for teaching and patiently guided me as we continued to develop a research project for the class (shout out to Alison Mills again here). Dr. Jim Burnette, Dr. Vinky Chetty, Alex Cortez, Isai Gonzalez and all the undergraduate learning assistants – Jacob Jauregui, Russel Angelo Arevalo, and Alondra Contreras were instrumental to getting the class project running smoothly. Additionally, teaching with BPSC104 Foundations in Plant Biology with Denise Mitchell, Dr. Kim Steiner, and Michael Guzman reinvigorated my enthusiasm for plants. Lastly, I am grateful to have participated in the University Teaching Certificate Program coordinated by J Selke and Ashley Harlow.

I would like to thank my co-advisor Dan Koenig and Danelle Seymour for the initial bioinformatics training and mentorship. In particular, Keely Brown, Chris Fiscus, and Jill Marzolino welcomed me into the Koenig lab and provided training. I also thank my committee members Julia Bailey-Serres and Meng Chen for their enthusiasm and fresh perspectives on my project.

I am grateful to the Cores and Facilities at UCR for the usage of their facilities and technical consultations: the microscopy Core (David Carter), the Genomics Core (Wei Zhang, Holly Clark, Clay Clark), the Bioinformatics Core (Brandon Le), the High Performance Computing Center (Thomas Girke, Emerson Jacobson, Austin Leong), and Agricultural Operations (Dave Wetovick and Hung Duy Lai). Dave in particular did an amazing job setting up and maintaining our field and his dedication was demonstrated by our beautiful plants.

My first three chapters were published in the European Journal of Cell Biology, the Plant Cell, and the Journal of Cell Science respectively and I am grateful to my co-

authors. Additionally, for Chapter 1, I am grateful to UCR lab members Stephanie Martinez, Lindy Allsman, Shreya Agarwal, Vivian Huang, Alondra Contreras, Rachel Strout, Adrian Garcia, Matthew Duong, Cassetty Habib, Mina Dalkiran for helpful comments. For Chapter 2, I am grateful to Professors Henrik Buschmann (Osnabrück University) and Laurie Smith (UCSD) and the reviewers for helpful comments. Finally for Chapter 3, I thank Jennifer Phan and other Rasmussen Laboratory members for help with the generation and propagation of genetic resources, and Dr. Marschal Bellinger for training. Dr. Meng Chen for procuring funds for the Zeiss 880 (NIH 3R01GM087388-06S2), and Dr. Marschal Bellinger (UCR) provided Zeiss 880 training.

Last but not least, I'd like to acknowledge my friends and family for their support over the past six years. My 2018 Plant Biology cohort members are talented, kind, and incredible scientists and I am grateful to have done my PhD alongside them. I've also been through so much with Stephanie Martinez and Albert Nguyen and I will miss our coffee and food hang outs. Thank you Sunhyun Chang for all the Pong pictures and I will miss hanging out with you and Femila Manoj. Also thank you to Jill Marzolino and Joy Hinshilwood for all of the food (Joy is the best cook) and the memories. My family in Riverside, my partner Micah and my two cats Soba and Gnocchi, provided greater than a dissertation's worth of support. I am also grateful to my parents, Micah's parents, Elise and Jordan, as well as my extended family in Hawai'i for their love and enthusiasm.

DEDICATION

For my parents and especially

my mother

who sacrificed much

for myself and my sister.

ABSTRACT OF THE DISSERTATION

Division Plane Orientation in Maize

by

Aimee Naomi Uyehara

Doctor of Philosophy, Graduate Program in Plant Biology
University of California, Riverside, June 2024
Dr. Carolyn G. Rasmussen, Chairperson

Proper cell division orientation is an important component to plant and animal growth and development. In contrast to animal cells which divide through the constriction of the contractile ring, plant cells divide through the expansion of a microtubule and actin structure, the phragmoplast, to a division site specified at the cell cortex. Plant cells are encased in a semi rigid cell wall and do not rotate or migrate, thus coordination of division site structures with the division site is very important. In Chapter 1, I discuss temporal, genetic, and synthetic redundancies that ensure plant cell division planes are positioned correctly. In Chapter 2, I examine and characterize the role of cortical telophase microtubules in positioning the phragmoplast through interactions with the division site protein TANGLED1 (TAN1). In Chapter 3, I demonstrate that TAN1 is also recruited independently of the preprophase band by the phragmoplast. Finally, in Chapter 4, I use bioinformatics and whole genome resequencing to identify new molecular players important to division plane orientation or cytokinesis in maize. Altogether these chapters provide new perspectives into the function of TAN1 in maize.

TABLE OF CONTENTS

CHAPTER 1:	
REDUNDANT MECHANISMS IN DIVISION PLANE POSITIONING	1
ABSTRACT	2
SUMMARY OF CURRENT MECHANISMS IN CELL DIVISION	2
TEMPORAL REDUNDANCY	6
GENETIC REDUNDANCY IN DIVISION PLANE ORIENTATION.....	14
Proteins important for PPB positioning.....	16
ROPs promote cell elongation required for division plane positioning	17
IRK/PXC2	21
GRAS Transcription Factors.....	21
Proteins important for PPB formation.....	22
IQ67 DOMAIN proteins.....	27
Proteins important for phragmoplast guidance or the maintenance of division plane orientation	28
POK1/POK2	28
Myosin XI and Myosin VIII	29
MAP65s.....	32
SYNTHETIC REDUNDANCY.....	35
CONCLUSIONS	39
REFERENCES	40

CHAPTER 2:	
CORTICAL MICROTUBULES CONTRIBUTE TO DIVISION PLANE POSITIONING DURING TELOPHASE IN MAIZE.....	58
ABSTRACT	59
INTRODUCTION	61
RESULTS	64
Analysis of cortical microtubule accumulation and orientation during telophase	64
Analysis of microtubule dynamics	70
TAN1 functions in microtubule plus-end capture	75
Interaction of cortical telophase microtubule arrays with the phragmoplast.....	83
Effects of cortical-telophase microtubule accumulation on the trajectory of phragmoplast expansion.....	87
DISCUSSION.....	96
MATERIALS AND METHODS.....	101
Plant growth and imaging conditions.....	101
Confocal microscopy.....	102
Quantification of microtubule array organization and coverage	103
Measuring microtubule dynamics.....	104
Statistical analysis.....	105
Accession numbers.....	106
AUTHOR CONTRIBUTIONS	106
REFERENCES	107

CHAPTER 3:	
DE NOVO TANGLED1 RECRUITMENT FROM THE PHRAGMOPLAST TO ABERRANT CELL PLATE FUSION SITES IN MAIZE.....	114
SUMMARY STATEMENT	115
ABSTRACT	115
INTRODUCTION	116
RESULTS AND DISCUSSION.....	119
Defects in dcd1 PPB formation reduce TAN1-YFP accumulation.....	119
Defective PPBs in dcd1 mutants cause division plane positioning defects.....	123
TAN1-YFP accumulates at misoriented cell plate insertion sites.	126
Actin and myosin XI OPAQUE1 (O1) facilitate TAN1-YFP accumulation at de novo cell plate insertion sites.....	131
MATERIALS AND METHODS.....	137
RESOURCE AVAILABILITY.....	137
EXPERIMENTAL MODEL DETAILS	137
METHOD DETAILS	138
QUANTIFICATION AND STATISTICAL ANALYSIS.....	141
RESOURCES TABLE.....	143
REFERENCES	145

CHAPTER 4: OTHER MOLECULAR PLAYERS INVOLVED WITH MAIZE DIVISION PLANE ORIENTATION AND CYTOKINESIS	150
ABSTRACT	151
INTRODUCTION	152
METHODS	154
EMS seed treatment	154
Plant Cultivation	154
Bulked Segregant Analysis (BSA) Material	154
DNA Extractions and Whole Genome Resequencing.....	155
Bulked segregant analysis bioinformatics pipeline for cyto3	156
EMS pollen mutagenesis	157
RESULTS	158
cytokinesis 3 (cyto3) is a maize mutant with defects in cytokinesis	158
Resequencing of cyto3, B73 and cyto3, W22(3).....	161
Mapping and candidate region identification	161
Generation of new cyto3 alleles using pollen EMS mutagenesis	169
CONCLUSIONS AND FUTURE DIRECTIONS	175
REFERENCES	176

LIST OF FIGURES

Chapter 1

Figure 1.1. Overview of mitotic microtubule and DNA structures and locations important in typical land plant division plane orientation.	4
Figure 1.2. Temporal redundancy during division plane orientation showing schematic examples of correctly oriented divisions, and when mitotic structures deviate from the “correctly oriented” position.	8
Figure 1.3. Temporal redundancy in protein recruitment.	13
Figure 1.4. Genetic redundancy in division plane orientation.	15
Figure 1.5. Modular redundancy in division plane orientation inspired by (Zinovyev et al., 2013).	34

Chapter 2

Figure 2.1 Cortical-telophase microtubules accumulate at the cortex before the phragmoplast contacts the cortex in wild-type maize epidermal cells.	66
Supplemental Figure S2.1. Cortical-telophase microtubules in wild-type maize epidermal cells, Arabidopsis root cells, and very sparse cortical-telophase microtubules in maize tan1 mutant epidermal cells.	67
Figure 2.2. Cortical-telophase microtubules are typically abundant and arranged towards the division site in wild-type cells but are more variable in abundance and organization in tan1 mutant cells.	69
Supplemental Figure S2.2: Propyzamide treatment of maize epidermal cells depolymerizes cortical telophase microtubules but does not depolymerize phragmoplast microtubules.	71
Figure 2.3. Cortical telophase microtubules pause at the division site near TAN1 puncta.	72
Supplemental Figure S2.3. Wild type and tangled1 microtubule dynamics during telophase.	80
Supplemental Figure S2.4. Examples of microtubule dynamics measurements using the Dynamic Kymograph plugin tool in Fiji.	82
Supplemental Figure S2.5: Description of the features of cells in telophase extracted for analysis.	84

Figure 2.4. Time-lapse images of cortical-telophase microtubules interacting with the phragmoplast using YFP-TUBULIN to label microtubules.....	86
Figure 2.5. Long-term uneven accumulation of cortical-telophase microtubules is correlated with changes in phragmoplast direction.....	89
Supplemental Figure S2.6. Short time-lapses (<5 minutes) of four different wild-type phragmoplasts showing little change in direction. Supports Figure 2.5. Purple dots indicate measured phragmoplast angle compared to predicted division site.....	91
Supplemental Figure S2.7. Longer timelapses (>8 minutes) of wild-type phragmoplasts with >10 degree changes in the direction of movement. (A, C) and (B, D) with < 10 degree changes in the direction of movement. Supports Figure 2.5.....	92
Supplemental Figure S2.8. Short timelapses (5 minutes or less) of five different tan1 phragmoplasts showing little change in direction, but frequently unevenly distributed cortical-telophase array. Supports Figure 2.5.....	94
Supplemental Figure S2.9. Longer timelapses (>12 minutes) of tan1 phragmoplast angle measurements compared to relative cortical microtubule accumulation. Supports Figure 2.5.....	95

Chapter 3

Figure 3.1. PPB formation and TAN1-YFP recruitment is defective in dcd1.....	121
Supplemental Figure S3.1. Confocal micrographs of divisions in wild type (WT) and dcd1 plants.....	122
Figure 3.2. Defective preprophase bands and TAN1 localization result in misoriented divisions.....	125
Figure 3.3. Cell plate insertion sites accumulate de novo TAN1-YFP. (A-D) CFP-TUBULIN (green) and TAN1-YFP (magenta) in various dividing cells. Carets (>) mark the division site and asterisks (*) mark de novo TAN1-YFP.....	129
Supplemental Figure S3.2. TAN1-YFP localization in wild type and the dcd1 add1 double mutant from prophase to early telophase.....	130
Supplemental Figure S3.3. TAN1-YFP localization patterns in dcd1 add1 embryos....	131
Figure 3.4. Actin and myosin XI motor protein OPAQUE1 increase TAN1 accumulation at de novo cell plate insertion sites.....	133
Supplemental Figure S3.4. Optimization of latrunculin B treatment for dcd1 and its wild-type sibling.....	134

Chapter 4

Figure 4.1. Overview of generation of EMS population.	159
Figure 4.2. cyto3 epidermal cells have defects in cytokinesis.	160
Figure 4.3. cyto3 is on chromosome 9.	163
Figure 4.4. Mapping analysis overview from Easymap v2 output.	164
Figure 4.5. Venn diagram of candidate gene models generated with different methods.	167
Figure 4.6. Noncomplementation of cyto3 resulted in the identification of two potential new alleles.	171
Figure 4.7. Sequencing of potential new alleles of cyto3.....	172

LIST OF TABLES

Chapter 2

Table 2.1. Quantification of individual interaction and bundling events between cortical-telophase microtubules and the phragmoplast.	74
Table 2.2. Percentage of cortical microtubule pausing at or passing through the division site in wild-type and tangled1 plants.	74
Supplemental Table S2.1. Summary of microtubule dynamics in wild-type and tangled1 cells across different locations at the cell cortex (supports Supplemental Figure S2.3).	81

Chapter 4

Table 4.1. Overview of sequencing experiments for cyto3 and tan64.	155
Table 4.2. Percent mapping and mean coverage of bulked segregant analysis populations.	156
Table 4.3 Number of fixed variants per chromosome	162
Table 4.4. List of candidates specific to cyto3, W22(3) and cyto3, B73(1) pools.	165
Table 4.5 Gene candidates shared between Easymap and Region of Interest	168
Table 4.6 Gene candidates shared between the Region of Interest and the Manual Filter	168
Table 4.7 Gene candidates shared between the Manual Filter and Easymap	169
Table 4.8. High effect variants as predicted by Variant Effect Predictor (VEP) for the 2 Mb candidate region spanning Chr9:19000000-21000000.	173
Table 4.9. Moderate effect variants from Chr9:19000000-21000000. For variants that had a similar predicted impact on the same gene model, the top variant was given.	174

CHAPTER 1:
REDUNDANT MECHANISMS IN DIVISION PLANE POSITIONING

Keywords:

Genetic redundancy, cell division, phragmoplast, cytokinesis, division plane orientation,
synthetic genetic interaction

ABSTRACT

Redundancies in plant cell division contribute to the maintenance of proper division plane orientation. Here we highlight three types of redundancy: 1) Temporal redundancy, or correction of earlier defects that results in proper final positioning, 2) Genetic redundancy, or functional compensation by homologous genes, and 3) Synthetic redundancy, or redundancy within or between pathways that contribute to proper division plane orientation. Understanding the types of redundant mechanisms involved provides insight into current models of division plane orientation and opens up new avenues for exploration.

SUMMARY OF CURRENT MECHANISMS IN CELL DIVISION

Cell division is a fundamental process where a cell divides into two new daughter cells. Cell division is essential for survival in all organisms and plays a vital role in plant growth and development. Plant cells do not migrate and instead control the location of new cells by positioning the division plane. Plant division plane orientation is established, maintained, and completed through the coordination of microtubule and actin arrays with division site proteins. A short description of the microtubule arrays and DNA structures observed in typical symmetric land plant divisions is shown in Figure 1.1. Symmetric cell divisions generate the same cell type while asymmetric divisions generate new cell types. For more on division plane determination in symmetric and asymmetric divisions, see reviews (Buschmann et al., 2019; Facette et al., 2019; Livanos et al., 2019; C. G. Rasmussen et al., 2018; Yi et al., 2022). For a synthesis of developmental and cell biological frameworks that modulate division plane orientation, please see (Facette et al., 2019; Glanc, 2022; Arvid Herrmann et al., 2021; Yi et al., 2022; Yi Zhang et al., 2023).

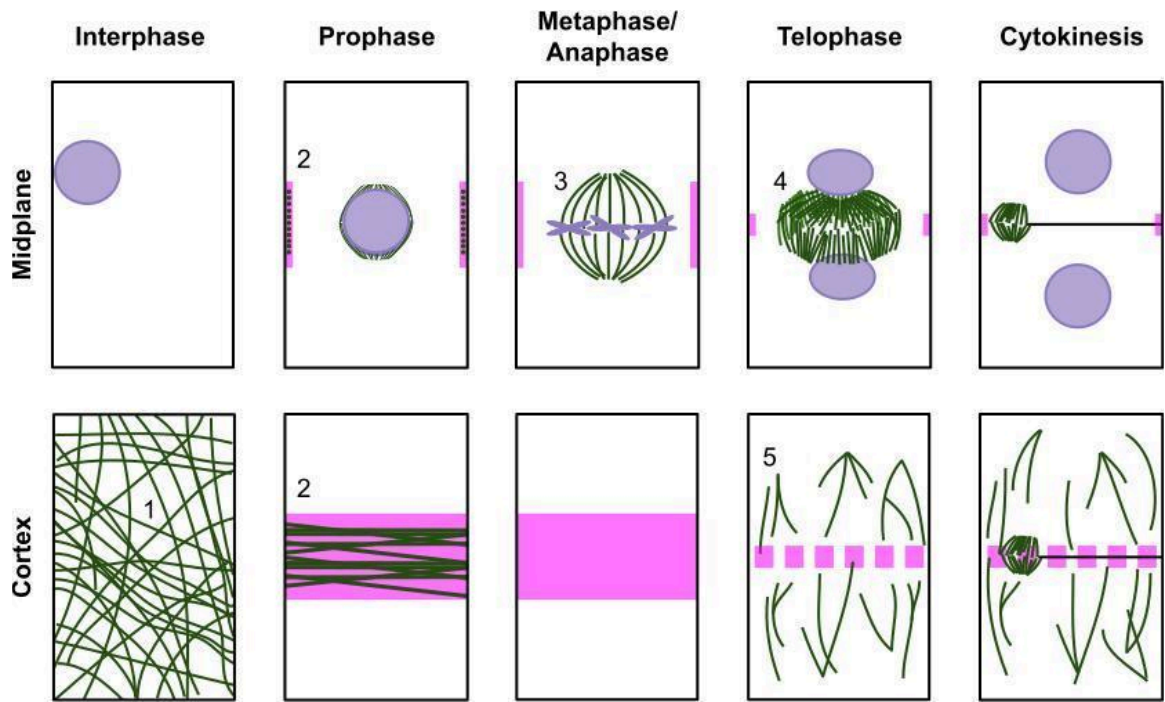


Figure 1.1. Overview of mitotic microtubule and DNA structures and locations important in typical land plant division plane orientation.

Typical land plant cells form five key microtubule arrays (green) during the cell cycle. The division site is marked in pink.

- 1) The interphase cortical microtubule array: During interphase, microtubules at the cell cortex, the region just underneath the plasma membrane, form a variety of cortical microtubule array organizations. Rapidly elongating cells form ordered arrays perpendicular to the growth axis while isotropically expanding cells tend to form more disordered microtubule arrays. These cortical interphase arrays contribute to positioning cellulose synthase complexes and generating new cell wall material. Therefore, the orientation of the interphase cortical microtubule array influences the direction of cell elongation (Dixit et al., 2004; Oda, 2015). Orientation of the interphase cortical microtubule array often, but not always, precedes orientation of the preprophase band (PPB), described below (Gunning et al., 1990).
- 2) The preprophase band (PPB): Increased microtubule dynamicity precedes the formation of the PPB ring at the cell cortex-during the last part of the G2 phase in the cell cycle (Vos et al., 2004). The PPB surrounds the nucleus (purple) and accurately predicts the future division site and cell plate insertion site (Mineyuki, 1999; Pickett-Heaps et al., 1966; A. Smertenko et al., 2017). While the PPB is disassembling, microtubules accumulate around the nuclear envelope to coalesce into an acentrosomal spindle. The cortical division zone, however, remains marked by division-site-localized proteins (pink) even though the PPB is no longer present.
- 3) The spindle: The spindle captures and separates chromosomes (purple) during metaphase and anaphase. Spindle formation is reviewed in (B. Liu et al., 2022; H. Zhang et al., 2011). After chromosome separation in anaphase, the spindle disassembles to form a plant specific structure called the phragmoplast.
- 4) The phragmoplast: The phragmoplast directs the formation of the cell plate. The cell plate transitions into the new cell wall after the completion of cytokinesis, reviewed in (Gu et al., 2022; Y.-R. J. Lee et al., 2019; A. Smertenko et al., 2017, 2018).
- 5) The cortical-telophase microtubule array: The cortical-telophase microtubule array contributes to positioning the phragmoplast. Cortical-telophase microtubules are added into the phragmoplast at the cortex to direct phragmoplast expansion at the division site (Bellinger et al., 2023). As the phragmoplast disassembles at the cell plate fusion site, the cell plate fuses with the mother cell plasma membrane to form the new cell wall.

A number of proteins and processes relevant to plant division plane orientation occur with some level of redundancy. Similar to other systems where redundancy is present, redundancies may contribute to the robustness of maintaining proper division plane positioning (Láruson et al., 2020). Open questions remain about why some processes are reinforced through redundant mechanisms and whether redundancy in division plane orientation contributes to phenotypic plasticity. Typical model systems used to understand division plane positioning include the dicot model *Arabidopsis thaliana* (*Arabidopsis*), monocots *Zea mays* (maize) and *Brachypodium distachyon*, and non-flowering models *Physcomitrium patens* (*P. patens*) and *Marchantia polymorpha* (*M. polymorpha*) although important discoveries have been found in other plants. This review focuses on genetic and non-genetic redundancies that contribute to proper division plane orientation.

Cell shape, size, and nuclear movement are closely intertwined with the onset of mitosis and division plane positioning. Plant cells grow to a certain size before they enter mitosis (Gutierrez, 2022). After asymmetric divisions generate small cells, S phase is delayed until cells reach a certain size (D'Ario et al., 2021). Prior to mitosis, the nucleus moves to the future division plane in both symmetrically and asymmetrically dividing cells through the coordinated action of microtubule and actin motor proteins (Facette et al., 2019; Frey et al., 2010). Proteins connecting the nucleus and the cytoskeleton are critical for positioning the PPB (Arif Ashraf et al., 2022). PPB positioning defects may result from errors in nuclear positioning but also reflect combinations of defective cell elongation, disorganized microtubule arrays, or failures in establishing polarity prior to asymmetric division (Pietra et al., 2013; L. Zhang et al., 2022). Some mutants discussed below have defects in cell elongation or microtubule orientation in interphase, which may

influence the position of the division plane and subsequently alter organ shape. Indeed, cell elongation prior to division typically favors a division bisecting the long axis of the cell (Martinez et al., 2018). The relationship between division plane orientation and cell shape is discussed in more detail in (Laruelle et al., 2022; Louveaux et al., 2016; Martinez et al., 2018; Moukhtar et al., 2019; C. G. Rasmussen et al., 2018). Identifying mutants that only alter PPB formation or positioning (some of which are discussed below) but do not seriously alter interphase microtubule orientation, polarity cues, or cell shape provide exceptionally valuable insight e.g. (Schaefer et al., 2017).

TEMPORAL REDUNDANCY

Cell division positioning is buffered through temporal redundancy. We use temporal redundancy to describe situations where alterations to division plane orientation are corrected later by another independent mechanism. Two examples of temporal redundancy discussed below are: 1) when defects in proper organization or positioning of mitotic structures (Figure 1.2), such as the spindle, does not alter the proper localization of the final division and 2) when protein recruitment to a specific location earlier in the cell cycle partially abrogates the need for that protein to be recruited later (Figure 1.3).

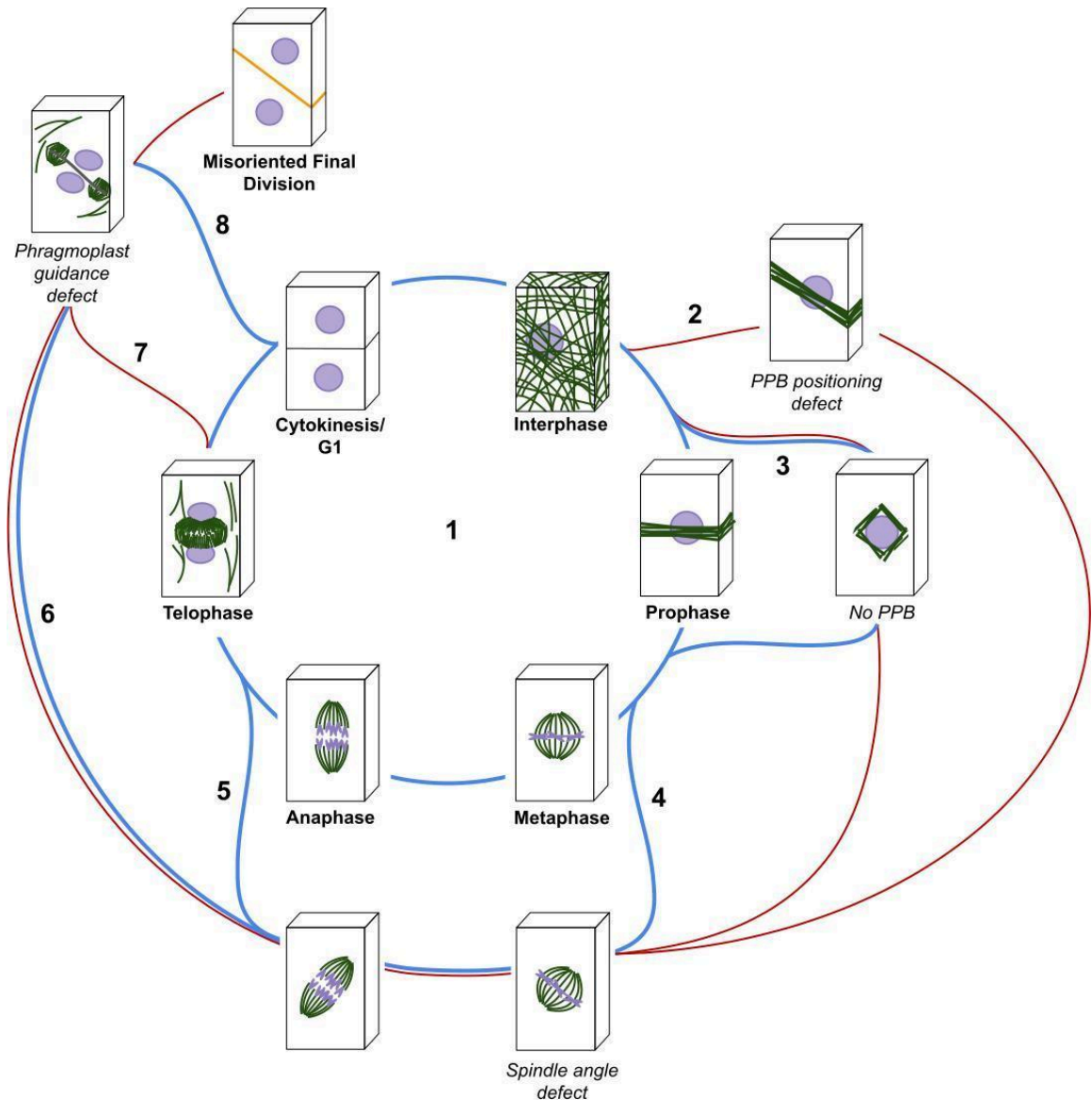


Figure 1.2. Temporal redundancy during division plane orientation showing schematic examples of correctly oriented divisions, and when mitotic structures deviate from the “correctly oriented” position.

Microtubule structures are green, DNA is purple, and black lines indicate the cell wall. The inner ring (clockwise starting from interphase) illustrates normal symmetric divisions with typical land-plant mitotic structures from interphase to cytokinesis (Pathway 1). Blue lines represent a cell-cycle progression that leads to a “correctly oriented” division. Red lines represent defects that may lead to an aberrantly positioned new cell wall (orange line). In Pathway 2, mispositioned PPBs result in misoriented spindles and phragmoplasts that lead to a final misoriented division. In Pathway 3, PPB formation does not occur which either results in wild-type division planes (blue line) or division-plane-orientation defects (red line). In Pathway 4, spindle rotation occurs both in mutant and non-mutant cells, but the tilt is corrected leading to normally positioned phragmoplasts (Pathway 5) or generating tilted phragmoplasts that are sometimes corrected later (Pathway 6). In Pathway 7, phragmoplast guidance defects result in misoriented divisions. Finally in Pathway 8, some misoriented phragmoplasts can be corrected as they near the cortical division site, but before cytokinesis is completed.

Plant cells are capable of robustly maintaining proper division plane orientation via dynamic re-positioning of mitotic structures (Figure 1.2, Pathway 1). Analysis of divisions with and without PPBs provides insight into the stabilizing function of the PPB and its contribution to efficient coordination of mitotic progression. Although the PPB facilitates efficient spindle formation, cells lacking PPBs still assemble functionally and morphologically normal spindles (Figure 1.2, Pathway 3). This includes both cells with defective/missing PPBs and those that always lack PPBs, such as the cells that will undergo meiosis (meiocytes) or some divisions in early diverging plants e.g. in (Chan et al., 2005; Higgins et al., 2016; Otegui et al., 2000; Rensing et al., 2020; Sakai et al., 2022). Unlike cells that have PPBs, cells that lack PPBs may require additional time for spindle coalescence as exemplified in *Arabidopsis* cultured cells (Chan et al., 2005). In addition, naturally PPB-less meiotic spindles often form incorrectly, taking additional time to realign to form a bipolar spindle in maize (Weiss et al., 2022; H. Zhang et al., 2011).

For cells that typically form PPBs, both spindle rotation and spindle morphology defects can be overcome to maintain proper division planes by corrective rotation of the phragmoplast (Figure 1.2, Pathways 4 and 5, or Pathways 4 and 6). Phragmoplast correction has been observed in bean, maize, and onion cells where imaging experiments revealed tilted spindles (e.g. >50% in maize epidermal cells), but normal final division orientations (Cleary et al., 1998; Oud et al., 1992; Palevitz, 1986). In onion guard mother cells, live cell imaging demonstrated correction of oblique spindle and phragmoplast angles occurs as the cell plate expands along the location previously marked by the PPB (Palevitz, 1986). In addition, in tobacco, when cells with PPBs are treated with microtubule depolymerizing drugs followed by washout, spindles formed that

are often tilted, but division positioning is typically corrected prior to cytokinesis (Marcus et al., 2005).

Corrections to spindle orientation are also observed in mutants with defects in spindle formation, morphology, and organization (Figure 1.2, Pathway 4 and 5 or Pathway 4 and 6). Mutants of the gene encoding the microtubule severing protein KATANIN1 (KTN1) make defective PPBs and have spindles that exhibit random rotations in *Arabidopsis* (Komis et al., 2017). However, the phragmoplasts eventually return to the former location of the PPB (Komis et al., 2017). Other mutants that produce highly elongated, mispositioned, or multipolar spindles also typically divide in the correct location. Examples include *Arabidopsis endosperm defective 1 (ede1)*, which is a mutant in an *AUGMIN8* homolog (Y.-R. J. Lee et al., 2017), and mutants lacking minus-end directed Kinesin 14A motors (*atk1* and *atk5*) (Ambrose et al., 2007; C. Chen et al., 2002; Hotta et al., 2022; Marcus et al., 2003).

Other redundant mechanisms that correct spindle mispositioning or multipolarity occur in cells lacking PPBs. In maize meiocytes, mutants in *Kinesin14A* have defects in spindle assembly and form multipolar spindles. However, multipolar spindles then coalesce to form bipolar spindles and division proceeds normally (Higgins et al., 2016; Weiss et al., 2022). This suggests that spindle correction also occurs in a PPB-independent manner. A similar redundancy is observed in *M. polymorpha* suspension cells which have centrosome-like structures called polar organizers that define the poles of the cell and promote the formation of the PPB. In the absence of the PPB but presence of multiple polar organizers, *Marchantia* suspension cells form multipolar prometaphase spindles that resolve into a bipolar arrangement for normal division progression (Buschmann et al., 2016).

Alternatively, in some divisions without PPBs, such as those observed in *P. patens*, meiocytes, or mutants, spindle orientation may play a greater role in determining division plane orientation. Here, we propose that the PPB may provide one or more corrective mechanisms because it recruits division site localized proteins that later adjust phragmoplast positioning. Therefore in the absence of a PPB, defects in spindle positioning may not be corrected later in the cell cycle. For example, the PPB-less divisions of male meiocytes in the Arabidopsis *atk1* mutant (mentioned above) have a more severe phenotype consisting of chromosome segregation defects than in PPB-containing mitotic divisions (C. Chen et al., 2002; Marcus et al., 2003). In addition, *P. patens* gametophore initial cells lack PPBs but instead make a microtubule structure called the gametosome, which predicts spindle positioning (Kosetsu et al., 2017). Spindle mispositioning in the asymmetric divisions of gametophore initials in the *P. patens* *TPX2* mutant results in aberrant division positioning (Kozgunova et al., 2022). Finally, greater variation in spindle angle was also observed in an Arabidopsis triple mutant (discussed below in the genetic redundancy section) that rarely produced PPBs called *tonneau recruiting motif (trm678)*. In the *trm678* mutant, spindle angle variation was correlated with variation in cell wall angle (Schaefer et al., 2017). However, confirming if spindle angle defects indeed lead to mispositioned final cell walls would require timelapse imaging. Together these examples suggest that in the absence of a PPB (e.g. in mutants such as *trm678*, some *P. patens*-divisions, and meiocytes), the spindle may play a greater role in division plane determination.

Spindle rotation and other defects are often compensated by phragmoplast guidance to the correct division plane (Pathway 8). In Arabidopsis, several proteins (discussed in more detail below) are hypothesized to guide the phragmoplast to the

correct division site by interacting with microtubules emanating from the phragmoplast called peripheral phragmoplast microtubules (Livanos et al., 2019). In maize, another mechanism is proposed to coordinate phragmoplast positioning with division site localized proteins. Cortical telophase microtubules, a population of microtubules that nucleates at the cell cortex independent from phragmoplast microtubules, were observed to interact with the phragmoplast and likely influence phragmoplast positioning (Bellinger et al., 2023). Interaction of these cortical telophase microtubules with division site localized proteins (discussed below) pre-orientates cortical telophase microtubules at the cell cortex ahead of phragmoplast expansion, thereby positioning the phragmoplast (Bellinger et al., 2023). These cortical telophase microtubules have been observed in both monocot and dicot species, suggesting that this type of phragmoplast positioning may be conserved through the plant lineage (Lucas, 2021; E. Panteris et al., 1995; Wick, 1985). Phragmoplast guidance is also mediated by both short and long range interactions between division site localized proteins, actin filaments, and microtubules. After centrifugation of dividing tobacco cells, long actin cables are observed connecting the displaced phragmoplast and the division site or former PPB location (Arima et al., 2018). Both classes of actin motor proteins, MYOSIN VIIIIs and MYOSIN XIIs, promote proper phragmoplast guidance (Abu-Abied et al., 2018; Huang et al., 2022; Nan et al., 2021; S.-Z. Wu et al., 2014). MYOSIN VIII coordinates actin filaments and microtubules at the phragmoplast and the division site to move the phragmoplast towards the division site (S.-Z. Wu et al., 2014).

Temporal Redundancy: Protein Recruitment

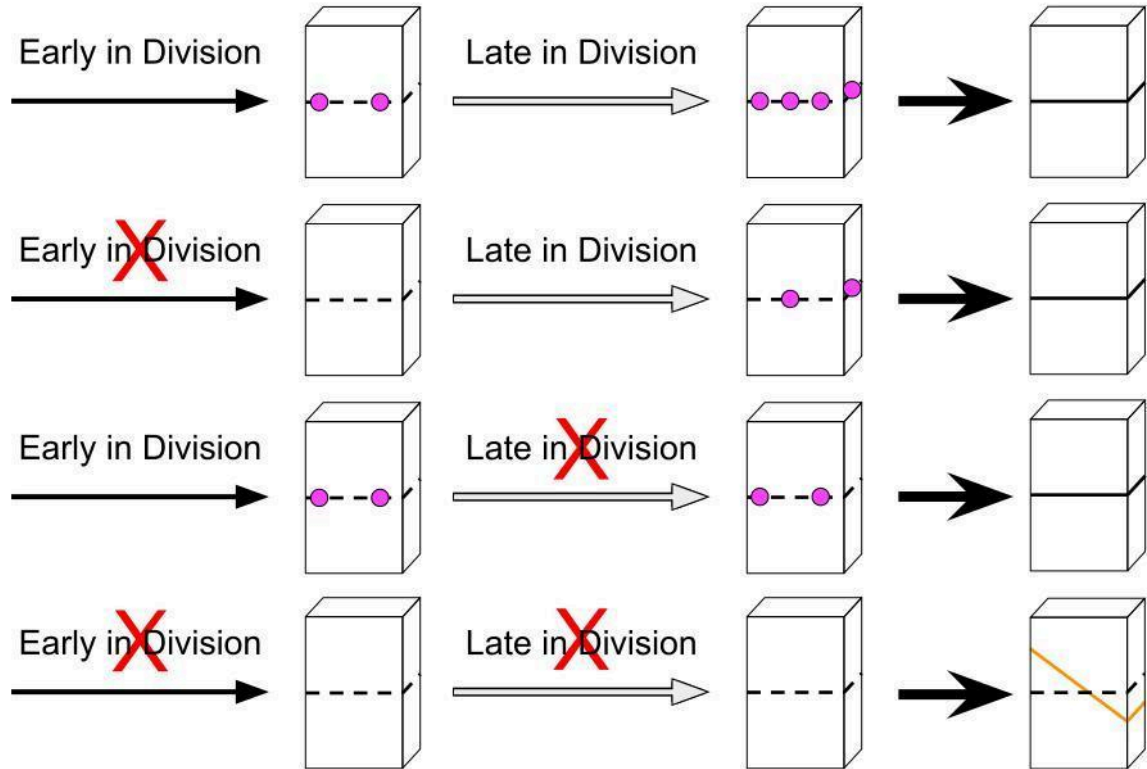


Figure 1.3. Temporal redundancy in protein recruitment.

In the wild-type example (top), early protein localization is reinforced by redundant, later recruitment to the same location. In the absence of either early or late recruitment (second and third from top), the protein is sufficient to maintain correct division plane orientation. Complete loss of recruitment results in a division plane orientation defect. Dotted lines represent the correct division site. Pink circles represent division site localized proteins. Solid orange line represents the final misoriented division.

A final example discusses temporal redundancy in terms of protein localization. TANGLED1 (TAN1) is a key division site localized protein recruited during both prophase and telophase by independent mechanisms (Carolyn G. Rasmussen et al., 2011), although only a part of the protein is only required for full function (Mills, Morris, et al., 2022). In Arabidopsis, this fragment accumulates at the division site during telophase, and interacts with another division site localized protein called PHRAGMOPLAST ORIENTING KINESIN1 (POK1) (Müller et al., 2006; Carolyn G. Rasmussen et al., 2011), which is described in more detail in the genetic redundancy section. Why then is TAN recruited to the division site during prophase? Recent data shows that when TAN1 is recruited during prophase, both TAN1-telophase recruitment and interaction with POK1 is less important for in vivo function. In other words, if TAN1 is already at the division site, there may be less need for it to be recruited again later and for interactions thought to mediate its telophase division site localization (Mills et al., 2022).

GENETIC REDUNDANCY IN DIVISION PLANE ORIENTATION

Genetic redundancy exists for some genes that are important for division plane orientation (Figure 1.4). Genetic redundancy (on the scale of the individual rather than a population) is defined as the ability of closely related genes (homologs) to functionally compensate for the absence of the other (Ascencio et al., 2013; Láruson et al., 2020). Single mutants have no or subtle phenotypes, whereas two or more mutant combinations in related genes show phenotypes with varying severity. In contrast, mutants in non-redundant genes, genes without homologs in the genome, often have noticeable phenotypes. Below, we highlight some examples of genetic redundancy involved in division plane positioning.

Genetic Redundancy

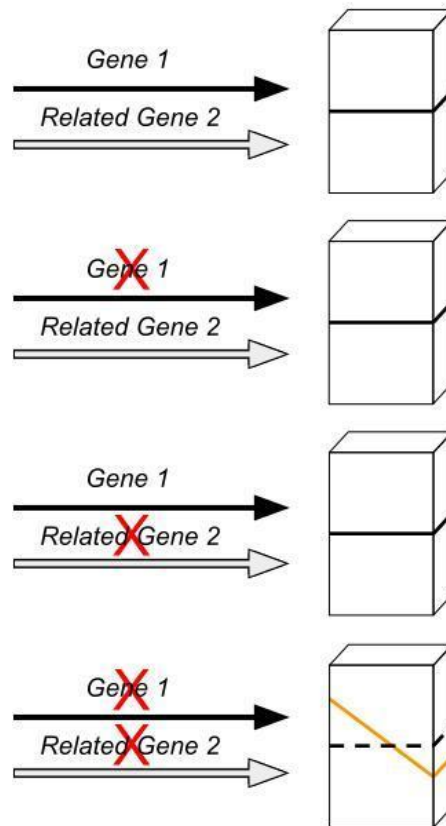


Figure 1.4. Genetic redundancy in division plane orientation.

In processes that involve two or more homologous genes within a family, some genes are able to functionally compensate for mutations within other related genes. For lower order mutants (e.g. single mutants shown here), this can result in a normally positioned division. Higher order mutants, such as the last example of the double mutant shown here, are required to observe division plane orientation defects (orange line).

Proteins important for PPB positioning

The first genes required for PPB positioning were discovered using forward genetic screens described below. Later, protein-protein interaction studies identified redundant partners that promote proper PPB positioning. As an example, we highlight the pathway that contributes to asymmetric divisions during stomatal formation in maize. The pathway required for PPB positioning and stomatal development in Arabidopsis has been beautifully and recently reviewed in (L. Chen, 2022; Guo et al., 2022; Arvid Herrmann et al., 2021).

The early components of the maize asymmetric subsidiary mother cell pathway were identified using forward genetics as many of the identified genes have non-redundant functions. Subsidiary mother cells divide into a subsidiary cell and pavement cell and begin with the polarized recruitment of BRICK to the subsidiary mother cell and guard mother cell interface. BRICK1 is a highly conserved component of the SCAR/WAVE (suppressor of cAR/WASP family/Verprolin-homologous protein) complex important for nucleating branched actin, first characterized in maize (Frank et al., 2002). Arabidopsis *brk1* mutants have aberrant actin organization and reduced trichome branching and pavement cell lobing (Djakovic et al., 2006; Le et al., 2006). Similarly maize *brick1* mutants with aberrant actin organization and form brick-shaped epidermal cells that lack lobes and have defects in subsidiary cell formation (Facette et al., 2015; Frank et al., 2002). BRICK1 is required for the recruitment of two catalytically dead leucine-rich-repeat receptor-like-kinases (LRR-RLK) PANGLOSS2 (PAN2) and PAN1 (Cartwright et al., 2009; Xiaoguo Zhang et al., 2012).

Redundant players important for subsidiary mother cell divisions were identified through protein-protein interactions. PAN2 is required to recruit PAN1 to the subsidiary

mother and guard cell interface, but they do not physically interact. Instead, PAN1 and PAN2 both interact with two members of the WEB1-PMI2-RELATED (WPR) protein family (Nan et al., 2023). Founding members of the WPR family, WEAK CHLOROPLAST MOVEMENT UNDER BLUE LIGHT 1 (WEB1) and PLASTED MOVEMENT IMPAIRED 2 (PMI2) promote actin nucleation during chloroplast movement (Kodama et al., 2010; Luesse et al., 2006; Suetsugu et al., 2017). WPRs are a large redundant family (16 in *A. thaliana* and 17 in maize) that share a coiled-coil domain which likely mediates protein-protein interactions (Nan et al., 2023). Four maize WPRs belonging to the WPR A and WPR B clades interact with each other, while WPRBs interact directly with PAN2 and PAN1. These WPRs polarly localize to the subsidiary mother cell face near the guard mother cell. PAN1 and PAN2 accumulation and interaction with these WPRs promote actin patch formation. Single *wpra* mutants have no phenotype, but double *wpra1 wpra2* mutants were not recovered and are therefore likely essential for viability (Nan et al., 2023). Similarly, the two *WPRB* genes are redundant: single mutants have no phenotype, while double mutants have subsidiary cell division defects. The WPRs may act redundantly to mediate PAN1 recruitment following polarization of BRIK1 and PAN2 (Nan et al., 2023). Finally, PAN1 is required for the recruitment of a class of small monomeric GTPase proteins found in plants called Rho-related GTPases of Plants (ROPs) (Facette et al., 2015), whose redundancy is discussed in more detail below.

ROPs promote cell elongation required for division plane positioning

ROPs act as molecular switches critical for coordinating polar growth via cytoskeletal rearrangements and vesicle trafficking (Craddock et al., 2012; E. Li et al., 2023; Nielsen, 2020; Ou et al., 2022; Z. Yang, 2008). Like other small GTPases, ROPs

cycle between an activated GTP-bound state and an inactive GDP-bound state mediated by guanine nucleotide exchange factors (GEFs) and GTPase-activating proteins (GAPs) respectively. Activated ROP-GTP interacts with ROP effectors. A final class of ROP regulators called guanine dissociation inhibitors (GDIs) inhibit ROP activity by sequestering ROP-GDP away from the plasma membrane. ROPs and their related proteins are often highly redundant. For example, in moss (*P. patens*), there are twelve GEFs, six ROPGAPs, and four GDIs. Silencing entire families of ROP regulators by RNAi results in loss of tip growth and highlights their role in cell expansion (Bascom et al., 2019). Arabidopsis has eleven highly similar ROPs, so overexpression or gain-of-function mutants have been used to overcome redundancy to reveal defects in directed cell expansion in root hairs, pollen tubes, during phloem development, and in epidermal cells (Fowler, 2009; Fu et al., 2005; Roszak et al., 2021; Z. Yang, 2002). Interestingly, a few proteins within the ROP signaling module may also play roles in division plane orientation. These include ROPs, ROP-GAP proteins (also known as PLECKSTRIN HOMOLOGY GAPS, PHGAPs), ROP-GEFs, and ROP effectors called ROP INTERACTING PARTNERS (RIPs) (Hasi et al., 2022; Rong et al., 2022; C. Zhang et al., 2022).

Two of the nine ROPs in maize play redundant roles in polarizing subsidiary mother cell divisions. Like Arabidopsis, maize ROPs can be classified based on post-translational modifications into two groups (Type-I or Type-II) which affect membrane targeting (Berken et al., 2008; Christensen et al., 2003a). Maize Type-I *rop2/rop2 rop9/+* mutants have defective subsidiary mother cell divisions due to failure to accumulate actin patches during polarization (Christensen et al., 2003b; Humphries et al., 2011). Maize ROPs are recruited by an initial BRICK/PAN polarizing signal

(discussed above) to promote actin patch formation. After ROP recruitment, the guard mother cell and the subsidiary mother cell expand (Facette et al., 2015).

P. patens and *M. polymorpha*, have fewer ROP genes than Arabidopsis and maize. In *P. patens*, all four ROP genes act redundantly to regulate polarized tip growth and individually contribute to plant size (Burkart et al., 2015). Quadruple *rop1234* mutants lose polar growth completely, resulting in diffusely growing spherical cells that lack branches (Cheng et al., 2020). Less severe triple ROP mutants *rop134* (Cheng et al., 2020) and *rop234* (Yi et al., 2020) exhibit defective placement of asymmetric branch divisions (Cheng et al., 2020). Similar phenotypes can be seen in cells treated with Latrunculin A, a drug that disrupts actin filaments, suggesting that ROPs regulate actin accumulation to promote branch initiation and then cell elongation (Yi et al., 2020). Division plane orientation defects in *rop234* mutants seem to be a consequence of failed branch expansion and failed nuclear migration (Yi et al., 2020). The sole ROP gene in *M. polymorpha* is most similar to *AtROP2* (Rong et al., 2022). *rop* mutant thallus cells had aberrant shapes and defects in cortical microtubule organization that likely contributed to more random division positioning. While it is known that *M. polymorpha* cells forms PPBs following the formation of polar organizers (perinuclear microtubule accumulations), whether PPBs were misplaced in *rop* mutants is unknown because they were not observed in these cells (Buschmann et al., 2016; Rong et al., 2022).

Arabidopsis *PHGAPs/RENs* are another example of redundant genes that impact division plane positioning. Mutants in Arabidopsis *PHGAPs/RENs* have aberrant PPB localization, potentially due to defects in cell elongation. PHGAPS are a class of pleckstrin homology ROP GTPase-activating proteins (GAPs) that promote GTP hydrolysis and thus inactivation of ROP (Stöckle et al., 2016). The founding member,

ROP ENHANCER1 (REN1), maintains pollen-tube tip growth through its regulation of ROP1 (Hwang et al., 2008). Two other closely related PHGAPs, PHGAP1/REN2 and PHGAP2/REN3, interact with ROP2 and are redundantly required for epidermal-cell lobing (Lauster et al., 2022). PHGAPs are stabilized by BRASSINOSTEROID INSENSITIVE 2 kinase-dependent phosphorylation, accumulating in pavement-cell indentations to deactivate ROP2 (C. Zhang et al., 2022). In addition to the role of PHGAPs in polar expansion, PHGAPs are recruited to the division site from metaphase to cytokinesis in the Arabidopsis root meristem (Stöckle et al., 2016). PHGAPs likely alter PPB positioning via their roles in cell elongation, although some other mechanism is possible. The role PHGAPs play at the division site remains unknown (Stöckle et al., 2016).

Other ROP-related proteins in Arabidopsis that influence the direction of cell division include a class of ROP effector proteins, interactor of constitutive active ROPs (ICRs)/ ROP interactive partners (RIPs) (Lavy et al., 2007; Nagawa et al., 2010), and the ROPGEFs (Roszak et al., 2021). Arabidopsis has five RIPs that all label cortical interphase microtubules (Hasi et al., 2022). Several double or triple mutant combinations have no phenotype while the two quadruple mutants *rip1245* and *rip1235* as well as the quintuple *rip12345* mutant generate narrower leaves due to less longitudinally-oriented PPBs leading to fewer transversely-oriented cells (Hasi et al., 2022). Thus far, mutants in another class of highly redundant ROP effectors, the ROP-interactive CRIB motif proteins (RICs), reveal functions in cell lobing in Arabidopsis (G. Wu et al., 2001) but no obvious function in *P. patens* (Bascom et al., 2019). Interestingly, individual overexpression of three Arabidopsis ROPGEFs (ROPGEF2, ROPGEF3, and ROPGEF5) activate ROPs to generate asymmetric periclinal divisions during phloem development

(Roszak et al., 2021). These ROPGEFs localize ubiquitously on the plasma membrane but are-depleted from the division site (Roszak et al., 2021), similar to the actin depleted zone (Emmanuel Panteris, 2008; Sano et al., 2005; Daniel Van Damme et al., 2007).

This suggests that ROP activity may be reduced at the division site

In summary, mutants of ROPs and ROP-related proteins demonstrate their roles in cell expansion and polar growth. Impacts on division plane placement may be indirect through alterations in cell shape mediated by cell expansion. However, the absence of ROPGEFs from the division site, and accumulation of PHGAPs at the division site may reflect more direct roles in division plane orientation.

IRK/PXC2

Preventing aberrant divisions is another critical role in division plane positioning played by two partially redundant leucine-rich-repeat receptor-like kinases (LRR-RLK) in Arabidopsis. One of them is INFLORESCENCE AND ROOT APICES RECEPTOR KINASE (IRK), a LRR-RLK that polarly localizes and is essential for preventing ectopic divisions in the endodermis and restricting stele width (Campos et al., 2020). A closely related LRR-RLK called PXY/TDR CORRELATED2 (PXC2) also restricts stele width. Double mutants have more frequent and aberrantly positioned divisions, wider steles and noticeable root growth defects: enhanced phenotypes are likely due to differences in gene expression domains (Goff et al., 2021).

GRAS Transcription Factors

The Arabidopsis GRAS family transcription factor SHORT-ROOT (SHR) together with another GRAS transcription factor, SCARECROW, promotes periclinal divisions in

the root to generate cortex and endodermal cell layers (Benfey et al., 1993; Koizumi et al., 2012). Arabidopsis SHR is a mobile protein that moves from the stele to the endodermis (Nakajima et al., 2001). Maize has three *SHR* homologs: *ZmSHR1*, *ZmSHR2*, and *ZmSHR2-h*, while *Setaria viridis* has two *SHR* homologs (Ortiz-Ramírez et al., 2021). In contrast to Arabidopsis, *ZmSHRs* are expressed in the endodermis and move to the cortex (Ortiz-Ramírez et al., 2021). While single mutants have no or slight phenotypes, maize and *S. viridis* double mutants have reduced cortical layer numbers, illustrating the redundant functions of two monocot *SHR* homologs in regulating root periclinal divisions (Ortiz-Ramírez et al., 2021). In *P. patens*, *SHR* homologs are also genetically redundant and play a role in division plane positioning of an asymmetric division that occurs in the phyllid (leaf) (Ishikawa et al., 2023). *P. patens* has two *SHR* homologs, *PpSHR1* and *PpSHR2* (Ishikawa et al., 2023; Moody et al., 2021). Double *ppshr1 ppshr2* mutants have defects in the orientation of a cell type called the most-medial lateral cell, resulting in narrower leaves and thicker midribs (Ishikawa et al., 2023). In most-medial lateral cells, *PpSHR* functions to promote longitudinal divisions instead of dividing along the path that minimizes surface area (Ishikawa et al., 2023).

Proteins important for PPB formation

One protein complex essential for PPB formation contains a core of five proteins called the TONNEAU1 (TON1)/TONNEAU1 RECRUITING MOTIF (TRM)/ PROTEIN PHOSPHATASE TYPE 2A (PP2A) (TTP) complex (Spinner et al., 2013). The complex contains a PP2A phosphatase holoenzyme composed of three subunits described below in more detail, a connector protein, TON1, and one or more proteins from the TRM family. Genes encoding proteins within the complexes are often redundant: double or

triple mutants are required to see a phenotype, which is typically altered cell elongation due to misorganized microtubule arrays (except in the *trm678* mutant where arrays appear normal, although this was not quantitatively analyzed) and no PPB. When core TTP components are removed, lethality is sometimes observed, suggesting that the TTP complex plays multiple vital roles in both interphase and mitotic cells. The TTP complex is targeted to specific locations by TRMs and the B'' regulatory subunit of PP2A.

PP2A holoenzymes play important roles in plant defense, regulating transcription factor stability, and signaling e.g. (Bheri et al., 2019; Bian et al., 2020; Máthé et al., 2019), but here we focus on its role in PPB formation. The PP2A heterotrimeric holoenzyme is composed of a scaffolding subunit (PP2AA), a regulatory B-type subunit that controls its localization, and a catalytic subunit (PP2AC). B-type subunits can be broken into B, B', and B'' families and function in substrate specificity or PP2A complex targeting. FASS/TON2 encodes a B'' type regulatory subunit (Camilleri et al., 2002). In Arabidopsis, *fass/ton2* mutants have defects in cortical-microtubule organization and lack PPBs (Camilleri et al., 2002; Kirik et al., 2012; McClinton et al., 1997; Torres-Ruiz et al., 1994). In maize, the B'' subunit is encoded by two homologs, *DISCORDIA1 (DCD1)* and *ALTERNATIVE DISCORDIA1 (ADD1)*. Similar to Arabidopsis *fass/ton2* loss-of-function mutants, maize *dcd1 add1* double mutants do not make PPBs and are seedling lethal. DCD1 and ADD1 localize to the division site from preprophase to metaphase (Wright et al., 2009) similar to FASS/TON2 (Kirik et al., 2012). Single *add1* mutants have no discernable phenotype (Wright et al., 2009). Single *dcd1* mutants have partially defective preprophase bands which disrupt subsidiary mother cell divisions but do not affect symmetric divisions (Wright et al., 2009). Perhaps symmetric divisions in

maize have additional redundant mechanisms to ensure proper division plane orientation not found in asymmetric divisions.

There are five copies of the Arabidopsis PP2A phosphatase catalytic subunit. Single *pp2ac-3* or *pp2ac-4* mutants do not have significant root growth, microtubule organization, and division positioning defects until combined into a double mutant (Ballesteros et al., 2013; Spinner et al., 2013; Yoon et al., 2018; Yue et al., 2016). A receptor-like kinase called ARABIDOPSIS CRINKLY4 (ACR4) phosphorylates PP2A-C3, while PP2A-C3 dephosphorylates ACR4. This cross-regulation is implicated in formative cell divisions within the Arabidopsis root (Yue et al., 2016). Similarly, three PP2AA-scaffolding subunits facilitate PP2A assembly and double or triple mutants are required to observe cells lacking PPBs (Spinner et al., 2013; H.-W. Zhou et al., 2004). Neither the scaffolding subunit double mutants (*pp2aa1-a3* or *pp2aa1-a2*) nor the catalytic subunit double mutant *pp2ac3-c4* make PPBs (Spinner et al., 2013). Enhanced phenotypes in higher order mutants reveal redundancies in the PP2A complex and its impact on PPB formation.

The original *ton1* mutant allele is actually a double mutant disrupting two tandemly-linked paralogs, *TON1a* and *TON1b* in Arabidopsis (Azimzadeh et al., 2008; Nacry et al., 1998; Traas et al., 1995). TON1a and TON1b are 86% identical at the amino acid level and both contain a serine-rich motif, a dimerization motif, and bind to the calcium-binding protein called centrin (Azimzadeh et al., 2008). TON1 also shares domains with human centrosome proteins and may be involved with microtubule nucleation (Azimzadeh et al., 2008). The double mutant produces a tiny plant with no PPBs and disordered microtubule arrays. In contrast, *ton1a-1* single mutants have a milder phenotype consisting of slightly slower root growth and misoriented symmetric

divisions mostly in the root epidermis (Yanwen Zhang et al., 2016). Disruption of the single gene *TON1* in *P. patens* leads to normally shaped but agravitropic vegetative cells and small, disorganized leafy gametophores with defects in PPB formation and cell elongation (Spinner et al., 2010).

A subset of highly redundant TON1 interactors, TRMs, were identified by yeast-two-hybrid screening that are required for both PPB positioning and formation. TRMs are a superfamily of 34 proteins that share a conserved C-terminal TON1 interacting motif. Some TRMs also contain microtubule-binding domains and FASS/TON2 interaction domains (Drevensek et al., 2012; Spinner et al., 2013). The founding *TRM* genes, called *LONGIFOLIA1 (LNG1)* and *LNG2*, were identified by a dominant mutant that overexpressed *LNG1/TRM2* in Arabidopsis, *Ing1-1D* (Y. K. Lee et al., 2006). The *Ing1-1D* overexpression produces aberrantly elongated cells leading to long, narrow leaves. Neither *Ing1* nor *Ing2* loss-of-function mutants have a noticeable phenotype. However, *Ing1 Ing2* double mutants have short, round leaves (Y. K. Lee et al., 2006). Progressively higher order mutant combinations generated cell elongation defects that led to shorter rounder leaves (Y. K. Lee et al., 2018). Whether these mutants have PPB positioning defects is unknown. In maize, a naturally-occurring mutation within the *LNG1/TRM2* gene *ZmLNG1*, alters leaf shape and plant architecture in specific genetic backgrounds. The mutation generates a protein that disrupts ZmLNG1 and ZmTON1 interactions but does not alter ZmLNG1 localization. *ZmLNG1* overexpression generates long, narrow leaves and kernels. Yeast-three-hybrid assays suggest that ZmLNG1 may act as a bridge between TON1 and Ovate Family Proteins (OFPS, discussed below) (Q. Wang et al., 2023).

While several *LNG/TRM* genes promote cell elongation, possibly due to modulation of interphase microtubule orientation or PPB location, other *TRM* genes are critical for PPB formation itself. A subset of three similar TRMs in Arabidopsis, *TRM6*, *TRM7* and *TRM8* (Drevensek et al., 2012), have partially redundant roles in PPB formation (Schaefer et al., 2017). Single and double mutants have minor phenotypes, but the triple *trm678* mutant has significantly impaired PPB formation (Schaefer et al., 2017). Triple *trm678* mutants do not have obvious growth defects but have increased spindle angle variance. Interestingly, division site localized proteins still accumulate, albeit less often than in wild-type cells (Huang et al., 2022; Schaefer et al., 2017). This suggests that a partial or defective PPB still accumulates in these mutants, and/or that division site protein localization is not strictly contingent on PPB formation.

Multiple TRMs interact with another class of plant-specific proteins called Ovate Family Proteins (OFPs) that likely alter PPB positioning or directional cell elongation, as mutants originally characterized in tomato produce elongated tomato fruits (Snouffer et al., 2019; van der Knaap et al., 2014; S. Wu et al., 2018). OFPs contain a conserved ~70 amino acid “ovate” motif in addition to protein-protein interaction domains (J. Liu et al., 2002). Multiple OFP family members are found across the land plants lineage: *P. patens* has 11, Arabidopsis has 19, and maize has 45 (D. Liu et al., 2014). Arabidopsis OFPs also interact with FASS/TON2 (Xiaowei Zhang et al., 2020). However, the founding OFP was a loss-of-function mutant in *OVATE* that produced elongated tomato fruits (J. Liu et al., 2002). Additional mutations in another *OFP* gene called *SIOFP20* led to highly elongated fruits in the *ovate* mutant background (S. Wu et al., 2018) indicating that redundant OFP functions can be revealed through higher order mutant combinations.

Indeed, single loss-of-function *ofp* mutants often do not have any phenotype (S. Wang et al., 2011).

Although OFPs and TRMs interact, they often have antagonistic effects on fruit or organ shape in diverse plant species e.g. (Colle et al., 2017; Lazzaro et al., 2018; Snouffer et al., 2019; Q. Wang et al., 2023; C. Yang et al., 2018; Zhao et al., 2018). TRM overexpression often generates elongated organs, while overexpression of OFPs often generates short, round organs (Snouffer et al., 2019). Transiently co-expressing OFPs with TRMs alters localization of one interacting partner or another (sometimes to microtubules or the cytosol), suggesting that both interactions and relative amounts are delicately balanced to generate proper localization eventually leading to correctly shaped organs (S. Wu et al., 2018).

IQ67 DOMAIN proteins

IQ67 DOMAIN proteins are a large family of plant-specific proteins (33 in Arabidopsis) that modulate cell shape, contain calmodulin binding motifs (IQ67) and often localize to microtubules (Bürstenbinder et al., 2013; Lazzaro et al., 2018; Liang et al., 2018; Hao Li et al., 2022; Yan Li et al., 2021; Yuanfeng Li et al., 2020; van der Knaap et al., 2014; B. Yang et al., 2022). Similar to the TRMs, a subset of three IQD proteins (IQD6,7 and 8) are also redundantly required for PPB formation as triple *iqd678* mutants result in 50% of cells without PPBs (Kumari et al., 2021). IQD8 fused to GFP rescues the *iqd678* mutant and marks a broad zone that encompasses the division site until cytokinesis and colocalizes with phragmoplast microtubules (Kumari et al., 2021). IQD678 are also important for the asymmetric divisions in the Arabidopsis embryo and likely indirectly contribute to division plane positioning by influencing cell shape through

auxin dependent cytoskeletal changes (Vaddepalli et al., 2021). Intriguingly, IQD8 interacts with PHGAP proteins, which are required for PPB placement (discussed above) and recruits them to microtubules when concurrently overexpressed in tobacco cells. IQD8 interacts with both PHRAGMOPLAST ORIENTING KINESIN1 (POK1) and POK2 discussed in more detail below (Kumari et al., 2021). In *iqd678* mutants, POK1 recruitment is delayed but eventually accumulates to wild-type levels (95%) by cytokinesis (Kumari et al., 2021).

Proteins important for phragmoplast guidance or the maintenance of division plane orientation

POK1/POK2

The homologs *POK1* and *POK2* encode two kinesin-12 class proteins in *A. thaliana* that localize to the division site from prophase to cytokinesis and together play critical roles in division plane orientation (A. Herrmann et al., 2018; Lipka et al., 2014; Müller et al., 2006). Both proteins have an N-terminal motor domain, coiled-coil domains, and a C-terminal cargo binding domain. Single mutants do not have division plane orientation defects. However, *pok1 pok2* double mutants have division plane orientation defects (Müller et al., 2006) due to defects in phragmoplast guidance, which often inserts the cell plate at a location different from the PPB (Lipka et al., 2014). POK1 also rescues the double mutant, suggesting functional redundancy (Lipka et al., 2014). However, phragmoplast expansion rates are significantly slower in *pok2* single mutants, indicating its distinct role (A. Herrmann et al., 2018). POK1 and POK2 have similar N-terminal motor domains but localize to the division site via C-terminal regions (A. Herrmann et al.,

2018; Lipka et al., 2014). The C-terminus mediates interaction with another division site localized protein TANGLED1, described in the next section (Müller et al., 2006). POK1 is actively recruited to the division site during prophase but is statically maintained in metaphase (Lipka et al., 2014). POK2 motor activity is diffusive and weakly processive towards microtubule plus-ends (Chugh et al., 2018). POK2-YFP noticeably accumulates in the phragmoplast midline and the division site, in contrast to POK1, which is primarily at the division site in wild-type cells (A. Herrmann et al., 2018; Lipka et al., 2014; Mills, Morris, et al., 2022). If POK1 is not recruited to the division site when interactions with other division site localized proteins are disrupted, it also accumulates in the phragmoplast midline and on the phragmoplast microtubules (Mills, Morris, et al., 2022). Perhaps in the absence of division-site recruiters and stabilizers, plus-end directed kinesins preferentially localize to the phragmoplast midline and the phragmoplast where microtubule plus-ends accumulate. POK1 interacts with the RAN-GTPASE-ACTIVATING-PROTEIN1 (RAN-GAP1), a protein that localizes to the division site and is likely required for division positioning with its redundant partner RAN-GAP2 (Xu et al., 2008). POK1 is actively maintained at the division site after the PPB disassembles through direct or indirect interactions with two other proteins, TANGLED1 (TAN1) and AUXIN INDUCED IN ROOT CULTURES9 (AIR9) (Mills, Morris, et al., 2022), which are discussed in more detail in the next section.

Myosin XI and Myosin VIII

POK1 and POK2 interact with other proteins including actin-binding motor proteins called myosins that transport cargo along actin filaments (Huang et al., 2022; Nan et al., 2021). Plants contain two myosin classes: MYOSIN XI, which contains a

similar domain structure as Myosin class V proteins from animals and fungi, and MYOSIN VIII, which is plant specific (Nebenführ et al., 2018). Interestingly, both MYOSIN XIs and MYOSIN VIIIs play critical but often highly redundant roles in division plane positioning in addition to their roles in cell elongation, nuclear and organelle movement, and cytoplasmic streaming (Bibeau et al., 2021; Haraguchi et al., 2018; Madison et al., 2015; Tominaga et al., 2012). In Arabidopsis, there are 13 MYOSIN XIs: 3 of them, MYOSIN XI-K, MYOSIN XI-1 (also called MYA1) and MYOSIN XI-2, are redundantly required for division plane positioning, particularly within the stele (Abu-Abied et al., 2018). The *myosin xi-k xi-1 xi-2* triple mutant generates additional lateral and adventitious roots and shows both unpolarized auxin transport efflux protein localization and lower auxin response in roots. MYOSIN XI-K-YFP rescues the triple myosin mutant and localizes to the division site during prophase, metaphase and telophase suggesting it may play a direct role in division plane positioning (Abu-Abied et al., 2018). The triple mutant was combined with a mutation in *MYOSIN XI-1* to generate a quadruple myosin mutant. Surprisingly, the quadruple mutant grew similarly to wild-type plants during the seedling stage. However, the quadruple mutant was hypersensitive to the microtubule-depolymerizing drug, oryzalin. Similar to MYOSIN XI-K-YFP, MYOSIN XI-1-YFP localized to the division site. MYOSIN XI-1 localization was dependent on a functional PPB, showing partially disrupted localization in the *trm678* triple mutant described above but no division site accumulation in the *fass/ton2* mutant. In addition, MYOSIN XI-K and XI-1 interact via co-immunoprecipitation and they are found together at the division site in puncta with other division site localized proteins including POK1, TAN1 and RAN-GAP1 (Huang et al., 2022).

In maize, a MYOSIN XI related to MYOSIN XI-I, called OPAQUE1 (O1) promotes phragmoplast guidance to the division site in asymmetric divisions and interacts with POK1 homologs and other myosins (Nan et al., 2021). The *o1* mutant has aberrant protein body accumulation in endosperm cells which produce the opaque kernel phenotype (G. Wang et al., 2012). Despite similarities in interactors, MYOSIN XIs also perform distinct, apparently non-conserved roles. For example, Arabidopsis MYOSIN XI-I is required for proper nuclear movement and nuclear shape (Muroyama et al., 2020; Tamura et al., 2013; X. Zhou et al., 2015), but the *o1* mutant does not have obvious defects in nuclear positioning or shape (Nan et al., 2021). Additionally, while several Arabidopsis MYOSIN XIs fused to fluorescence proteins localize to the division site and the phragmoplast midline (Abu-Abied et al., 2018; Huang et al., 2022), immunolocalization shows that maize O1 localizes only to the phragmoplast midline (Nan et al., 2021). In *P. patens*, the two MYOSIN XIs are redundantly required for polarized growth via interaction with a RAB monomeric GTPase and also play roles in vesicle clustering and trafficking (Galotto et al., 2021; Orr et al., 2020). MYOSIN XI accumulates at the growing tip prior to actin filaments (Furt et al., 2013) and localizes to the spindle and phragmoplast midline but not at the division site (Sun et al., 2018). These recent exciting breakthroughs and differences among MYOSIN XIs illuminate the need to determine how MYOSIN XIs promote proper division plane positioning possibly through interaction with POKs or other proteins at the division site or the phragmoplast midline.

The plant-specific myosins, MYOSIN VIII, also play critical roles in division plane positioning, although their interaction with other division-site localized proteins is still unknown. *MYOSIN VIII* genes are found in large and sometimes partially redundant

families. Deleting one, two, and up to five *MYOSIN VIII*s in *P. patens* generates progressively smaller plants, with the quintuple mutant most severely affected (S.-Z. Wu et al., 2011). In addition, quintuple mutants have defects in division plane positioning that can be mostly rescued by overexpression of one MYOSIN VIII. MYOSIN VIII localizes to the division site both in *P. patens*-PPB-independent divisions, and in PPB-containing tobacco cells (S.-Z. Wu et al., 2014). MYOSIN VIII also localizes to plasmodesmata, plasma membrane, microtubule and actin filaments (Golomb et al., 2008; Kastner et al., 2022; L. Liu et al., 2001; S.-Z. Wu et al., 2014). In *P. patens*, division site localization requires an intact actin cytoskeleton (S.-Z. Wu et al., 2014). While mutants in a single MYOSIN VIII, *arabidopsis thaliana myosin1 (atm1)*, have slower growth and less dividing root cells, division plane orientation was not assessed (Olatunji et al., 2022). It will be interesting to determine whether MYOSIN VIIIs interact with division site localized proteins.

MAP65s

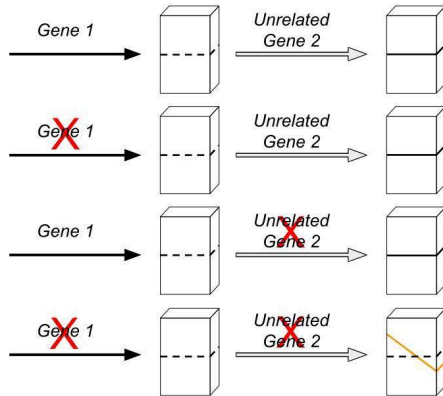
In addition to interacting with MYOSIN XI, POK2 also interacts with several members of the MICROTUBULE ASSOCIATED PROTEIN65 (MAP65) family: MAP65-1, MAP65-3 and MAP65-5 (A. Herrmann et al., 2018). The founding MAP65 protein was identified through a robust interaction with microtubules, including *in vitro* bundling (Chang-Jie et al., 1993). MAP65s typically bundle parallel or antiparallel microtubules with shallow contact angles (Hashimoto, 2015; A. P. Smertenko et al., 2004; Tulin et al., 2012). MAP65 gene families tend to be large (9 in Arabidopsis), and have variable regions that provide specificity within subfamilies. In addition, expression,

phosphoregulation, and localization of MAP65 proteins is variable (Hussey et al., 2002; Sasabe et al., 2012; A. P. Smertenko et al., 2008).

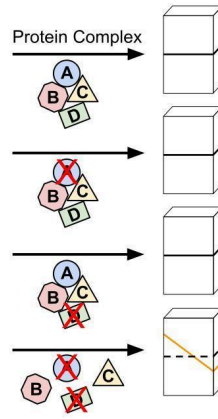
Unlike other MAP65s, MAP65-3 and MAP65-4 exhibit mitosis-specific expression and are together essential for cytokinesis (Haoge Li et al., 2017; Daniël Van Damme et al., 2004). MAP65-3 plays a critical and non-redundant role in antiparallel microtubule bundling within the phragmoplast (Ho et al., 2011). *map65-3/pleiade* mutants are small and have defects in cytokinesis (Müller et al., 2004) that cannot be rescued with *MAP65-1* driven by the *MAP65-3* promoter (Ho et al., 2012). MAP65-3 localizes to the phragmoplast midline (Müller et al., 2004) and interacts with many proteins including POK2 (A. Herrmann et al., 2018). Other MAP65s are also important in cytokinesis as demonstrated through exacerbated cytokinetic defects in MAP65-3 double mutants with MAP65-1, MAP65-2, or MAP65-4 respectively (Haoge Li et al., 2017; Sasabe et al., 2011). Interestingly, *map65-1 map65-2* double mutants do not have defects in division positioning or cytokinesis and instead function redundantly in cell expansion (Lucas et al., 2012; Sasabe et al., 2011). *map65-4* mutants have no noticeable phenotypes until combined with *map65-3* mutants but double mutants are not viable due to cytokinesis failures. MAP65-4 localizes to the division site and the phragmoplast midline, but its function at the division site is not yet known (Haoge Li et al., 2017).

A Synthetic Redundancy within Pathways

i. Accumulation of partial pathway mutations



ii. Mutations within a complex



B Synthetic Redundancy between Pathways

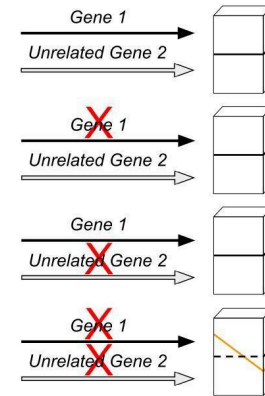


Figure 1.5. Modular redundancy in division plane orientation inspired by (Zinovyev et al., 2013).

(A) Synthetic enhancement within pathways can occur (i) through accumulation of partial pathway mutations in genes (black and gray arrows) within the same pathway or (ii) through mutations within a complex that lead to complex disassembly. (B) Schematic of genes (black and gray arrows) that occur in two distinct but redundant pathways that contribute to correct division plane orientation. Loss of components in one pathway does not result in a phenotype. However, loss of both pathways results in a synthetically enhanced division plane orientation defect. Orange lines represent final misoriented divisions.

SYNTHETIC REDUNDANCY

In this section we discuss another type of redundancy that is mediated not by homologous genes, but by unrelated genes. The framework for understanding synthetic genetic interactions has been described (Zinovyev et al., 2013). Unrelated genes may contribute redundant functions through involvement in the same pathway (Figure 1.5A-i, ii) or in different pathways (Figure 1.5B). Within a singular genetic pathway, loss of an unrelated gene may represent a “partial loss of function” (Figure 1.5A). Alternatively, unrelated genes may contribute to similar functions, likely in genetically parallel pathways that converge on a single phenotypic output (Figure 1.5B). For both within or between pathway redundancies, when one gene or the other is disrupted there is no or little obvious phenotype, but the double mutant has a synthetic or synergistic phenotype, described as “synthetic sick” or “synthetic lethal”. The most comprehensive analysis of synthetic sick or synthetic lethal mutants comes from a systematic double mutant screen in budding yeast. This screen identified many unexpected genetic interactions between unrelated genes (Tong et al., 2001). Alternatively, synthetic lethality screens have led to treatments of human cancers: poly(ADP-ribose) polymerase (PARP) inhibitors are synthetically lethal with mutations in *Breast Cancer gene1 (BRCA1)* or *BRCA2* (Turk et al., 2018).

One type of synthetic genetic interaction is observed when two genes from different parts of a single pathway are mutated (Figure 1.5A-i). Several examples came from a screen that generated double mutants focused on the MITOGEN ACTIVATED PROTEIN KINASE (MAPK) pathway in Arabidopsis. Single mutants in different parts of the MAPK pathway have minor growth phenotypes, while the double mutants show synthetic short-root phenotypes (Su et al., 2016). This conserved MAPK pathway is

essential for cytokinesis, reviewed in (Sasabe et al., 2012). An additional example of a synthetic genetic interaction occurs in *pan1 pan2* double mutants which have ~3X more asymmetric division defects than single mutants (Xiaoguo Zhang et al., 2012). PAN1 and PAN2 are two different LRR-RLK proteins that accumulate during different times during the developmental sequence of subsidiary mother cell division (Facette et al., 2015).

When unrelated genes contribute to a singular pathway, partial-loss-of-function mutant alleles are enhanced by additional “within-complex” mutant alleles (Figure 1.5A-ii). Two fascinating examples took advantage of weak alleles of *fass/ton2* to screen for enhancers. A new allele of *ton1a* was identified as a *ton2-15* enhancer (Kirik et al., 2012). TON1A protein directly interacts with FASS/TON2 (Spinner et al., 2013), suggesting that the “synthetic” phenotype may be caused by loss of multiple components within a complex. Another use of a different weak *fass/ton2* allele showed strong genetic enhancement when combined with *pp2aa1*, *pp2aa2* or *pp2aa3* mutants. The PP2AA proteins also interact directly with FASS/TON2 in the TTP complex (Spinner et al., 2013).

Another partial-loss-of-function mutant enhanced by additional “within complex” mutant alleles occurs during asymmetric divisions that produce the subsidiary cells in maize (BRICK/PAN/ROP pathway described earlier). Combining *rop2* homozygous mutants with *rop9* heterozygotes (*rop2/rop2 rop9/+*) generates a mild subsidiary cell division-positioning defect, likely representing a partial loss of ROP Type I function. Combining this with the *pan1* mutant (which by itself has ~20% defective subsidiary cells) generates plants with >50% defective subsidiary cells. This synthetic enhanced phenotype is consistent with their physical interaction (Humphries et al., 2011).

A synthetic double mutant with defects in growth and division plane orientation was recently identified through the combination of a mutant in *TANGLED1 (TAN1)*, which

encodes a microtubule-binding protein that localizes to the division site, together with a mutant in *AUXIN INDUCED IN ROOT CULTURES9 (AIR9)*, which encodes an unrelated microtubule-binding protein that localizes to the division site in preprophase and late telophase in *Arabidopsis* (Buschmann et al., 2006, 2015; Walker et al., 2007). The current hypothesis is that TAN1 and AIR9 function in two separate but functionally redundant pathways (schematically outlined in Figure 1.5B) that maintain division plane orientation in *Arabidopsis* because no interaction between them has been identified (Mir et al., 2018). *TAN1* was originally identified in maize, in which *tan1* mutants are short and have defects in phragmoplast guidance to the division site (Cleary et al., 1998; Martinez et al., 2017; Smith et al., 1996). *TAN1* is found in plants either as a single gene (e.g. *Arabidopsis* (Walker et al., 2007)) or is within a small family with a few paralogs (e.g. sorghum or maize). *TAN1* is plant-specific and in maize, it encodes a protein that binds, bundles and crosslinks microtubules in vitro (Martinez et al., 2020; Smith et al., 2001) and likely captures microtubules in vivo to position the expanding phragmoplast at the division site (Bellinger et al., 2023). In *Arabidopsis*, *tan1* and *air9* single mutants do not have significant division plane or growth defects. However, *tan1 air9* double mutants exhibit a synthetically enhanced phenotype, consisting of short, slow-growing plants with phragmoplast guidance defects. Unexpectedly, TAN1 and AIR9 functionally converge on their ability to maintain POK1 at the division site after metaphase. While POK1 localizes to the division site in either single mutant, POK1 is not maintained at the division site in *tan1 air9* double mutants after metaphase (Mills, Morris, et al., 2022). It will be interesting to determine whether AIR9 directly interacts with POK1 similar to the direct interaction between TAN1 and POK1.

The synthetic *tan1 air9* double mutant phenotype in Arabidopsis is rescued by transforming it with TAN1 constructs, allowing identification of TAN1 domains that are critical for its function in growth and division plane positioning (Mills, Morris, et al., 2022; Mills & Rasmussen, 2022; Mir et al., 2018). The first ~130 amino acids of TAN1 (TAN1₁₋₁₃₂) localize to the division site primarily during telophase, are necessary and sufficient for POK1 interaction, and fully rescued the *tan1 air9* double mutant (Carolyn G. Rasmussen et al., 2011). Disrupting the interaction between TAN1 and POK1 in the *tan1 air9* double mutant causes phragmoplast guidance defects (Mills, Morris, et al., 2022).

Another example of genes likely functioning in a parallel pathway was identified in the monocot *Brachypodium distachyon*. *BdPOLAR* was identified by its reduced RNA accumulation (D. Zhang et al., 2022) in a mutant which fails to form subsidiary cells (Raissig et al., 2017). POLAR is a plant-specific polarly-localized protein that accumulates during Arabidopsis stomatal development. Unlike the *Atpolar* mutants that have no phenotype (Pillitteri et al., 2011), *Bdpolar* mutants have misoriented subsidiary cell divisions, which are greatly enhanced by combination with *Bdpan1* mutants. Since *BdPOLAR* and *BdPAN1* localize to opposite domains of the subsidiary mother cell, it is likely that they are in parallel pathways, although *BpPOLAR* requires *BdPAN1* to localize correctly (D. Zhang et al., 2022).

CONCLUSIONS

Multiple types of redundancy make identifying the specific roles of proteins implicated in division plane positioning an exciting challenge. After protein-protein interactions identify additional components, high-throughput methods of gene editing such as CRISPR-Cas9 may be used to generate higher order mutants in genetically redundant pathways. Additional insight into synthetic redundancy may be provided by enhancer screens. Finally, detailed mechanistic studies will be required to unravel situations with temporal redundancy.

REFERENCES

- Abu-Abied, M., Belausov, E., Hagay, S., Peremyslov, V., Dolja, V., & Sadot, E. (2018). Myosin XI-K is involved in root organogenesis, polar auxin transport, and cell division. *Journal of Experimental Botany*, *69*(12), 2869–2881.
- Ambrose, J. C., & Cyr, R. (2007). The kinesin ATK5 functions in early spindle assembly in Arabidopsis. *The Plant Cell*, *19*(1), 226–236.
- Arif Ashraf, M., Liu, L., & Facette, M. R. (2022). An outer nuclear membrane protein promotes a polarized nuclear position and the future division plane during asymmetric cell division. In bioRxiv (p. 2022.08.26.505454). doi: 10.1101/2022.08.26.505454
- Arima, K., Tamaoki, D., Mineyuki, Y., Yasuhara, H., Nakai, T., Shimmen, T., Yoshihisa, T., & Sonobe, S. (2018). Displacement of the mitotic apparatuses by centrifugation reveals cortical actin organization during cytokinesis in cultured tobacco BY-2 cells. *Journal of Plant Research*. doi: 10.1007/s10265-018-1047-4
- Ascencio, D., & DeLuna, A. (2013). Genetic Redundancy. In W. Dubitzky, O. Wolkenhauer, K.-H. Cho, & H. Yokota (Eds.), *Encyclopedia of Systems Biology* (pp. 824–827). New York, NY: Springer New York.
- Azimzadeh, J., Nacry, P., Christodoulidou, A., Drevensek, S., Camilleri, C., Amiour, N., Parcy, F., Pastuglia, M., & Bouchez, D. (2008). Arabidopsis TONNEAU1 proteins are essential for preprophase band formation and interact with centrin. *The Plant Cell*, *20*(8), 2146–2159.
- Ballesteros, I., Domínguez, T., Sauer, M., Paredes, P., Duprat, A., Rojo, E., Sanmartín, M., & Sánchez-Serrano, J. J. (2013). Specialized functions of the PP2A subfamily II catalytic subunits PP2A-C3 and PP2A-C4 in the distribution of auxin fluxes and development in Arabidopsis. In *The Plant Journal* (Vol. 73, Issue 5, pp. 862–872). doi: 10.1111/tpj.12078
- Bascom, C., Jr, Burkart, G. M., Mallett, D. R., O'Sullivan, J. E., Tomaszewski, A. J., Walsh, K., & Bezanilla, M. (2019). Systematic survey of the function of ROP regulators and effectors during tip growth in the moss *Physcomitrella patens*. *Journal of Experimental Botany*, *70*(2), 447–457.
- Benfey, P. N., Linstead, P. J., Roberts, K., Schiefelbein, J. W., Hauser, M.-T., & Aeschbacher, R. A. (1993). Root development in Arabidopsis: four mutants with dramatically altered root morphogenesis. *Development*, *119*(1), 57–70.
- Berken, A., & Wittinghofer, A. (2008). Structure and function of Rho-type molecular switches in plants. *Plant Physiology and Biochemistry: PPB / Societe Francaise de Physiologie Vegetale*, *46*(3), 380–393.
- Bheri, M., & Pandey, G. K. (2019). PP2A phosphatases take a giant leap in the post-genomics era. *Current Genomics*, *20*(3), 154–171.

- Bian, C., Guo, X., Zhang, Y., Wang, L., Xu, T., DeLong, A., & Dong, J. (2020). Protein phosphatase 2A promotes stomatal development by stabilizing SPEECHLESS in Arabidopsis. *Proceedings of the National Academy of Sciences of the United States of America*, *117*(23), 13127–13137.
- Bibeau, J. P., Galotto, G., Wu, M., Tüzel, E., & Vidali, L. (2021). Quantitative cell biology of tip growth in moss. *Plant Molecular Biology*. doi: 10.1007/s11103-021-01147-7
- Burkart, G. M., Baskin, T. I., & Bezanilla, M. (2015). A family of ROP proteins that suppresses actin dynamics, and is essential for polarized growth and cell adhesion. *Journal of Cell Science*, *128*(14), 2553–2564.
- Bürstenbinder, K., Savchenko, T., Müller, J., Adamson, A. W., Stamm, G., Kwong, R., Zipp, B. J., Dinesh, D. C., & Abel, S. (2013). Arabidopsis Calmodulin-binding Protein IQ67-Domain 1 Localizes to Microtubules and Interacts with Kinesin Light Chain-related Protein-1*. *The Journal of Biological Chemistry*, *288*(3), 1871–1882.
- Buschmann, H., Chan, J., Sanchez-Pulido, L., Andrade-Navarro, M. A., Doonan, J. H., & Lloyd, C. W. (2006). Microtubule-associated AIR9 recognizes the cortical division site at preprophase and cell-plate insertion. *Current Biology: CB*, *16*(19), 1938–1943.
- Buschmann, H., Dols, J., Kopischke, S., Peña, E. J., Andrade-Navarro, M. A., Heinlein, M., Szymanski, D. B., Zachgo, S., Doonan, J. H., & Lloyd, C. W. (2015). Arabidopsis KCBP interacts with AIR9 but stays in the cortical division zone throughout mitosis via its MyTH4-FERM domain. *Journal of Cell Science*, *128*(11), 2033–2046.
- Buschmann, H., Holtmannspötter, M., Borchers, A., O'Donoghue, M.-T., & Zachgo, S. (2016). Microtubule dynamics of the centrosome-like polar organizers from the basal land plant *Marchantia polymorpha*. *The New Phytologist*, *209*(3), 999–1013.
- Buschmann, H., & Müller, S. (2019). Update on plant cytokinesis: rule and divide. *Current Opinion in Plant Biology*, *52*, 97–105.
- Camilleri, C., Azimzadeh, J., Pastuglia, M., Bellini, C., Grandjean, O., & Bouchez, D. (2002). The Arabidopsis TONNEAU2 gene encodes a putative novel protein phosphatase 2A regulatory subunit essential for the control of the cortical cytoskeleton. *The Plant Cell*, *14*(4), 833–845.
- Campos, R., Goff, J., Rodriguez-Furlan, C., & Van Norman, J. M. (2020). The Arabidopsis Receptor Kinase IRK Is Polarized and Represses Specific Cell Divisions in Roots. *Developmental Cell*, *52*(2), 183–195.e4.
- Cartwright, H. N., Humphries, J. A., & Smith, L. G. (2009). PAN1: a receptor-like protein that promotes polarization of an asymmetric cell division in maize. *Science*, *323*(5914), 649–651.

- Chang-Jie, J., & Sonobe, S. (1993). Identification and preliminary characterization of a 65 kDa higher-plant microtubule-associated protein. *Journal of Cell Science*, 105 (Pt 4), 891–901.
- Chan, J., Calder, G., Fox, S., & Lloyd, C. (2005). Localization of the microtubule end binding protein EB1 reveals alternative pathways of spindle development in *Arabidopsis* suspension cells. *The Plant Cell*, 17(6), 1737–1748.
- Chen, C., Marcus, A., Li, W., Hu, Y., Calzada, J.-P. V., Grossniklaus, U., Cyr, R. J., & Ma, H. (2002). The *Arabidopsis* ATK1 gene is required for spindle morphogenesis in male meiosis. *Development*, 129(10), 2401–2409.
- Cheng, X., Mwaura, B. W., Chang Stauffer, S. R., & Bezanilla, M. (2020). A Fully Functional ROP Fluorescent Fusion Protein Reveals Roles for This GTPase in Subcellular and Tissue-Level Patterning. *The Plant Cell*, 32(11), 3436–3451.
- Chen, L. (2022). Emerging roles of protein phosphorylation in regulation of stomatal development. *Journal of Plant Physiology*, 280, 153882.
- Christensen, T. M., Vejlupkova, Z., Sharma, Y. K., Arthur, K. M., Spatafora, J. W., Albright, C. A., Meeley, R. B., Duvick, J. P., Quatrano, R. S., & Fowler, J. E. (2003a). Conserved Subgroups and Developmental Regulation in the Monocot *rop* Gene Family. In *Plant Physiology* (Vol. 133, Issue 4, pp. 1791–1808). doi: 10.1104/pp.103.029900
- Christensen, T. M., Vejlupkova, Z., Sharma, Y. K., Arthur, K. M., Spatafora, J. W., Albright, C. A., Meeley, R. B., Duvick, J. P., Quatrano, R. S., & Fowler, J. E. (2003b). Conserved subgroups and developmental regulation in the monocot *rop* gene family. *Plant Physiology*, 133(4), 1791–1808.
- Chugh, M., Reißner, M., Bugiel, M., Lipka, E., Herrmann, A., Roy, B., Müller, S., & Schäffer, E. (2018). Phragmoplast Orienting Kinesin 2 Is a Weak Motor Switching between Processive and Diffusive Modes. *Biophysical Journal*, 115(2), 375–385.
- Cleary, A. L., & Smith, L. G. (1998). The Tangled1 gene is required for spatial control of cytoskeletal arrays associated with cell division during maize leaf development. *The Plant Cell*, 10(11), 1875–1888.
- Colle, M., Weng, Y., Kang, Y., Ophir, R., Sherman, A., & Grumet, R. (2017). Variation in cucumber (*Cucumis sativus* L.) fruit size and shape results from multiple components acting pre-anthesis and post-pollination. *Planta*, 246(4), 641–658.
- Craddock, C., Lavagi, I., & Yang, Z. (2012). New insights into Rho signaling from plant ROP/Rac GTPases. *Trends in Cell Biology*, 22(9), 492–501.
- D'Ario, M., Tavares, R., Schiessl, K., Desvoyes, B., Gutierrez, C., Howard, M., & Sablowski, R. (2021). Cell size controlled in plants using DNA content as an internal scale. *Science*, 372(6547), 1176–1181.

- Dixit, R., & Cyr, R. (2004). The cortical microtubule array: from dynamics to organization. *The Plant Cell*, 16(10), 2546–2552.
- Djakovic, S., Dyachok, J., Burke, M., Frank, M. J., & Smith, L. G. (2006). BRICK1/HSPC300 functions with SCAR and the ARP2/3 complex to regulate epidermal cell shape in Arabidopsis. *Development*, 133(6), 1091–1100.
- Drevensek, S., Gousset, M., Duroc, Y., Christodoulidou, A., Steyaert, S., Schaefer, E., Duvernois, E., Grandjean, O., Vantard, M., Bouchez, D., & Pastuglia, M. (2012). The Arabidopsis TRM1-TON1 interaction reveals a recruitment network common to plant cortical microtubule arrays and eukaryotic centrosomes. *The Plant Cell*, 24(1), 178–191.
- Facette, M. R., Park, Y., Sutimantanapi, D., Luo, A., Cartwright, H. N., Yang, B., Bennett, E. J., Sylvester, A. W., & Smith, L. G. (2015). The SCAR/WAVE complex polarizes PAN receptors and promotes division asymmetry in maize. *Nature Plants*, 1, 14024.
- Facette, M. R., Rasmussen, C. G., & Van Norman, J. M. (2019). A plane choice: coordinating timing and orientation of cell division during plant development. *Current Opinion in Plant Biology*, 47, 47–55.
- Fowler, J. E. (2009). *Integrated G Proteins Signaling in Plants* (S. Yalovsky, F. Baluška, & A. Jones (eds.)). Springer Berlin Heidelberg.
- Frank, M. J., & Smith, L. G. (2002). A small, novel protein highly conserved in plants and animals promotes the polarized growth and division of maize leaf epidermal cells. *Current Biology: CB*, 12(10), 849–853.
- Frey, N., Klotz, J., & Nick, P. (2010). A kinesin with calponin-homology domain is involved in premitotic nuclear migration. *Journal of Experimental Botany*, 61(12), 3423–3437.
- Furt, F., Liu, Y.-C., Bibeau, J. P., Tüzel, E., & Vidali, L. (2013). Apical myosin XI anticipates F-actin during polarized growth of *Physcomitrella patens* cells. *The Plant Journal: For Cell and Molecular Biology*, 73(3), 417–428.
- Fu, Y., Gu, Y., Zheng, Z., Wasteneys, G., & Yang, Z. (2005). Arabidopsis interdigitating cell growth requires two antagonistic pathways with opposing action on cell morphogenesis. *Cell*, 120(5), 687–700.
- Galotto, G., Wisanpitayakorn, P., Bibeau, J. P., Liu, Y.-C., Furt, F., Pierce, E. C., Simpson, P. J., Tüzel, E., & Vidali, L. (2021). Myosin XI drives polarized growth by vesicle focusing and local enrichment of F-actin in *Physcomitrium patens*. *Plant Physiology*, 187(4), 2509–2529.
- Glanc, M. (2022). Plant cell division from the perspective of polarity. *Journal of Experimental Botany*, 73(16), 5361–5371.

- Goff, J., & Van Norman, J. M. (2021). Polarly localized receptor-like kinases PXC2 and IRK act redundantly during Arabidopsis root development in the radial axis. In bioRxiv (p. 2021.02.11.429611). doi: 10.1101/2021.02.11.429611
- Golomb, L., Abu-Abied, M., Belausov, E., & Sadot, E. (2008). Different subcellular localizations and functions of Arabidopsis myosin VIII. *BMC Plant Biology*, 8, 3.
- Gunning, B., & Sammut, M. (1990). Rearrangements of Microtubules Involved in Establishing Cell Division Planes Start Immediately after DNA Synthesis and Are Completed just before Mitosis. *The Plant Cell*, 2(12), 1273–1282.
- Guo, X., & Dong, J. (2022). Protein polarization: Spatiotemporal precisions in cell division and differentiation. *Current Opinion in Plant Biology*, 68, 102257.
- Gutierrez, C. (2022). A Journey to the Core of the Plant Cell Cycle. *International Journal of Molecular Sciences*, 23(15). doi: 10.3390/ijms23158154
- Gu, Y., & Rasmussen, C. G. (2022). Cell biology of primary cell wall synthesis in plants. *The Plant Cell*, 34(1), 103–128.
- Haraguchi, T., Ito, K., Duan, Z., Rula, S., Takahashi, K., Shibuya, Y., Hagino, N., Miyatake, Y., Nakano, A., & Tominaga, M. (2018). Functional Diversity of Class XI Myosins in Arabidopsis thaliana. *Plant & Cell Physiology*, 59(11), 2268–2277.
- Hashimoto, T. (2015). Microtubules in plants. *The Arabidopsis Book / American Society of Plant Biologists*, 13, e0179.
- Hasi, Q., & Kakimoto, T. (2022). ROP Interactive Partners are Involved in the Control of Cell Division Patterns in Arabidopsis Leaves. *Plant & Cell Physiology*, 63(8), 1130–1139.
- Herrmann, A., Livanos, P., Lipka, E., & Gadeyne, A. (2018). Dual localized kinesin-12 POK 2 plays multiple roles during cell division and interacts with MAP 65-3. *EMBO*. Retrieved from <https://www.embojournal.org/doi/abs/10.15252/embr.201846085>
- Herrmann, A., & Torii, K. U. (2021). Shouting out loud: signaling modules in the regulation of stomatal development. *Plant Physiology*, 185(3), 765–780.
- Higgins, D. M., Nannas, N. J., & Dawe, R. K. (2016). The Maize Divergent spindle-1 (dv1) Gene Encodes a Kinesin-14A Motor Protein Required for Meiotic Spindle Pole Organization. *Frontiers in Plant Science*, 7, 1277.
- Ho, C.-M. K., Hotta, T., Guo, F., Roberson, R. W., Lee, Y.-R. J., & Liu, B. (2011). Interaction of antiparallel microtubules in the phragmoplast is mediated by the microtubule-associated protein MAP65-3 in Arabidopsis. *The Plant Cell*, 23(8), 2909–2923.
- Ho, C.-M. K., Lee, Y.-R. J., Kiyama, L. D., Dinesh-Kumar, S. P., & Liu, B. (2012). Arabidopsis microtubule-associated protein MAP65-3 cross-links antiparallel microtubules toward their plus ends in the phragmoplast via its distinct C-terminal microtubule binding domain. *The Plant Cell*, 24(5), 2071–2085.

- Hotta, T., Lee, Y.-R. J., Higaki, T., Hashimoto, T., & Liu, B. (2022). Two Kinesin-14A Motors Oligomerize to Drive Poleward Microtubule Convergence for Acentrosomal Spindle Morphogenesis in *Arabidopsis thaliana*. *Frontiers in Cell and Developmental Biology*, *10*, 949345.
- Huang, C. H., Peng, F. L., Lee, Y.-R. J., & Liu, B. (2022). The microtubular preprophase band recruits Myosin XI to the division site for plant cytokinesis. In bioRxiv (p. 2022.11.08.515512). doi: 10.1101/2022.11.08.515512
- Humphries, J. A., Vejlupkova, Z., Luo, A., Meeley, R. B., Sylvester, A. W., Fowler, J. E., & Smith, L. G. (2011). ROP GTPases act with the receptor-like protein PAN1 to polarize asymmetric cell division in maize. *The Plant Cell*, *23*(6), 2273–2284.
- Hussey, P. J., Hawkins, T. J., Igarashi, H., Kaloriti, D., & Smertenko, A. (2002). The plant cytoskeleton: recent advances in the study of the plant microtubule-associated proteins MAP-65, MAP-190 and the *Xenopus* MAP215-like protein, MOR1. *Plant Molecular Biology*, *50*(6), 915–924.
- Hwang, J.-U., Vernoud, V., Szumlanski, A., Nielsen, E., & Yang, Z. (2008). A tip-localized RhoGAP controls cell polarity by globally inhibiting Rho GTPase at the cell apex. *Current Biology: CB*, *18*(24), 1907–1916.
- Ishikawa, M., Fujiwara, A., Kosetsu, K., Horiuchi, Y., Kamamoto, N., Umakawa, N., Tamada, Y., Zhang, L., Matsushita, K., Palfalvi, G., Nishiyama, T., Kitasaki, S., Masuda, Y., Shiroza, Y., Kitagawa, M., Nakamura, T., Cui, H., Hiwatashi, Y., Kabeya, Y., ... Kofuji, R. (2023). GRAS transcription factors regulate cell division planes in moss overriding the default rule. *Proceedings of the National Academy of Sciences*, *120*(4), e2210632120.
- Kastner, C., Wagner, V. C., Fratini, M., Dobritzsch, D., Fuszard, M., Heilmann, M., & Heilmann, I. (2022). The pollen-specific class VIII-myosin ATM2 from *Arabidopsis thaliana* associates with the plasma membrane through a polybasic region binding anionic phospholipids. *Biochimie*, *203*, 65–76.
- Kirik, A., Ehrhardt, D. W., & Kirik, V. (2012). TONNEAU2/FASS regulates the geometry of microtubule nucleation and cortical array organization in interphase *Arabidopsis* cells. *The Plant Cell*, *24*(3), 1158–1170.
- Kodama, Y., Suetsugu, N., Kong, S.-G., & Wada, M. (2010). Two interacting coiled-coil proteins, WEB1 and PMI2, maintain the chloroplast photorelocation movement velocity in *Arabidopsis*. *Proceedings of the National Academy of Sciences of the United States of America*, *107*(45), 19591–19596.
- Koizumi, K., Hayashi, T., & Gallagher, K. L. (2012). SCARECROW reinforces SHORT-ROOT signaling and inhibits periclinal cell divisions in the ground tissue by maintaining SHR at high levels in the endodermis. *Plant Signaling & Behavior*, *7*(12), 1573–1577.

- Komis, G., Luptovčiak, I., Ovečka, M., Samakovli, D., Šamajová, O., & Šamaj, J. (2017). Katanin Effects on Dynamics of Cortical Microtubules and Mitotic Arrays in *Arabidopsis thaliana* Revealed by Advanced Live-Cell Imaging. *Frontiers in Plant Science*, *8*, 866.
- Kosetsu, K., Murata, T., Yamada, M., Nishina, M., Boruc, J., Hasebe, M., Van Damme, D., & Goshima, G. (2017). Cytoplasmic MTOCs control spindle orientation for asymmetric cell division in plants. *Proceedings of the National Academy of Sciences of the United States of America*, *114*(42), E8847–E8854.
- Kozgunova, E., Yoshida, M. W., Reski, R., & Goshima, G. (2022). Spindle motility skews division site determination during asymmetric cell division in *Physcomitrella*. *Nature Communications*, *13*(1), 2488.
- Kumari, P., Dahiya, P., Livanos, P., Zergiebel, L., Kölling, M., Poeschl, Y., Stamm, G., Hermann, A., Abel, S., Müller, S., & Bürstenbinder, K. (2021). IQ67 DOMAIN proteins facilitate preprophase band formation and division-plane orientation. *Nature Plants*, *7*(6), 739–747.
- Laruelle, E., Belcram, K., Trubuil, A., Palauqui, J.-C., & Andrey, P. (2022). Large-scale analysis and computer modeling reveal hidden regularities behind variability of cell division patterns in *Arabidopsis thaliana* embryogenesis. *eLife*, *11*. doi: 10.7554/eLife.79224
- Láruson, Á. J., Yeaman, S., & Lotterhos, K. E. (2020). The Importance of Genetic Redundancy in Evolution. *Trends in Ecology & Evolution*, *35*(9), 809–822.
- Lauster, T., Stöckle, D., Gabor, K., Haller, T., Krieger, N., Lotz, P., Mayakrishnan, R., Späth, E., Zimmermann, S., Livanos, P., & Müller, S. (2022). *Arabidopsis* pavement cell shape formation involves spatially confined ROPGAP regulators. *Current Biology: CB*, *32*(3), 532–544.e7.
- Lavy, M., Bloch, D., Hazak, O., Gutman, I., Poraty, L., Sorek, N., Sternberg, H., & Yalovsky, S. (2007). A Novel ROP/RAC effector links cell polarity, root-meristem maintenance, and vesicle trafficking. *Current Biology: CB*, *17*(11), 947–952.
- Lazzaro, M. D., Wu, S., Snouffer, A., Wang, Y., & van der Knaap, E. (2018). Plant Organ Shapes Are Regulated by Protein Interactions and Associations With Microtubules. *Frontiers in Plant Science*, *9*, 1766.
- Lee, Y. K., Kim, G.-T., Kim, I.-J., Park, J., Kwak, S.-S., Choi, G., & Chung, W.-I. (2006). LONGIFOLIA1 and LONGIFOLIA2, two homologous genes, regulate longitudinal cell elongation in *Arabidopsis*. *Development*, *133*(21), 4305–4314.
- Lee, Y. K., Rhee, J. Y., Lee, S. H., Chung, G. C., Park, S. J., Segami, S., Maeshima, M., & Choi, G. (2018). Functionally redundant LNG3 and LNG4 genes regulate turgor-driven polar cell elongation through activation of XTH17 and XTH24. *Plant Molecular Biology*. doi: 10.1007/s11103-018-0722-0

- Lee, Y.-R. J., Hiwatashi, Y., Hotta, T., Xie, T., Doonan, J. H., & Liu, B. (2017). The Mitotic Function of Augmin Is Dependent on Its Microtubule-Associated Protein Subunit EDE1 in *Arabidopsis thaliana*. *Current Biology: CB*, 27(24), 3891–3897.e4.
- Lee, Y.-R. J., & Liu, B. (2019). Microtubule nucleation for the assembly of acentrosomal microtubule arrays in plant cells. *The New Phytologist*, 222(4), 1705–1718.
- Le, J., Mallery, E. L., Zhang, C., Brankle, S., & Szymanski, D. B. (2006). Arabidopsis BRICK1/HSPC300 is an essential WAVE-complex subunit that selectively stabilizes the Arp2/3 activator SCAR2. *Current Biology: CB*, 16(9), 895–901.
- Liang, H., Zhang, Y., Martinez, P., Rasmussen, C. G., Xu, T., & Yang, Z. (2018). The Microtubule-Associated Protein IQ67 DOMAIN5 Modulates Microtubule Dynamics and Pavement Cell Shape. *Plant Physiology*, 177(4), 1555–1568.
- Li, E., Zhang, Y.-L., Qin, Z., Xu, M., Qiao, Q., Li, S., Li, S.-W., & Zhang, Y. (2023). Signaling network controlling ROP-mediated tip growth in *Arabidopsis* and beyond. *Plant Communications*, 4(1), 100451.
- Li, H., Han, J., Chen, L., Han, N., Hu, Y., Ge, Q., Ren, Z., & Wang, L. (2022). Ectopic Expression of CsSUN in Tomato Results in Elongated Fruit Shape via Regulation of Longitudinal Cell Division. *International Journal of Molecular Sciences*, 23(17). doi: 10.3390/ijms23179973
- Li, H., Sun, B., Sasabe, M., Deng, X., Machida, Y., Lin, H., Julie Lee, Y.-R., & Liu, B. (2017). Arabidopsis MAP65-4 plays a role in phragmoplast microtubule organization and marks the cortical cell division site. *The New Phytologist*, 215(1), 187–201.
- Lipka, E., Gadeyne, A., Stöckle, D., Zimmermann, S., De Jaeger, G., Ehrhardt, D. W., Kirik, V., Van Damme, D., & Müller, S. (2014). The Phragmoplast-Orienting Kinesin-12 Class Proteins Translate the Positional Information of the Preprophase Band to Establish the Cortical Division Zone in *Arabidopsis thaliana*. *The Plant Cell*, 26(6), 2617–2632.
- Liu, B., & Lee, Y.-R. J. (2022). Spindle Assembly and Mitosis in Plants. *Annual Review of Plant Biology*, 73, 227–254.
- Liu, D., Sun, W., Yuan, Y., Zhang, N., Hayward, A., Liu, Y., & Wang, Y. (2014). Phylogenetic analyses provide the first insights into the evolution of OVATE family proteins in land plants. *Annals of Botany*, 113(7), 1219–1233.
- Liu, J., Van Eck, J., Cong, B., & Tanksley, S. D. (2002). A new class of regulatory genes underlying the cause of pear-shaped tomato fruit. *Proceedings of the National Academy of Sciences of the United States of America*, 99(20), 13302–13306.
- Liu, L., Zhou, J., & Pesacreta, T. C. (2001). Maize myosins: diversity, localization, and function. *Cell Motility and the Cytoskeleton*, 48(2), 130–148.
- Livanos, P., & Müller, S. (2019). Division Plane Establishment and Cytokinesis. *Annual Review of Plant Biology*, 70, 239–267.

- Li, Y., Deng, M., Liu, H., Li, Y., Chen, Y., Jia, M., Xue, H., Shao, J., Zhao, J., Qi, Y., An, L., Yu, F., & Liu, X. (2020). ABNORMAL SHOOT 6 interacts with KATANIN 1 and SHADE AVOIDANCE 4 to promote cortical microtubule severing and ordering in *Arabidopsis*. *Journal of Integrative Plant Biology*. doi: 10.1111/jipb.13003
- Li, Y., Huang, Y., Wen, Y., Wang, D., Liu, H., Li, Y., Zhao, J., An, L., Yu, F., & Liu, X. (2021). The domain of unknown function 4005 (DUF4005) in an *Arabidopsis* IQD protein functions in microtubule binding. *The Journal of Biological Chemistry*, 100849.
- Louveaux, M., Julien, J.-D., Mirabet, V., Boudaoud, A., & Hamant, O. (2016). Cell division plane orientation based on tensile stress in *Arabidopsis thaliana*. *Proceedings of the National Academy of Sciences of the United States of America*, 113(30), E4294–E4303.
- Lucas, J. R. (2021). Appearance of microtubules at the cytokinesis to interphase transition in *Arabidopsis thaliana*. *Cytoskeleton*, 78(7), 361–371.
- Lucas, J. R., & Shaw, S. L. (2012). MAP65-1 and MAP65-2 promote cell proliferation and axial growth in *Arabidopsis* roots. In *The Plant Journal* (p. no – no). doi: 10.1111/j.1365-313x.2012.05002.x
- Luesse, D. R., DeBlasio, S. L., & Hangarter, R. P. (2006). Plastid movement impaired 2, a new gene involved in normal blue-light-induced chloroplast movements in *Arabidopsis*. *Plant Physiology*, 141(4), 1328–1337.
- Madison, S. L., Buchanan, M. L., Glass, J. D., McClain, T. F., Park, E., & Nebenführ, A. (2015). Class XI Myosins Move Specific Organelles in Pollen Tubes and Are Required for Normal Fertility and Pollen Tube Growth in *Arabidopsis*. *Plant Physiology*, 169(3), 1946–1960.
- Marcus, A. I., Dixit, R., & Cyr, R. J. (2005). Narrowing of the preprophase microtubule band is not required for cell division plane determination in cultured plant cells. *Protoplasma*, 226(3-4), 169–174.
- Marcus, A. I., Li, W., Ma, H., & Cyr, R. J. (2003). A kinesin mutant with an atypical bipolar spindle undergoes normal mitosis. *Molecular Biology of the Cell*, 14(4), 1717–1726.
- Martinez, P., Allsman, L. A., Brakke, K. A., Hoyt, C., Hayes, J., Liang, H., Neher, W., Rui, Y., Roberts, A. M., Moradifam, A., Goldstein, B., Anderson, C. T., & Rasmussen, C. G. (2018). Predicting Division Planes of Three-Dimensional Cells by Soap-Film Minimization. *The Plant Cell*, 30(10), 2255–2266.
- Martinez, P., Dixit, R., Balkunde, R. S., Zhang, A., O’Leary, S. E., Brakke, K. A., & Rasmussen, C. G. (2020). TANGLED1 mediates microtubule interactions that may promote division plane positioning in maize. *The Journal of Cell Biology*, 219(8). doi: 10.1083/jcb.201907184

- Martinez, P., Luo, A., Sylvester, A., & Rasmussen, C. G. (2017). Proper division plane orientation and mitotic progression together allow normal growth of maize. *Proceedings of the National Academy of Sciences of the United States of America*, 114(10), 2759–2764.
- Máthé, C., Garda, T., Freytag, C., & M-Hamvas, M. (2019). The Role of Serine-Threonine Protein Phosphatase PP2A in Plant Oxidative Stress Signaling-Facts and Hypotheses. *International Journal of Molecular Sciences*, 20(12). doi: 10.3390/ijms20123028
- McClinton, R. S., & Sung, Z. R. (1997). Organization of cortical microtubules at the plasma membrane in Arabidopsis. *Planta*, 201(3), 252–260.
- Mills, A. M., Morris, V. H., & Rasmussen, C. G. (2022). Localization of PHRAGMOPLAST ORIENTING KINESIN1 at the division site depends on the microtubule binding proteins TANGLED1 and AUXIN-INDUCED IN ROOT CULTURES9 in Arabidopsis. *The Plant Cell*. doi: 10.1093/plcell/koac266
- Mills, A. M., & Rasmussen, C. G. (2022). Defects in division plane positioning in the root meristematic zone affect cell organization in the differentiation zone. *Journal of Cell Science*. doi: 10.1242/jcs.260127
- Mineyuki, Y. (1999). The Preprophase Band of Microtubules: Its Function as a Cytokinetic Apparatus in Higher Plants. In K. W. Jeon (Ed.), *International Review of Cytology* (Vol. 187, pp. 1–49). Academic Press.
- Mir, R., Morris, V. H., Buschmann, H., & Rasmussen, C. G. (2018). Division Plane Orientation Defects Revealed by a Synthetic Double Mutant Phenotype. *Plant Physiology*, 176(1), 418–431.
- Moody, L. A., Kelly, S., Clayton, R., Weeks, Z., Emms, D. M., & Langdale, J. A. (2021). NO GAMETOPHORES 2 Is a Novel Regulator of the 2D to 3D Growth Transition in the Moss *Physcomitrella patens*. *Current Biology: CB*, 31(3), 555–563.e4.
- Moukhtar, J., Trubuil, A., Belcram, K., Legland, D., Khadir, Z., Urbain, A., Palauqui, J.-C., & Andrey, P. (2019). Cell geometry determines symmetric and asymmetric division plane selection in Arabidopsis early embryos. *PLoS Computational Biology*, 15(2), e1006771.
- Müller, S., Han, S., & Smith, L. G. (2006). Two kinesins are involved in the spatial control of cytokinesis in Arabidopsis thaliana. *Current Biology: CB*, 16(9), 888–894.
- Müller, S., Smertenko, A., Wagner, V., Heinrich, M., Hussey, P. J., & Hauser, M.-T. (2004). The plant microtubule-associated protein AtMAP65-3/PLE is essential for cytokinetic phragmoplast function. *Current Biology: CB*, 14(5), 412–417.
- Muroyama, A., Gong, Y., & Bergmann, D. C. (2020). Opposing, Polarity-Driven Nuclear Migrations Underpin Asymmetric Divisions to Pattern Arabidopsis Stomata. *Current Biology: CB*. doi: 10.1016/j.cub.2020.08.100

- Nacry, P., Camilleri, C., Courtial, B., Caboche, M., & Bouchez, D. (1998). Major Chromosomal Rearrangements Induced by T-DNA Transformation in *Arabidopsis*. In *Genetics* (Vol. 149, Issue 2, pp. 641–650). doi: 10.1093/genetics/149.2.641
- Nagawa, S., Xu, T., & Yang, Z. (2010). RHO GTPase in plants: Conservation and invention of regulators and effectors. *Small GTPases*, 1(2), 78–88.
- Nakajima, K., Sena, G., Nawy, T., & Benfey, P. N. (2001). Intercellular movement of the putative transcription factor SHR in root patterning. *Nature*, 413(6853), 307–311.
- Nan, Q., Char, S. N., Yang, B., Bennett, E. J., Yang, B., & Facette, M. R. (2023). Polarly localized WPR proteins interact with PAN receptors and the actin cytoskeleton during maize stomatal development. *The Plant Cell*, 35(1), 469–487.
- Nan, Q., Liang, H., Mendoza, J., Liu, L., Fulzele, A., Wright, A., Bennett, E. J., Rasmussen, C. G., & Facette, M. R. (2021). The OPAQUE1/DISCORDIA2 myosin XI is required for phragmoplast guidance during asymmetric cell division in maize. In bioRxiv (p. 2021.08.29.458084). doi: 10.1101/2021.08.29.458084
- Nebenführ, A., & Dixit, R. (2018). Kinesins and Myosins: Molecular Motors that Coordinate Cellular Functions in Plants. *Annual Review of Plant Biology*, 69, 329–361.
- Nielsen, E. (2020). The Small GTPase Superfamily in Plants: A Conserved Regulatory Module with Novel Functions. *Annual Review of Plant Biology*, 71, 247–272.
- Oda, Y. (2015). Cortical microtubule rearrangements and cell wall patterning. *Frontiers in Plant Science*, 6, 236.
- Olatunji, D., Clark, N. M., & Kelley, D. R. (2022). The Class VIII myosin ATM1 is required for root apical meristem function. In bioRxiv (p. 2022.11.30.518567). doi: 10.1101/2022.11.30.518567
- Orr, R. G., Furt, F., Warner, E. L., Agar, E. M., Garbarino, J. M., Cabral, S. E., Dubuke, M. L., Butt, A. M., Munson, M., & Vidali, L. (2020). Rab-E and its interaction with myosin XI are essential for polarized cell growth. *The New Phytologist*. doi: 10.1111/nph.17023
- Ortiz-Ramírez, C., Guillotin, B., Xu, X., Rahni, R., Zhang, S., Yan, Z., Coqueiro Dias Araujo, P., Demesa-Arevalo, E., Lee, L., Van Eck, J., Gingeras, T. R., Jackson, D., Gallagher, K. L., & Birnbaum, K. D. (2021). Ground tissue circuitry regulates organ complexity in maize and *Setaria*. *Science*, 374(6572), 1247–1252.
- Otegui, M., & Staehelin, L. A. (2000). Cytokinesis in flowering plants: more than one way to divide a cell. *Current Opinion in Plant Biology*, 3(6), 493–502.
- Oud, J. L., & Nanninga, N. (1992). Cell shape, chromosome orientation and the position of the plane of division in *Vicia faba* root cortex cells. *Journal of Cell Science*, 103(3), 847–855.

- Ou, H., & Yi, P. (2022). ROP GTPase-dependent polarity establishment during tip growth in plants. *The New Phytologist*, 236(1), 49–57.
- Palevitz, B. A. (1986). Division plane determination in guard mother cells of *Allium*: Video time-lapse analysis of nuclear movements and phragmoplast rotation in the cortex. *Developmental Biology*, 117(2), 644–654.
- Panteris, E. (2008). Cortical actin filaments at the division site of mitotic plant cells: a reconsideration of the “actin-depleted zone.” *The New Phytologist*, 179(2), 334–341.
- Panteris, E., Apostolakos, P., & Galatis, B. (1995). Telophase-interphase transition in taxol-treated *Triticum* root cells: cortical microtubules appear without the prior presence of a radial perinuclear array. *Protoplasma*, 188(1), 78–84.
- Pickett-Heaps, J. D., & Northcote, D. H. (1966). Organization of microtubules and endoplasmic reticulum during mitosis and cytokinesis in wheat meristems. *Journal of Cell Science*, 1(1), 109–120.
- Pietra, S., Gustavsson, A., Kiefer, C., Kalmbach, L., Hörstedt, P., Ikeda, Y., Stepanova, A. N., Alonso, J. M., & Grebe, M. (2013). Arabidopsis SABRE and CLASP interact to stabilize cell division plane orientation and planar polarity. *Nature Communications*, 4, 2779.
- Pillitteri, L. J., Peterson, K. M., Horst, R. J., & Torii, K. U. (2011). Molecular profiling of stomatal meristemoids reveals new component of asymmetric cell division and commonalities among stem cell populations in *Arabidopsis*. *The Plant Cell*, 23(9), 3260–3275.
- Raissig, M. T., Matos, J. L., Gil, M. X. A., Kornfeld, A., Bettadapur, A., Abrash, E., Allison, H. R., Badgley, G., Vogel, J. P., Berry, J. A., & Bergmann, D. C. (2017). Mobile MUTE specifies subsidiary cells to build physiologically improved grass stomata. *Science*, 355(6330), 1215–1218.
- Rasmussen, C. G., & Bellinger, M. (2018). An overview of plant division-plane orientation. *The New Phytologist*. Retrieved from <https://nph.onlinelibrary.wiley.com/doi/abs/10.1111/nph.15183>
- Rasmussen, C. G., Sun, B., & Smith, L. G. (2011). Tangled localization at the cortical division site of plant cells occurs by several mechanisms. *Journal of Cell Science*, 124(Pt 2), 270–279.
- Rensing, S. A., Goffinet, B., Meyberg, R., Wu, S.-Z., & Bezanilla, M. (2020). The Moss *Physcomitrium* (*Physcomitrella*) patens: A Model Organism for Non-Seed Plants. *The Plant Cell*, 32(5), 1361–1376.

- Rong, D., Zhao, S., Tang, W., Luo, N., He, H., Wang, Z., Ma, H., Huang, Y., Yao, X., Pan, X., Lv, L., Xiao, J., Liu, R., Nagawa, S., & Yamamuro, C. (2022). ROP signaling regulates spatial pattern of cell division and specification of meristem notch. *Proceedings of the National Academy of Sciences of the United States of America*, *119*(47), e2117803119.
- Roszak, P., Heo, J.-O., Blob, B., Toyokura, K., Sugiyama, Y., de Luis Balaguer, M. A., Lau, W. W. Y., Hamey, F., Cirrone, J., Madej, E., Bouatta, A. M., Wang, X., Guichard, M., Ursache, R., Tavares, H., Verstaen, K., Wendrich, J., Melnyk, C. W., Oda, Y., ... Helariutta, Y. (2021). Cell-by-cell dissection of phloem development links a maturation gradient to cell specialization. *Science*, *374*(6575), eaba5531.
- Sakai, Y., Higaki, T., Ishizaki, K., Nishihama, R., Kohchi, T., & Hasezawa, S. (2022). Migration of prospindle before the first asymmetric division in germinating spore of *Marchantia polymorpha*. *Plant Biotechnology*, *39*(1), 5–12.
- Sano, T., Higaki, T., Oda, Y., Hayashi, T., & Hasezawa, S. (2005). Appearance of actin microfilament “twin peaks” in mitosis and their function in cell plate formation, as visualized in tobacco BY-2 cells expressing GFP-fimbrin. *The Plant Journal: For Cell and Molecular Biology*, *44*(4), 595–605.
- Sasabe, M., Kosetsu, K., Hidaka, M., Murase, A., & Machida, Y. (2011). Arabidopsis thaliana MAP65-1 and MAP65-2 function redundantly with MAP65-3/PLEIADE in cytokinesis downstream of MPK4. *Plant Signaling & Behavior*, *6*(5), 743–747.
- Sasabe, M., & Machida, Y. (2012). Regulation of organization and function of microtubules by the mitogen-activated protein kinase cascade during plant cytokinesis. *Cytoskeleton*, *69*(11), 913–918.
- Schaefer, E., Belcram, K., Uyttewaal, M., Duroc, Y., Goussot, M., Legland, D., Laruelle, E., de Tautzia-Moreau, M.-L., Pastuglia, M., & Bouchez, D. (2017). The preprophase band of microtubules controls the robustness of division orientation in plants. *Science*, *356*(6334), 186–189.
- Smertenko, A., Assaad, F., Baluška, F., Bezanilla, M., Buschmann, H., Drakakaki, G., Hauser, M.-T., Janson, M., Mineyuki, Y., Moore, I., Müller, S., Murata, T., Otegui, M. S., Panteris, E., Rasmussen, C., Schmit, A.-C., Šamaj, J., Samuels, L., Staehelin, L. A., ... Žárský, V. (2017). Plant Cytokinesis: Terminology for Structures and Processes. *Trends in Cell Biology*, *27*(12), 885–894.
- Smertenko, A., Hewitt, S. L., Jacques, C. N., Kacprzyk, R., Liu, Y., Marcec, M. J., Moyo, L., Ogden, A., Oung, H. M., Schmidt, S., & Serrano-Romero, E. A. (2018). Phragmoplast microtubule dynamics - a game of zones. *Journal of Cell Science*, *131*(2), jcs203331.
- Smertenko, A. P., Chang, H.-Y., Wagner, V., Kaloriti, D., Fenyk, S., Sonobe, S., Lloyd, C., Hauser, M.-T., & Hussey, P. J. (2004). The Arabidopsis microtubule-associated protein AtMAP65-1: molecular analysis of its microtubule bundling activity. *The Plant Cell*, *16*(8), 2035–2047.

- Smertenko, A. P., Kaloriti, D., Chang, H.-Y., Fiserova, J., Opatrny, Z., & Hussey, P. J. (2008). The C-terminal variable region specifies the dynamic properties of Arabidopsis microtubule-associated protein MAP65 isotypes. *The Plant Cell*, *20*(12), 3346–3358.
- Smith, L. G., Gerttula, S. M., Han, S., & Levy, J. (2001). Tangled1: a microtubule binding protein required for the spatial control of cytokinesis in maize. *The Journal of Cell Biology*, *152*(1), 231–236.
- Smith, L. G., Hake, S., & Sylvester, A. W. (1996). The tangled-1 mutation alters cell division orientations throughout maize leaf development without altering leaf shape. *Development*, *122*(2), 481–489.
- Snouffer, A., Kraus, C., & van der Knaap, E. (2019). The shape of things to come: ovate family proteins regulate plant organ shape. *Current Opinion in Plant Biology*, *53*, 98–105.
- Spinner, L., Gadeyne, A., Belcram, K., Gousso, M., Moison, M., Duroc, Y., Eeckhout, D., De Winne, N., Schaefer, E., Van De Slijke, E., Persiau, G., Witters, E., Gevaert, K., De Jaeger, G., Bouchez, D., Van Damme, D., & Pastuglia, M. (2013). A protein phosphatase 2A complex spatially controls plant cell division. *Nature Communications*, *4*, 1863.
- Spinner, L., Pastuglia, M., Belcram, K., Pegoraro, M., Gousso, M., Bouchez, D., & Schaefer, D. G. (2010). The function of TONNEAU1 in moss reveals ancient mechanisms of division plane specification and cell elongation in land plants. *Development*, *137*(16), 2733–2742.
- Stöckle, D., Herrmann, A., Lipka, E., Lauster, T., Gavidia, R., Zimmermann, S., & Müller, S. (2016). Putative RopGAPs impact division plane selection and interact with kinesin-12 POK1. *Nature Plants*, *2*, 16120.
- Suetsugu, N., & Wada, M. (2017). Two Coiled-Coil Proteins, WEB1 and PMI2, Suppress the Signaling Pathway of Chloroplast Accumulation Response that Is Mediated by Two Phototropin-Interacting Proteins, RPT2 and NCH1, in Seed Plants. *International Journal of Molecular Sciences*, *18*(7). doi: 10.3390/ijms18071469
- Sun, H., Furt, F., & Vidali, L. (2018). Myosin XI localizes at the mitotic spindle and along the cell plate during plant cell division in *Physcomitrella patens*. *Biochemical and Biophysical Research Communications*, *506*(2), 409–421.
- Su, S.-H., & Krysan, P. J. (2016). A double-mutant collection targeting MAP kinase related genes in Arabidopsis for studying genetic interactions. *The Plant Journal: For Cell and Molecular Biology*, *88*(5), 867–878.
- Tamura, K., Iwabuchi, K., Fukao, Y., Kondo, M., Okamoto, K., Ueda, H., Nishimura, M., & Hara-Nishimura, I. (2013). Myosin XI-i links the nuclear membrane to the cytoskeleton to control nuclear movement and shape in Arabidopsis. *Current Biology: CB*, *23*(18), 1776–1781.

- Tominaga, M., & Nakano, A. (2012). Plant-Specific Myosin XI, a Molecular Perspective. *Frontiers in Plant Science*, 3, 211.
- Tong, A. H., Evangelista, M., Parsons, A. B., Xu, H., Bader, G. D., Pagé, N., Robinson, M., Raghbizadeh, S., Hogue, C. W., Bussey, H., Andrews, B., Tyers, M., & Boone, C. (2001). Systematic genetic analysis with ordered arrays of yeast deletion mutants. *Science*, 294(5550), 2364–2368.
- Torres-Ruiz, R. A., & Jürgens, G. (1994). Mutations in the FASS gene uncouple pattern formation and morphogenesis in Arabidopsis development. *Development*, 120(10), 2967–2978.
- Traas, J., Bellini, C., Nacry, P., Kronenberger, J., Bouchez, D., & Caboche, M. (1995). Normal differentiation patterns in plants lacking microtubular preprophase bands. *Nature*, 375(6533), 676.
- Tulin, A., McClerklin, S., Huang, Y., & Dixit, R. (2012). Single-molecule analysis of the microtubule cross-linking protein MAP65-1 reveals a molecular mechanism for contact-angle-dependent microtubule bundling. *Biophysical Journal*, 102(4), 802–809.
- Turk, A. A., & Wisinski, K. B. (2018). PARP inhibitors in breast cancer: Bringing synthetic lethality to the bedside. *Cancer*, 124(12), 2498–2506.
- Vaddepalli, P., de Zeeuw, T., Strauss, S., Bürstenbinder, K., Liao, C.-Y., Ramalho, J. J., Smith, R. S., & Weijers, D. (2021). Auxin-dependent control of cytoskeleton and cell shape regulates division orientation in the Arabidopsis embryo. *Current Biology: CB*, 31(22), 4946–4955.e4.
- Van Damme, D., Van Poucke, K., Boutant, E., Ritzenthaler, C., Inzé, D., & Geelen, D. (2004). In vivo dynamics and differential microtubule-binding activities of MAP65 proteins. *Plant Physiology*, 136(4), 3956–3967.
- Van Damme, D., Vanstraelen, M., & Geelen, D. (2007). Cortical division zone establishment in plant cells. *Trends in Plant Science*, 12(10), 458–464.
- van der Knaap, E., Chakrabarti, M., Chu, Y. H., Clevenger, J. P., Illa-Berenguer, E., Huang, Z., Keyhaninejad, N., Mu, Q., Sun, L., Wang, Y., & Wu, S. (2014). What lies beyond the eye: the molecular mechanisms regulating tomato fruit weight and shape. *Frontiers in Plant Science*, 5, 227.
- Vos, J. W., Dogterom, M., & Emons, A. M. C. (2004). Microtubules become more dynamic but not shorter during preprophase band formation: a possible “search-and-capture” mechanism for microtubule translocation. *Cell Motility and the Cytoskeleton*, 57(4), 246–258.
- Walker, K. L., Müller, S., Moss, D., Ehrhardt, D. W., & Smith, L. G. (2007). Arabidopsis TANGLED identifies the division plane throughout mitosis and cytokinesis. *Current Biology: CB*, 17(21), 1827–1836.

- Wang, G., Wang, F., Wang, G., Wang, F., Zhang, X., Zhong, M., Zhang, J., Lin, D., Tang, Y., Xu, Z., & Song, R. (2012). Opaque1 encodes a myosin XI motor protein that is required for endoplasmic reticulum motility and protein body formation in maize endosperm. *The Plant Cell*, *24*(8), 3447–3462.
- Wang, Q., Fan, J., Cong, J., Chen, M., Qiu, J., Liu, J., Zhao, X., Huang, R., Liu, H., & Huang, X. (2023). Natural variation of ZmLNG1 alters organ shapes in maize. *The New Phytologist*, *237*(2), 471–482.
- Wang, S., Chang, Y., Guo, J., Zeng, Q., Ellis, B. E., & Chen, J.-G. (2011). Arabidopsis ovate family proteins, a novel transcriptional repressor family, control multiple aspects of plant growth and development. *PLoS One*, *6*(8), e23896.
- Weiss, J. D., McVey, S. L., Stinebaugh, S. E., Sullivan, C. F., Dawe, R. K., & Nannas, N. J. (2022). Frequent Spindle Assembly Errors Require Structural Rearrangement to Complete Meiosis in *Zea mays*. *International Journal of Molecular Sciences*, *23*(8). doi: 10.3390/ijms23084293
- Wick, S. M. (1985). Immunofluorescence microscopy of tubulin and microtubule arrays in plant cells. III. Transition between mitotic/cytokinetic and interphase microtubule arrays. *Cell Biology International Reports*, *9*(4), 357–371.
- Wright, A. J., Gallagher, K., & Smith, L. G. (2009). discordia1 and alternative discordia1 function redundantly at the cortical division site to promote preprophase band formation and orient division planes in maize. *The Plant Cell*, *21*(1), 234–247.
- Wu, G., Gu, Y., Li, S., & Yang, Z. (2001). A genome-wide analysis of Arabidopsis Rop-interactive CRIB motif-containing proteins that act as Rop GTPase targets. *The Plant Cell*, *13*(12), 2841–2856.
- Wu, S.-Z., & Bezanilla, M. (2014). Myosin VIII associates with microtubule ends and together with actin plays a role in guiding plant cell division. *eLife*, *3*, e03498.
- Wu, S., Zhang, B., Keyhaninejad, N., Rodríguez, G. R., Kim, H. J., Chakrabarti, M., Illa-Berenguer, E., Taitano, N. K., Gonzalo, M. J., Díaz, A., Pan, Y., Leisner, C. P., Halterman, D., Buell, C. R., Weng, Y., Jansky, S. H., van Eck, H., Willemsen, J., Monforte, A. J., ... van der Knaap, E. (2018). A common genetic mechanism underlies morphological diversity in fruits and other plant organs. *Nature Communications*, *9*(1), 4734.
- Wu, S.-Z., Ritchie, J. A., Pan, A.-H., Quatrano, R. S., & Bezanilla, M. (2011). Myosin VIII regulates protonemal patterning and developmental timing in the moss *Physcomitrella patens*. *Molecular Plant*, *4*(5), 909–921.
- Xu, X. M., Zhao, Q., Rodrigo-Peirís, T., Brkljacic, J., He, C. S., Müller, S., & Meier, I. (2008). RanGAP1 is a continuous marker of the Arabidopsis cell division plane. *Proceedings of the National Academy of Sciences of the United States of America*, *105*(47), 18637–18642.

- Yang, B., Stamm, G., Bürstenbinder, K., & Voiniciuc, C. (2022). Microtubule-associated IQD9 orchestrates cellulose patterning in seed mucilage. *The New Phytologist*, 235(3), 1096–1110.
- Yang, C., Ma, Y., He, Y., Tian, Z., & Li, J. (2018). OsOFP19 modulates plant architecture by integrating the cell division pattern and brassinosteroid signaling. *The Plant Journal: For Cell and Molecular Biology*, 93(3), 489–501.
- Yang, Z. (2002). Small GTPases: versatile signaling switches in plants. *The Plant Cell*, 14 Suppl(Suppl), S375–S388.
- Yang, Z. (2008). Cell polarity signaling in Arabidopsis. *Annual Review of Cell and Developmental Biology*, 24, 551–575.
- Yi, P., & Goshima, G. (2020). Rho of Plants GTPases and Cytoskeletal Elements Control Nuclear Positioning and Asymmetric Cell Division during *Physcomitrella patens* Branching. *Current Biology: CB*. doi: 10.1016/j.cub.2020.05.022
- Yi, P., & Goshima, G. (2022). Division site determination during asymmetric cell division in plants. *The Plant Cell*, 34(6), 2120–2139.
- Yoon, J.-T., Ahn, H.-K., & Pai, H.-S. (2018). The subfamily II catalytic subunits of protein phosphatase 2A (PP2A) are involved in cortical microtubule organization. *Planta*, 248(6), 1551–1567.
- Yue, K., Sandal, P., Williams, E. L., Murphy, E., Stes, E., Nikonorova, N., Ramakrishna, P., Czyzewicz, N., Montero-Morales, L., Kumpf, R., Lin, Z., van de Cotte, B., Iqbal, M., Van Bel, M., Van De Slijke, E., Meyer, M. R., Gadeyne, A., Zipfel, C., De Jaeger, G., ... De Smet, I. (2016). PP2A-3 interacts with ACR4 and regulates formative cell division in the Arabidopsis root. *Proceedings of the National Academy of Sciences of the United States of America*, 113(5), 1447–1452.
- Zhang, C., Lauster, T., Tang, W., Houbaert, A., Zhu, S., Eeckhout, D., De Smet, I., De Jaeger, G., Jacobs, T. B., Xu, T., Müller, S., & Russinova, E. (2022). ROPGAP-dependent interaction between brassinosteroid and ROP2-GTPase signaling controls pavement cell shape in Arabidopsis. *Current Biology: CB*, 32(3), 518–531.e6.
- Zhang, D., Spiegelhalder, R. P., Abrash, E. B., Nunes, T. D. G., Hidalgo, I., Anleu Gil, M. X., Jesenofsky, B., Lindner, H., Bergmann, D. C., & Raissig, M. T. (2022). Opposite polarity programs regulate asymmetric subsidiary cell divisions in grasses. *eLife*, 11. doi: 10.7554/eLife.79913
- Zhang, H., & Dawe, R. K. (2011). Mechanisms of plant spindle formation. *Chromosome Research: An International Journal on the Molecular, Supramolecular and Evolutionary Aspects of Chromosome Biology*, 19(3), 335–344.
- Zhang, L., & Ambrose, C. (2022). CLASP balances two competing cell division plane cues during leaf development. *Nature Plants*. doi: 10.1038/s41477-022-01163-5

- Zhang, X., Facette, M., Humphries, J. A., Shen, Z., Park, Y., Sutimantanapi, D., Sylvester, A. W., Briggs, S. P., & Smith, L. G. (2012). Identification of PAN2 by Quantitative Proteomics as a Leucine-Rich Repeat–Receptor-Like Kinase Acting Upstream of PAN1 to Polarize Cell Division in Maize. *The Plant Cell*, *24*(11), 4577–4589.
- Zhang, X., Wu, J., Yu, Q., Liu, R., Wang, Z.-Y., & Sun, Y. (2020). AtOFPs regulate cell elongation by modulating microtubule orientation via direct interaction with TONNEAU2. *Plant Science: An International Journal of Experimental Plant Biology*, *292*, 110405.
- Zhang, Y., Iakovidis, M., & Costa, S. (2016). Control of patterns of symmetric cell division in the epidermal and cortical tissues of the Arabidopsis root. *Development*, *143*(6), 978–982.
- Zhang, Y., Xu, T., & Dong, J. (2023). Asymmetric cell division in plant development. *Journal of Integrative Plant Biology*, *65*(2), 343–370.
- Zhao, D.-S., Li, Q.-F., Zhang, C.-Q., Zhang, C., Yang, Q.-Q., Pan, L.-X., Ren, X.-Y., Lu, J., Gu, M.-H., & Liu, Q.-Q. (2018). GS9 acts as a transcriptional activator to regulate rice grain shape and appearance quality. *Nature Communications*, *9*(1), 1240.
- Zhou, H.-W., Nussbaumer, C., Chao, Y., & DeLong, A. (2004). Disparate roles for the regulatory A subunit isoforms in Arabidopsis protein phosphatase 2A. *The Plant Cell*, *16*(3), 709–722.
- Zhou, X., Groves, N. R., & Meier, I. (2015). Plant nuclear shape is independently determined by the SUN-WIP-WIT2-myosin XI-i complex and CRWN1. *Nucleus*, *6*(2), 144–153.
- Zinovyev, A., Kuperstein, I., Barillot, E., & Heyer, W.-D. (2013). Synthetic lethality between gene defects affecting a single non-essential molecular pathway with reversible steps. *PLoS Computational Biology*, *9*(4), e1003016.

CHAPTER 2:
CORTICAL MICROTUBULES CONTRIBUTE TO DIVISION PLANE POSITIONING
DURING TELOPHASE IN MAIZE

Marschal A. Bellinger^{1,2 †}, Aimee N. Uyehara^{1,2}, Lindy Allsman², Pablo Martinez^{3, ‡},
Michael C. McCarthy⁴, and Carolyn G. Rasmussen^{2,3*}

¹ Co-first authors, equal contribution

²Department of Botany and Plant Sciences, Center for Plant Cell Biology, Institute for Integrative Genome Biology, University of California, Riverside, CA, USA.

[†]Current Address: White Rabbit Group, Seattle, WA, USA.

³Biochemistry Graduate Group, University of California, Riverside, USA.

[‡]Current Address: Fulgent Genetics, El Monte, CA USA.

⁴Radical Research, LLC, Riverside CA, USA.

*Correspondence to: crasmu@ucr.edu

Short title: Cortical microtubules promote division positioning Cortical microtubules position divisions

One sentence summary: Microtubules accumulate at the cell cortex during telophase and interact with the plant division machinery to direct its movement towards the division site.

ABSTRACT

Cell divisions are accurately positioned to generate cells of the correct size and shape. In plant cells, the new cell wall is built in the middle of the cell by vesicles trafficked along an antiparallel microtubule and a microfilament array called the phragmoplast. The phragmoplast expands towards a specific location at the cell cortex called the division site, but how it accurately reaches the division site is unclear. We observed microtubule arrays that accumulate at the cell cortex during the telophase transition in maize (*Zea mays*) leaf epidermal cells. Before the phragmoplast reaches the cell cortex, these cortical-telophase microtubules transiently interact with the division site. Increased microtubule plus-end capture and pausing occur when microtubules contact the division site-localized protein TANGLED1 or other closely associated proteins. Microtubule capture and pausing align the cortical microtubules perpendicular to the division site during telophase. Once the phragmoplast reaches the cell cortex, cortical-telophase microtubules are incorporated into the phragmoplast primarily by parallel bundling. The addition of microtubules into the phragmoplast promotes fine-tuning of the positioning at the division site. Our hypothesis is that division site-localized proteins such as TANGLED1 organize cortical microtubules during telophase to mediate phragmoplast positioning at the final division plane.

IN A NUTSHELL

Background: Both cell division and proper orientation of the division are important for plant development and growth. Cell division is initiated in the middle of the cell by a structure called the phragmoplast. The phragmoplast is composed of filaments including microtubules and it expands outwards to form the new cell wall. Phragmoplast positioning is mediated by proteins that localize in a ring at the future division location or division site. It is not known how these proteins promote division positioning.

Question: How do proteins at the division site contribute to the phragmoplast reaching the correct location?

Findings: We propose a potential mechanism linking phragmoplast positioning with division site localized proteins using maize epidermal cells expressing a live-cell microtubule marker. We discovered that an extensive network of microtubule filaments accumulates at the cell periphery and are captured at the division site by a microtubule binding protein called TANGLED1, leading to microtubules that are oriented perpendicular to the division site. Pre-oriented microtubules are added into the phragmoplast as it reaches the cell periphery to accurately direct the movement of the phragmoplast.

Next steps: Whether microtubules participate in division positioning and how TANGLED1 might modulate their dynamics in other plant cells is not yet known.

INTRODUCTION

Cell division in plants occurs via the transport of vesicles along an antiparallel microtubule array called the phragmoplast to build a new cell wall (Smertenko et al., 2017). The phragmoplast grows towards the cell cortex via microtubule nucleation on pre-existing phragmoplast microtubules. Microtubule-dependent microtubule nucleation on the phragmoplast is mediated by gamma-tubulin and augmin-complex proteins (Murata et al., 2013; Lee et al., 2017; Lee and Liu, 2019; Hotta et al., 2012; Nakaoka et al., 2012). Microtubule bundling in the phragmoplast may be mediated by MICROTUBULE ORGANIZATION 1 (MOR1)/TMBP200/GEM1, which localizes to the phragmoplast and also crosslinks microtubules in vitro (Yasuhara et al., 2002; Hamada et al., 2004). This activity is consistent with its role in rapid phragmoplast expansion, as demonstrated by quantitative live-cell imaging (Kawamura et al., 2006). In addition to nucleation and bundling, microtubule disassembly at the phragmoplast lagging edge also promotes phragmoplast expansion. Mitogen Activated Protein Kinase (MAPK) phosphorylates MAP65-1, which in turn reduces the microtubule bundling efficiency of MAP65-1. MAP65-1 phosphorylation allows lagging edge microtubules to disassemble, thereby promoting phragmoplast expansion (Sasabe et al., 2006; Sasabe and Machida, 2012). MAP65-1 is also phosphorylated by alpha Aurora Kinase, which similarly promotes timely phragmoplast expansion (Boruc et al., 2016). PHRAGMOPLAST ORIENTING KINESIN2 (POK2) promotes timely phragmoplast expansion, possibly through interaction with the phragmoplast midzone crosslinker MAP65-3 (Herrmann et al. 2018).

Although there has been progress in identifying factors that mediate phragmoplast expansion, how the phragmoplast is directed towards a specific cortical location, called the division site, is still unknown (Livanos and Müller, 2019; Rasmussen and Bellinger, 2018). In land plants, the location of the future division site can be accurately predicted by a microtubule and microfilament structure that assembles during the G2 phase of the cell cycle at the cell cortex called the preprophase band (PPB). Several proteins co-localize with the PPB and remain at the division site until division is completed. These division-site-localized proteins promote phragmoplast guidance to the division site: phragmoplasts in mutant cells often do not return to the division site (Müller et al., 2006; Martinez et al., 2017; Cleary and Smith, 1998). Several division-site-localized proteins are microtubule- or microfilament-bundling or motor proteins (Wu and Bezanilla, 2014; Müller et al., 2006; Hermann et al., 2018; Martinez et al., 2020), suggesting that division site positioning may be mediated by local alterations in cytoskeletal dynamics.

Current models of division plane positioning propose that division-site and phragmoplast-localized proteins pull or push cytoskeletal filaments within the phragmoplast to guide it to the division site. More specifically, these models propose that microtubules attached to and nucleated from the phragmoplast (peripheral microtubules) interact with division-site-localized proteins such as the PHRAGMOPLAST ORIENTING KINESIN2 (POK2) or MYOSINVIII (Chugh et al., 2018; Wu and Bezanilla, 2014). A proposed function of POK2, a microtubule plus-end directed kinesin, is to bind peripheral microtubules and, through plus-end directed movement, push them away from the division site, thereby positioning the phragmoplast (Chugh et al., 2018). MYOSINVIII, a division site-localized protein that also localizes to the plus ends of peripheral phragmoplast microtubules, mediates an interaction between microtubules and actin

filaments to guide the phragmoplast to the division site (Wu and Bezanilla, 2014). The microtubule-binding protein TANGLED1 (TAN1) localizes to the division site in maize (*Zea mays*) and Arabidopsis (*Arabidopsis thaliana*) (Walker et al., 2007; Martinez et al., 2017). In vitro, TAN1 bundles and promotes transient microtubule capture and crosslinking. Furthermore, it co-localizes with a small population of phragmoplast microtubules at the division site in vivo and promotes timely phragmoplast expansion (Martinez et al., 2017; Martinez et al., 2020). Maize *tan1* mutants have defects in phragmoplast guidance to the division site, indicating that TAN1 contributes to positioning the phragmoplast, but the underlying mechanisms are not yet clear (Cleary and Smith, 1998; Martinez et al., 2017).

The plant cell at telophase has often been considered devoid of microtubules outside of the phragmoplast (Smertenko et al., 2017). However, many reports indicate that both microtubules and microtubule nucleators such as gamma tubulin are present at the cell cortex during telophase in monocots, dicots, ferns, and moss (Kong et al., 2010; Liu et al., 1995; Wick, 1985; Panteris et al., 1995; Wu and Bezanilla, 2014; Gunning et al., 1978). Additionally, in dicots, microtubules nucleated from the nuclear envelope in late telophase contact the cell cortex but their function was not described (Van Damme and Geelen, 2008; Chan et al., 2005). More recently, cortical microtubules were shown to accumulate independently of the nuclear envelope in Arabidopsis during late telophase (Lucas, 2021). A previously proposed function of cortical-telophase microtubules is to repopulate the cortex for microtubule reorganization during G1 (Flanders et al., 1990).

Here we demonstrate that cortical microtubules are organized by a transient interaction with the division site, specifically near TAN1 puncta, in maize during telophase. This

interaction may be directly mediated by the division site-localized protein TAN1. The cortical-telophase microtubules are pre-arranged via interactions with TAN1 or other nearby proteins at the division site. Cortical-telophase microtubules are then added by parallel bundling into the phragmoplast at the cortex. Therefore, cortical-telophase microtubules direct the movement of the phragmoplast towards the division site in maize cells.

RESULTS

Analysis of cortical microtubule accumulation and orientation during telophase

Live-cell imaging of symmetrically dividing maize leaf epidermal cells revealed an unexpected population of cell-cortex-localized microtubules that typically accumulated during telophase ($n = 45/49$ cells) (Figure 2.1A, 2.1B, Supplemental Figure S2.1A, B). Cortical microtubules were sparse or nonexistent during metaphase (10% $n = 2/20$ cells from 8 plants, Supplemental Figure S2.1G, S2.1H) and anaphase (0% $n = 0/8$ cells from 8 plants). These cortical-telophase microtubules were spatially distinct from the phragmoplast and accumulated before the phragmoplast reached the cortex, as shown by time lapse imaging (Figure 2.1A, and 2.1B). We measured the density of cortical-telophase microtubules using the BoneJ plug-in in ImageJ (Doube et al., 2010), as described in the Materials and Methods section. Using confocal z-stacks with 0.5 μm resolution, we observed that the cortical-telophase array started to accumulate when the phragmoplast was as far as 3 to 4.5 microns away from the cell cortex (5% density, $n = 2$ cells). When the phragmoplast was between 0.5 and 1.5 microns from the cell cortex, the cortical-telophase array covered 33% of the cortex ($n = 6$ cells, standard error (SE) $\pm 7\%$). The density of the cortical-telophase microtubules increased as the leading edge of

the phragmoplast neared the cell cortex. The density of the cortical-telophase array when the phragmoplast touched the cortex was 39% (n= 24 cells, SE \pm 4%, from 12 plants). Together, these results indicate that cortical-telophase microtubules accumulate during telophase but before the phragmoplast reaches the cortex.

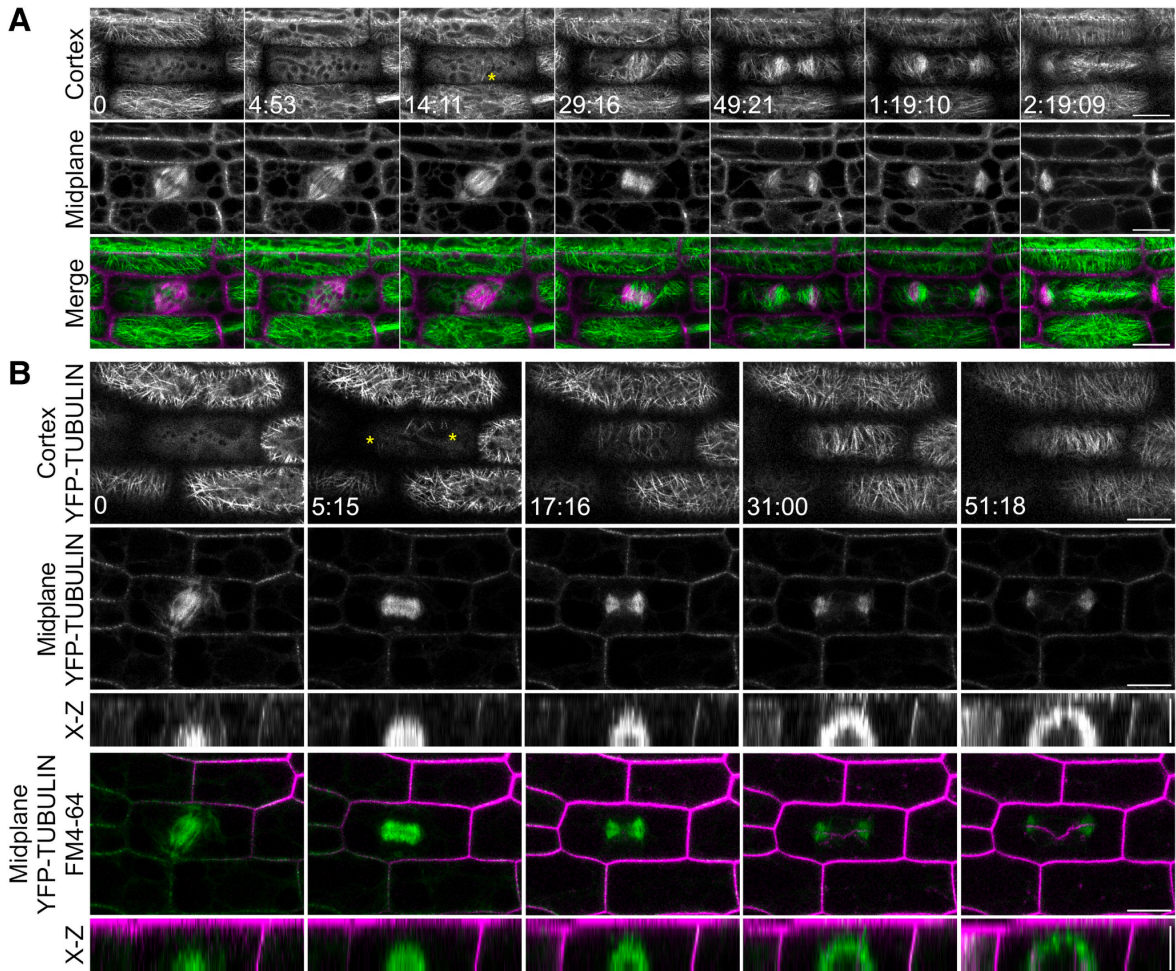
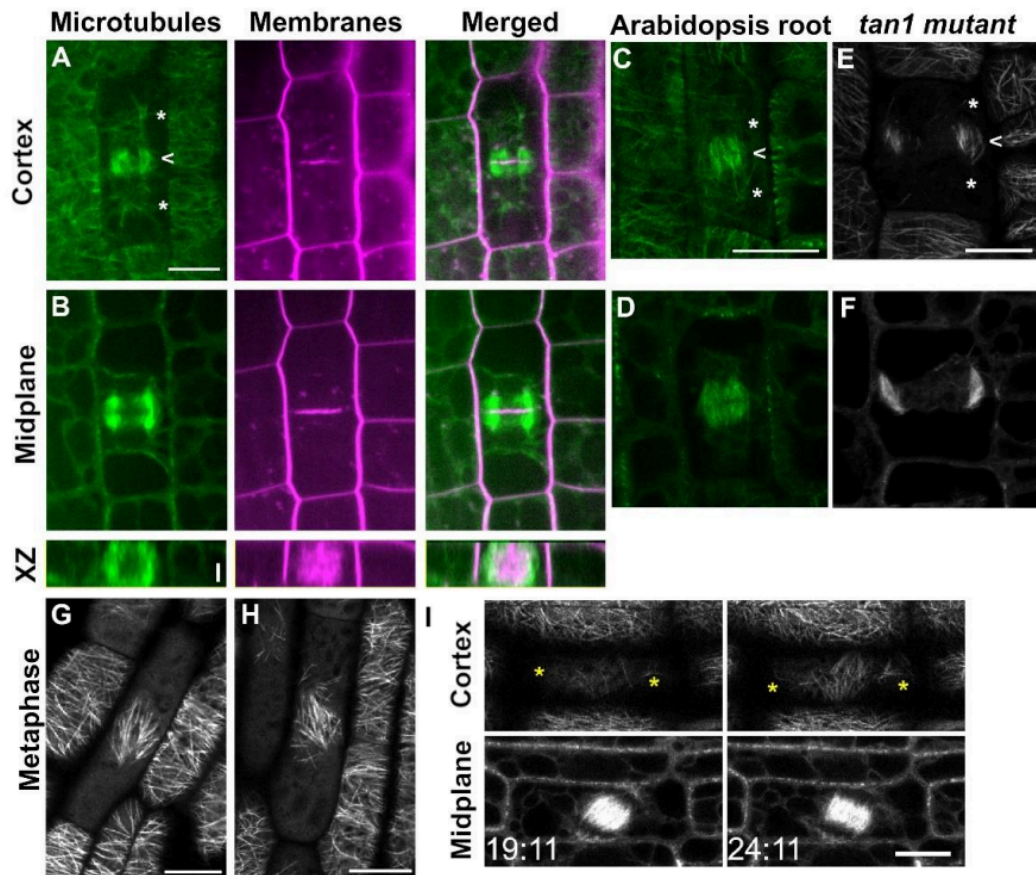


Figure 2.1 Cortical-telophase microtubules accumulate at the cortex before the phragmoplast contacts the cortex in wild-type maize epidermal cells.

Times are indicated in hours:minutes:seconds at the bottom left corner. A) Timelapse imaging of a cell expressing YFP-TUBULIN from metaphase to telophase. Microtubules at the cortex (top panel), microtubules at the midplane (middle panel), and merged images (cortex: green, and midplane: magenta; bottom panel) are shown. Cortical-telophase microtubules faintly accumulate at 14:11, with more accumulating by 29:16; additional intermediary timepoints shown in Supplementary Figure S2.1. B) Timelapse imaging of microtubules from anaphase to telophase. Merged images (cortex: green, and cell plate and plasma membrane dyed with FM-4-64: magenta). X-Z projections show that the cortical telophase arrays accumulate before the phragmoplast reaches the cell cortex. Bar is 10 μm for X-Y images and $\sim 10 \mu\text{m}$ for the X-Z projection (estimated due to sample drift). Images were acquired using a Zeiss LSM 880 equipped with Airyscan at 100x (NA=1.46).



Supplemental Figure S2.1. Cortical-telophase microtubules in wild-type maize epidermal cells, Arabidopsis root cells, and very sparse cortical-telophase microtubules in maize *tan1* mutant epidermal cells.

Supports Figure 2.1 and Figure 2.2. Microtubules are labeled with YFP-TUBULIN in green, membranes are labeled with FM4-64 in magenta. Cortical telophase microtubules (asterisks) were distinct from phragmoplast microtubules (arrowhead). A) A single Z-slice of the cortex of a maize epidermal cell in telophase surrounded by interphase cells. The phragmoplast has already reached the cortex in the middle of the cell (arrowhead) but has not reached the edges. The cortical-telophase microtubules are indicated with asterisks. B) Midplane indicates the middle of the cell. XZ image is a rotated projection along the XZ axis of the phragmoplast, scale bar is 5 μm . C) Single Z-slice showing the cortex and corresponding cortical telophase microtubules (asterisks) in *A. thaliana* root cell with a phragmoplast that has already reached the cortex (arrowhead). D) Typical mid-plane view of the phragmoplast. E) Maize *tan1* mutant epidermal cells have sparse or no cortical microtubules. Single Z-slice showing the cortex and sparse cortical-telophase microtubules (asterisks), with a phragmoplast that already reached the cortex (arrowhead). F) Typical mid-plane view of a *tan1* mutant phragmoplast. G) Single Z-slice of the cell cortex of a maize cell in metaphase shows no independent cortical microtubules, microtubules are associated with the spindle. H) Single Z-slice of the cell cortex of another maize epidermal cell in metaphase shows very sparse cortical microtubules Bar is 10 μm . I) Two additional timepoints between 14:11 and 29:16 highlighting the accumulation of cortical-telophase microtubules. Bar is 10 μm .

Cortical-telophase microtubules were present in over 90% of wild-type cells during telophase (n =173/190 cells from 26 plants, Figure 2.2A). Cortical-telophase microtubule arrays covered $33 \pm 2\%$ (mean \pm standard error (SE) of the cell cortex (Figure 2.2D), with an average anisotropy of 0.12 ± 0.01 arbitrary units (Figure 2.2B). These anisotropy values (reflecting the relative orientation of cortical-telophase arrays) were similar to those of microtubule arrays in Arabidopsis shoot meristems during interphase (Boudaoud et al., 2014). The cortical-telophase microtubules were on average typically arranged into anti-parallel arrays perpendicular to the division site (~50% within 10 degrees of perpendicular relative to the phragmoplast midline, n = 38 microtubule arrays from 19 cells, 7 plants, Figure 2.2D), with most plus-ends facing the division site. We also observed cortical telophase microtubule arrays in Arabidopsis root cells (Supplemental Figure S2.1C). The results were similar to previous reports showing microtubule-nucleating protein accumulation at the cell cortex e.g. (Kong et al., 2010; Vavrdová et al., 2019; Lucas, 2021) or cortical microtubules in moss (*Physcomitrium patens*) e.g. (Wu and Bezanilla, 2014). Therefore, cortical-telophase microtubule arrays were abundant and on average oriented perpendicular to the division site during telophase in maize epidermal cells. Although they are difficult to see, cortical-telophase microtubules may be a conserved feature of plant cells.

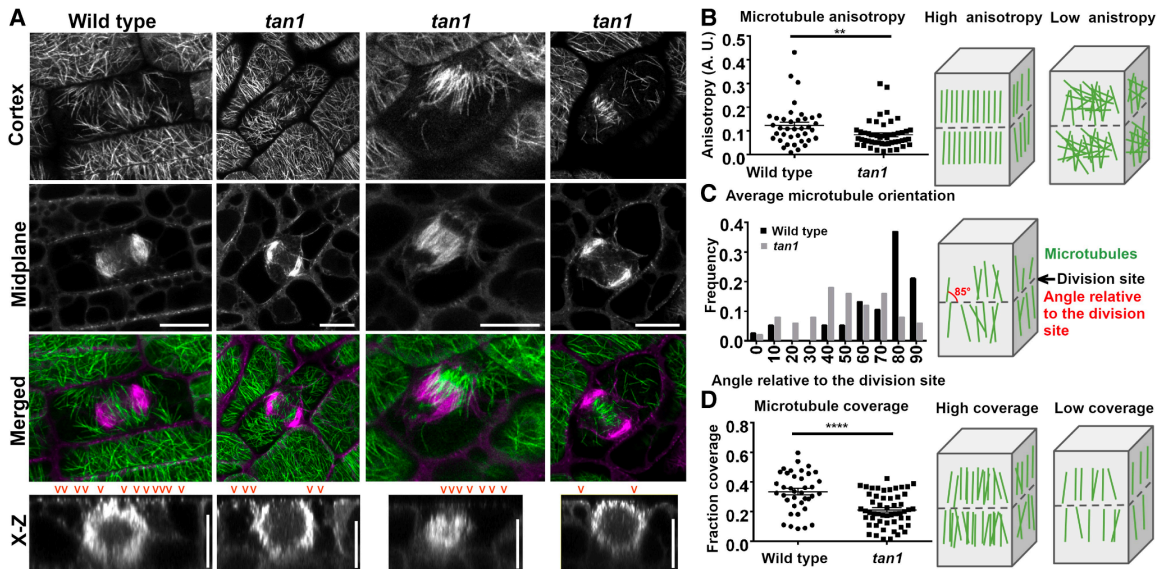
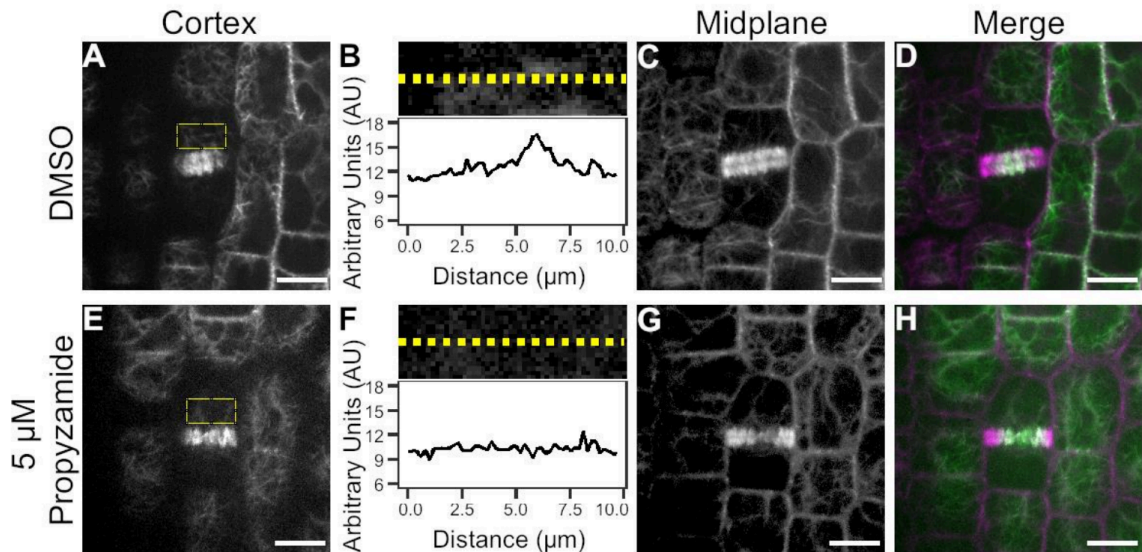


Figure 2.2. Cortical-telophase microtubules are typically abundant and arranged towards the division site in wild-type cells but are more variable in abundance and organization in *tan1* mutant cells.

A) a wild-type maize epidermal cell with abundant cortical-telophase microtubules (far left), *tan1* mutant cells with abundant (left), asymmetric (middle) or sparse cortical-telophase microtubules (right). Merged images show midplane view (magenta) and cortex view (green). X-Z shows the X-Z projection, with orange arrowheads indicating cortical microtubules at the top of the cell. (B) Cortical-telophase microtubule array anisotropy, $n = 38$ wild-type arrays (19 cells from 5 plants) and 50 *tan1* arrays (25 cells from 9 plants) with median and quartiles indicated by black bars (two-tailed Mann-Whitney test p -value = 0.005). Schematic diagrams of cells with high and low anisotropy (right). (C) Histogram of the average microtubule orientation of the cortical-telophase microtubule array ($n = 38$ arrays for wild-type and 50 for *tan1* mutant cells, two-tailed Mann-Whitney test comparing angle values, p value <0.001). Schematic diagram showing angle measurements compared to the division site (D) Relative cortical-telophase coverage, represented as a fraction, was significantly higher in wild-type (38 arrays) than *tan1* (54 arrays) cells, two-tailed Mann-Whitney test, median and quartiles are indicated with black bars (p value <0.0001). Schematic diagrams with examples of high and low microtubule coverage. Micrographs were taken under a Zeiss LSM 880 (Airyscan, 100X, NA=1.46). Bars are 10 μ m.

Analysis of microtubule dynamics

To assess whether cortical-telophase microtubules had different properties compared to phragmoplast microtubules, we treated maize epidermal cells with the microtubule destabilizer propyzamide (5 μ M). Propyzamide inhibits microtubule assembly by binding to beta-tubulin (Young and Lewandowski, 2000). Cortical-telophase microtubules were more sensitive to 5 μ M propyzamide treatment than phragmoplast microtubules. The majority of cortical telophase microtubules were depolymerized within 30-minutes of treatment (Supplementary Figure S2.2, n = 50/56 cells from 3 plants). After an additional 30 minutes, all remaining cortical telophase microtubules were disassembled. By contrast, interphase cortical microtubules were intact after 30 minutes of propyzamide treatment, depolymerizing after 45 minutes to 1 hr after treatment (n = 117 cells from 2 plants). By contrast, phragmoplast microtubules were resistant to propyzamide treatment and remained intact after 1 hour (n = 68/68 phragmoplasts). When incubated with DMSO (negative control), cortical telophase microtubules were still intact 30 minutes after treatment (n = 34/69 cortical-telophase microtubule arrays). Phragmoplast (n = 62) and interphase microtubules (n = 82 cells) were also intact. Together, these results indicate that cortical-telophase microtubules are more sensitive to treatment with 5 μ M propyzamide than either interphase cortical microtubules or phragmoplast microtubules, suggesting that they are more likely to be single, highly dynamic and unbundled microtubules that are distinct from the phragmoplast, which is consistent with our imaging data.



Supplemental Figure S2.2: Propyzamide treatment of maize epidermal cells depolymerizes cortical telophase microtubules but does not depolymerize phragmoplast microtubules.

Supports Figure 2.1 and Figure 2.2. A) Cells treated with DMSO (negative control) showing intact cortical-telophase microtubules. Box indicates region used in line scan in panel B. B) Line scan showing arbitrary fluorescence intensity measured at the cortex indicating intact cortical telophase microtubules. C) Midplane of the cell, showing the phragmoplast D) Merged Image, with cortex false colored green, and midplane false colored magenta. E) Cells treated with 5 μM Propyzamide for 30 minutes lacking cortical-telophase microtubules. Box indicates region used in line scan in panel F. F) Line scan showing arbitrary fluorescence intensity indicating lack of intact cortical-telophase microtubules. G) Midplane of the cell, showing the phragmoplast H) Merged image, with cortex false colored green, and midplane false colored magenta. Scale bars are 10 μm.

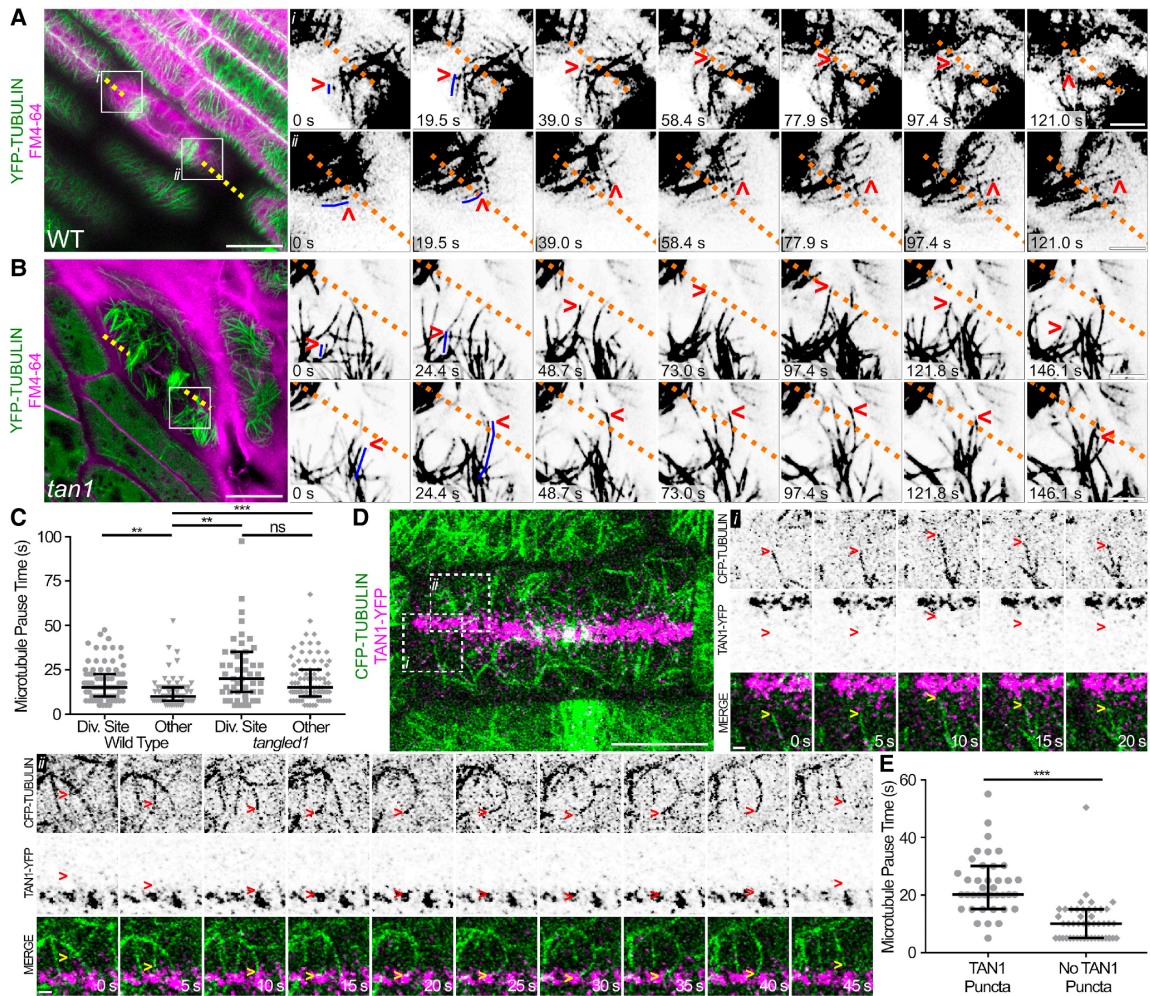


Figure 2.3. Cortical telophase microtubules pause at the division site near TAN1 puncta.

A-B) Time-lapse images of cortical telophase microtubules (YFP-TUBULIN, green) pausing at the division site (top panels) or passing (bottom panels) through the division site ahead of the phragmoplast in wild-type (A) and *tangled1* (B) cells. Red arrowheads indicate the microtubule plus end. Dotted lines in time-lapse insets mark the division site, as predicted through extension of FM4-64 cell plate staining (magenta). Scale bar is 10 μ m and 5 μ m in insets. (C) Dot plot of microtubule pause times (s) at division site and other cortex locations in wild type and *tan1*. Bars represent median with interquartile range. (D) Time-lapse images of a wild-type cell cortex with cortical telophase microtubules and cortical TAN1 localization. Cortical telophase microtubules ahead of the phragmoplast pause at the division site with no TAN1 puncta (i, top panel) and at the division site with TAN1-puncta (ii, bottom panel). Microtubules are labeled with CFP-TUBULIN (green) and TAN1 by TAN1-YFP (magenta). Arrowheads indicate the respective microtubule plus-end. Scale bar is 10 microns and 1 micron in insets. (E) Dot plot comparing microtubule pause times (s) at division site locations with or without TAN1 puncta in wild-type cells expressing TAN1-YFP. Each dot represents one microtubule pause time. Error bars are median with interquartile range. P-values ns not significant, * <0.05, ** <0.01, *** <0.001 by Kruskal-Wallis & Dunn's Test. Images were acquired using a Zeiss LSM 880 equipped with Airyscan with a 100X (NA=1.46) lens.

To understand how cortical-telophase microtubules formed-arrays with their plus-ends facing the division site, we examined individual microtubules interacting with the division site in addition to other locations within the cell (Supplemental Table S2.1 and Supplemental Data Set S1). In wild-type cells, microtubule plus-ends were transiently stabilized by pausing or capture at the division site (Figure 2.3A, 2.3C, I Movie 1). When cortical-telophase microtubules contacted the division site, 59.4% of microtubules paused ($n = 60/101$ microtubules, 4 cells, 3 plants, Table 2.1), 4.9% underwent immediate catastrophe after touching the division site, and 35.6% passed through the division site without altering of their trajectories. When cortical-telophase microtubules interacted with the division site, 59% ($n = 53/90$) buckled, indicating that the microtubule was still growing as it was transiently captured at the division site. Median pausing or capture time was 15 seconds at the division site but 10.0 seconds in other locations (Figure 2.3A, 3C, Table 2.2, p value = 0.03). Transient stabilization of microtubule plus-ends at the division site may promote overall perpendicular orientation.

Table 2.1. Quantification of individual interaction and bundling events between cortical-telophase microtubules and the phragmoplast.

(A) Summary of cortical-telophase microtubule bundling times and angles with the phragmoplast. (B) Summary of cortical-telophase microtubule interaction types with the phragmoplast. (B) Fisher's exact test was used, and significant differences are indicated by (**) $P < 0.01$, (****) $P < 0.0001$. Phragmoplast-interacting MTs: WT ($n = 252$, 5 cells, 3 individuals), *tan1* ($n = 163$, 5 cells, 3 individuals).

A

Sample	Phragmoplast trailing edge			Phragmoplast leading edge		
	Time bundled (Seconds, mean +/- SEM)	Angle bundled (Degrees, mean +/- SEM)	Proportion of microtubules (% , n)	Time bundled (Seconds, mean +/- SEM)	Angle bundled (Degrees, mean +/- SEM)	Proportion of microtubules (% , n)
Wild type	45.75 +/- 6.781	26.57 +/- 1.804	34 (86)	108.6 +/- 6.922	21.48 +/- 1.113	66 (166)
<i>tangled1</i>	****63.07 +/- 6.305	28.44 +/- 1.901	**47 (77)	97.96 +/- 7.745	25.14 +/- 2.032	**53 (86)
P value	0.0001	ns	0.0074	ns	ns	0.0074

B

Sample	Phragmoplast interaction types			
	Depolymerized (% , n)	Stayed (% , n)	Severed (% , n)	Stabilized (% ,n)
Wild type	22 (54)	78 (197)	37 (94)	41 (103)
<i>tangled1</i>	**10 (16)	**90 (147)	**56 (92)	34 (55)
P value	0.0019	0.0019	0.002	ns

Table 2.2. Percentage of cortical microtubule pausing at or passing through the division site in wild-type and *tangled1* plants.

Comparison of microtubule interactions with the division site between wild type ($n = 3$ plants, 4 cells) and *tangled1* ($n = 4$ plants, 4 cells). P-values ns not significant, *** ≤ 0.001 by Fisher's Exact Test.

	Wild Type	<i>tangled1</i>
% Pause	59.4% (60/101)	27% (26/96)***
% Pass	35.6% (36/101)	65% (62/96)***
% Depolymerize	4.9 % (5/101)	8% (8/96) ^{ns}

To determine if microtubule pausing at the division site was due to contact with opposing microtubules, we examined how often microtubules contacted antiparallel microtubules at the division site. Microtubule pausing at the cortical division site ahead of the phragmoplast did not typically occur through antiparallel interactions with microtubules located on the other side of the division site. For wild-type cortical-telophase microtubules, antiparallel contact at the division site occurred 13% of the time ($n = 8/61$ microtubules from 12 cells from 6 plants). This number of antiparallel contacts was similar to the number of cortical-telophase microtubule contacts that did not occur at the division site, 2%, ($n = 1/48$ microtubules from 12 cells from 6 plants, no significant difference, two-tailed Fisher's Exact Test). Similarly, 25% of phragmoplast leading-edge microtubules had antiparallel contacts at the division site ($n = 5/20$ microtubules from 8 cells, 5 plants, no significant difference compared to cortical-telophase microtubules at the division site, two-tailed Fisher's Exact Test). Together, these results suggest that cortical-telophase microtubules did not pause at the division site solely due to contact with antiparallel microtubules. Instead, microtubules paused at the division site regardless of whether a microtubule from the other side was present, suggesting that a protein (or proteins) located at the division site mediated microtubule pausing.

TAN1 functions in microtubule plus-end capture

To analyze the role of the microtubule binding protein TAN1 in microtubule plus-end capture, we measured microtubule plus-end pausing using time-lapse imaging of wild-type cells expressing both TAN1-YFP and CFP-TUBULIN. TAN1-YFP forms discrete puncta at the division site during telophase (Figure 2.3D, Movie 2) (Rasmussen et al., 2011; Walker et al., 2007; Martinez et al., 2017). In time-lapse images, cortical

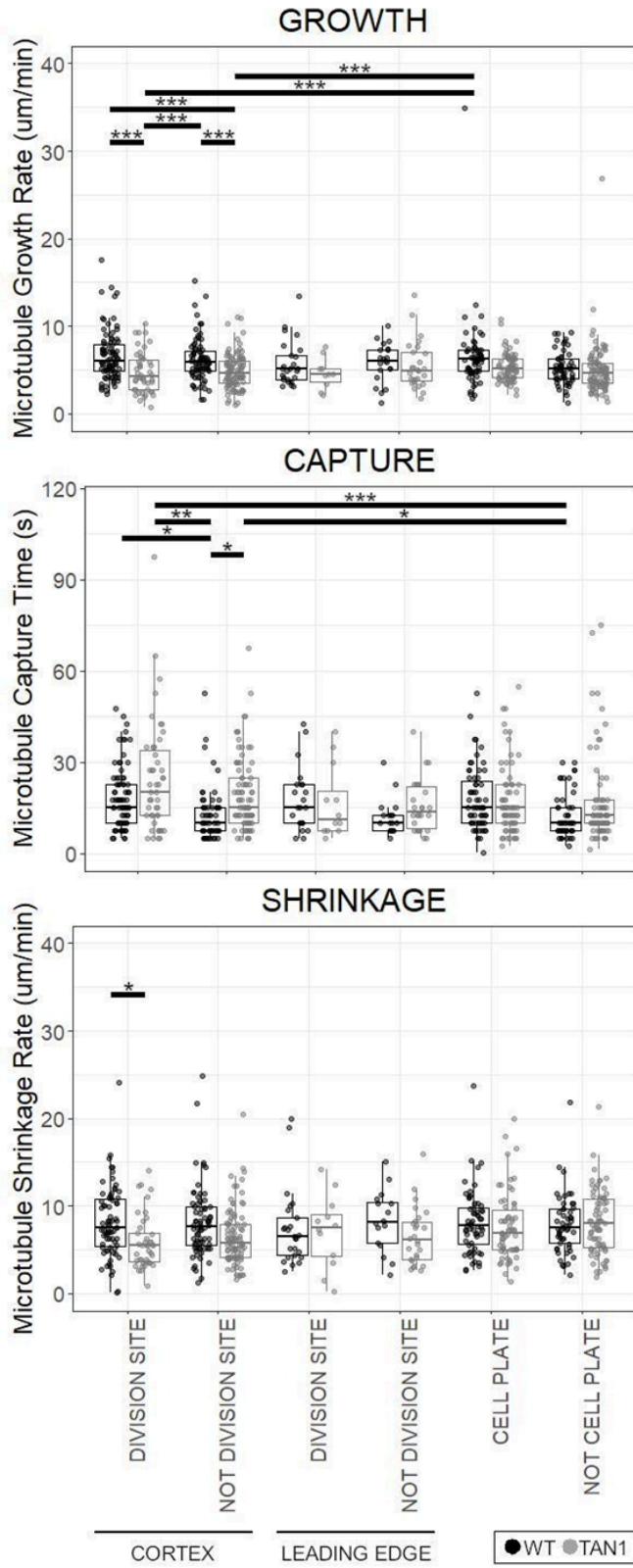
telophase microtubules appear to interact with stable TAN1 puncta the division site (Movie 2). We found that cortical-telophase microtubules remained near TAN1-YFP puncta longer than other regions within the division site in wild-type maize cells (Figure 2.3D, 2.3E). Microtubule plus-ends paused near TAN-YFP1 puncta for ~20 seconds (20 ± 1.6 s, median \pm SEM, $n = 39$ microtubules, 4 plants). By contrast, microtubule plus-ends that contacted regions of the division site distinct from TAN1-YFP puncta paused for ~10 seconds (10 ± 1.1 , median \pm SEM $n = 48$ microtubules, 4 plants, Figure 2.3E). Together, these findings suggest that TAN1 or other division-site localized proteins in close proximity (within Airy Scan resolution limits of ~150 nm) promote cortical microtubule plus-end pausing or capture during telophase. This microtubule interaction is consistent with the results of in vitro dynamic assays where TAN1 transiently captured microtubules at high contact angles (Martinez et al., 2020). Together, these results suggest that TAN1 or other nearby division site-localized proteins increase microtubule pausing or capture at the division site, which over time leads to cortical telophase arrays that are on average perpendicular to the division site, as observed in Figure 2.2C.

We hypothesized that loss of TAN1 from the division site would lead to defects in cortical-telophase microtubule organization, so we examined cortical-telophase microtubules in the maize *tan1* mutant. Cortical-telophase microtubule arrays were sparse or missing in nearly 30% of *tan1* cells ($n = 24/122$ cells from 24 plants, e.g., Supplemental Figure S2.1E, S2.1F).

When cortical-telophase arrays were present in *tan1* cells, they were often unevenly distributed (asymmetric) (Figure 2.2A). Furthermore, cortical-telophase microtubule arrays in the *tan1* mutant were less anisotropic (Figure 2.2B) than wild-type cortical-telophase arrays. In addition, unlike wild-type cortical-telophase arrays, *tan1* mutant arrays were not typically oriented toward the division site (Figure 2.2C, median orientation 49.5 +/- 3 degrees relative to the phragmoplast midline, $P < 0.0001$ Mann-Whitney test). These data suggest that TAN1 promotes proper cortical-telophase microtubule array organization.

In contrast to wild-type cells, cortical-telophase microtubules were not transiently stabilized at the division site in *tan1* mutant cells, showing no significant difference in microtubule pausing at the division site versus other cortical locations (Figure 2.3B, 2.3C, Supplemental Figure S2.3, Supplemental Data Set S1 Kruskal-Wallis Test and Dunn's Test, $p = 0.11$ (adjusted p -value = 1)). Unlike wild-type cells, where ~60% of cortical telophase microtubules paused at the division site, significantly fewer cortical telophase microtubules paused in the *tan1* mutant (27%, $n = 26/96$, Fisher's Exact Test, p value < 0.00001 , Table 2.2). Instead, the majority of cortical-telophase microtubules in the *tan1* mutant grew past the division site without any alteration in their trajectories (65% $n = 62/96$, example in Figure 2.3B, 6 cells from 5 plants, Table 2.2) or shrunk immediately (8%, $n = 8/96$). Microtubules that interacted with the division site displayed similar buckling frequency compared to wild-type cortical microtubules (58%, $n = 22/38$ compared to 59%, 53/90, p value = 1, Fisher's Exact Test). TAN1 also plays a role in mediating other microtubule dynamics during telophase, as measured using the Dynamic Kymograph Plugin in Fiji (Zhou et al., 2020) Supplemental Figure S2.4). Microtubule growth, shrinkage, and pause during telophase tended to be slower in *tan1*

mutants compared to wild type (Supplemental Figure S2.3). These data, together with the finding that microtubule pausing or capture increased at TAN1 puncta, suggest that TAN1 directly or indirectly promotes both microtubule plus-end capture and shrinkage at the division site.

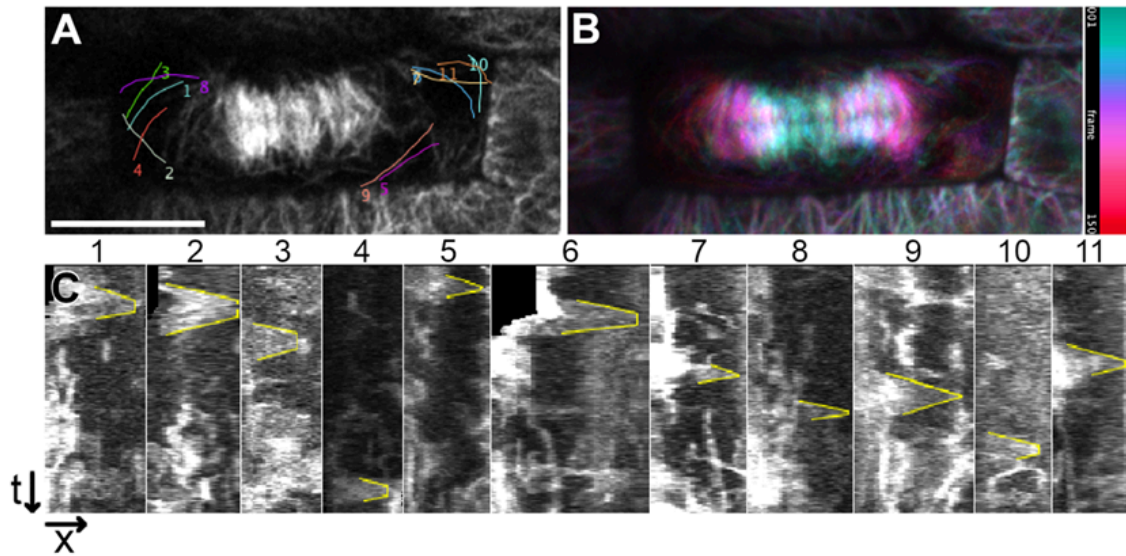


Supplemental Figure S2.3. Wild type and tangled1 microtubule dynamics during telophase.

Supports Figure 2.3 and Figure 2.4. Boxplots of microtubule growth and shrinkage rates and microtubule capture times. Horizontal lines on boxplot are 1st quartile, median, and 3rd quartile respectively. Each dot represents an individual microtubule measurement. P-values ns not significant, * <0.05, ** < 0.01, *** <0.001 by Kruskal-Wallis & Dunn's Test. For more summary values, see Supplemental Table S2.1 and Supplemental Dataset 1.

Supplemental Table S2.1. Summary of microtubule dynamics in wild-type and tangled1 cells across different locations at the cell cortex (supports Supplemental Figure S2.3).

Wild Type	N		GROWTH		CAPTURE		SHRINK	
	Plants	Cells	N MTs	Median \pm SE ($\mu\text{m}/\text{min}$)	N MTs	Median \pm SE (s)	N MTs	Median \pm SE ($\mu\text{m}/\text{min}$)
Cortical Microtubule - Division Site	6	12	69	6 \pm 0.3	61	15 \pm 1.1	61	7.6 \pm 0.5
Cortical Microtubule - Not Division Site	6	12	59	5.9 \pm 0.3	48	10 \pm 1.2	60	7.7 \pm 0.5
Phragmoplast Leading Edge - Division Site	5	8	22	5.1 \pm 0.5	20	15 \pm 2.1	21	6.5 \pm 0.9
Phragmoplast Leading Edge - Not Division Site	4	5	16	6 \pm 0.5	9	10 \pm 1.4	12	8.1 \pm 0.9
Cell Plate	4	9	53	6.2 \pm 0.5	52	15 \pm 1.3	52	7.7 \pm 0.5
Not Cell Plate	5	8	47	5.1 \pm 0.2	45	10 \pm 1.1	47	7.5 \pm 0.5
<i>tangled1</i>	N		GROWTH		CAPTURE		SHRINK	
	Plants	Cells	N MTs	Median \pm SE ($\mu\text{m}/\text{min}$)	N MTs	Median \pm SE (s)	N MTs	Median \pm SE ($\mu\text{m}/\text{min}$)
Cortical Microtubule - Division Site	8	11	35	4.2 \pm 0.3	33	20 \pm 2.7	33	5.5 \pm 0.5
Cortical Microtubule - Not Division Site	8	11	70	4.6 \pm 0.2	65	15 \pm 1.3	66	5.8 \pm 0.4
Phragmoplast Leading Edge - Division site	5	7	9	4.5 \pm 0.6	10	11 \pm 3.4	10	7.5 \pm 1.2
Phragmoplast Leading Edge - Not Division site	5	8	21	4.8 \pm 0.5	18	14 \pm 1.7	21	6.1 \pm 0.6
Cell Plate	4	8	56	5.2 \pm 0.2	52	15 \pm 1.4	54	6.9 \pm 0.5
Not Cell Plate	5	9	65	4.6 \pm 0.3	60	13 \pm 1.6	63	8 \pm 0.4



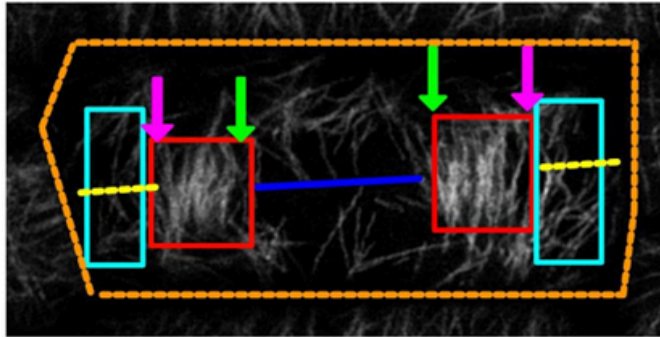
Supplemental Figure S2.4. Examples of microtubule dynamics measurements using the Dynamic Kymograph plugin tool in Fiji.

Supports Supplemental Table S2.1 and Figure 2.4 (A) Position of microtubule ROIs overlaid on the first frame of a timelapse image. (B) Time projection of timelapse in (A), where early frames are colored blue and later frames are colored red. (C) Kymographs of microtubules 1-11 from (A) annotated with ROIs to measure growth, capture, and shrinkage rates or times. Scale bar is 10 μm .

Interaction of cortical telophase microtubule arrays with the phragmoplast

We hypothesized that when the phragmoplast reached the cortex, it would interact with cortical telophase microtubules. To examine how cortical telophase microtubule arrays interacted with the phragmoplast, we used time-lapse imaging. Cortical-telophase microtubules were typically added into the phragmoplast by parallel bundling, as described below. To assess how individual microtubules from the cortical-telophase array interacted with the phragmoplast, we first identified sites of microtubule nucleation at the cortex from cortical telophase microtubules that were clearly distinct from the phragmoplast. Next, we determined how these microtubules interacted with the phragmoplast. An annotated micrograph describes the terms used here, such as leading and lagging edges (Supplemental Figure S2.5).

Cell cortex in late telophase



-  Phragmoplast
-  Phragmoplast disassembled and cell plate inserted
-  Cortical-telophase microtubules in front of the phragmoplast
-  Leading edge of the phragmoplast
-  Lagging edge of the phragmoplast
-  Division site ahead of the phragmoplast
-  Cell edges

Supplemental Figure S2.5: Description of the features of cells in telophase extracted for analysis.

Supports Figure 2.4 and Figure 2.5. The phragmoplast is indicated in red, the cell plate region, where the phragmoplast is already disassembled, is shown in dark blue. Cortical telophase microtubules ahead of the phragmoplast are indicated in teal. The leading of the phragmoplast is indicated in magenta, while the lagging edge is indicated in green. The division site ahead of the phragmoplast is indicated with a dashed yellow line, while the cell edges are indicated with a dashed orange line.

When cortical-telophase microtubules contacted the phragmoplast, most (78%, n = 197/252 microtubules from 5 cells from 3 plants) were incorporated into the leading edge of the phragmoplast by parallel bundling (Figure 2.4G, Movie 3, Movie 4). After bundling into the phragmoplast, the microtubules would either remain connected to the original cortical-telophase array during the 252 second timelapse (41%, n = 103/252, Figure 2.4G) or become fully incorporated into the phragmoplast by severing the connection between the cortical-telophase array and the phragmoplast (37%, n = 94/251, Figure 2.4E, Movie 5). We speculate that severing was performed by the microtubule severing protein KATANIN, which localizes to the distal phragmoplast (Panteris et al., 2011; Nakamura et al., 2010), possibly via the microtubule-binding protein MACET4/CORD4 (Schmidt and Smertenko, 2019; Sasaki et al., 2019). The remaining cortical telophase microtubules that contacted the phragmoplast underwent catastrophe after touching the phragmoplast (22%, n = 55/252, Figure 2.4F, Movie 6). Most (66%, n = 166/252) cortical telophase microtubules interacted with the leading edge, although others interacted with the lagging edge (n = 86/252) and then primarily were incorporated into the phragmoplast by low-angle parallel bundling (<45 degrees, Table 2.1).

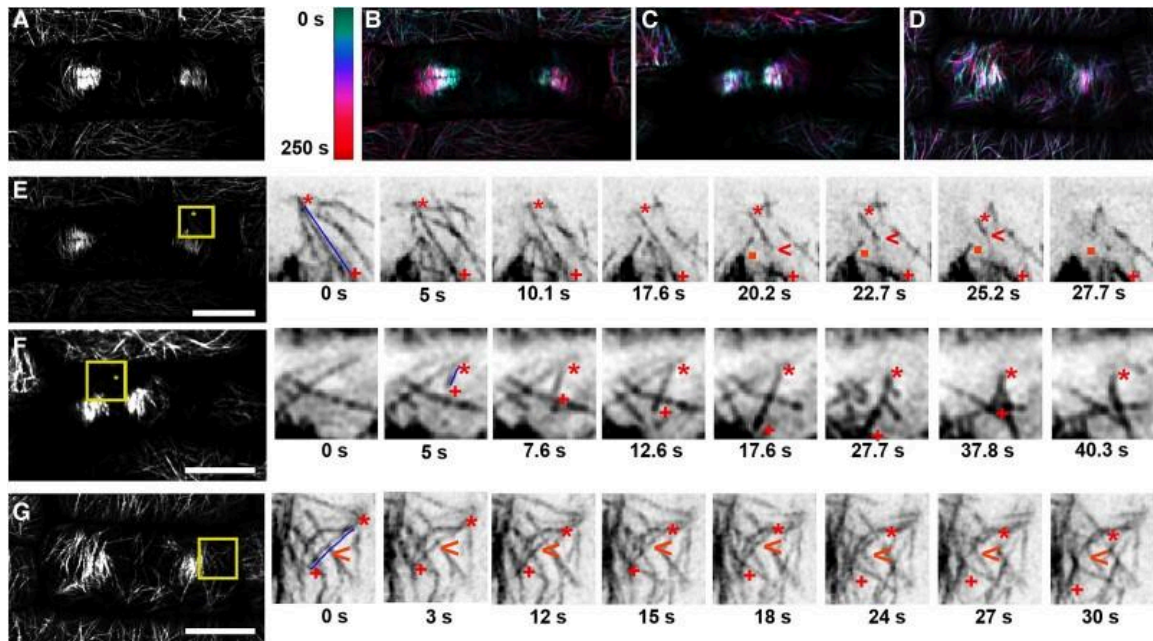


Figure 2.4. Time-lapse images of cortical-telophase microtubules interacting with the phragmoplast using YFP-TUBULIN to label microtubules.

A) A single early snapshot of a maize dividing cell during telophase with surrounding interphase cells. B) Color-coded time projection showing the movement of the phragmoplast and cortical-telophase microtubules of the cell in A). C) Time projection of cell in F), D) time projection of cell in G). E) The cell shown in A) at a later time point. Representative example of severing leading to the incorporation of a cortical-telophase microtubule into the phragmoplast. Microtubules of interest are indicated with an adjacent blue line; red asterisks indicate the cortical-telophase microtubule minus ends and red pluses indicate the microtubule plus end. Red arrowheads show severing followed by depolymerization. The orange square marks the new microtubule minus end after severing. F) Representative example of depolymerization of a cortical-telophase microtubule following contact with the phragmoplast. G) Representative bundling of a cortical-telophase microtubule into the phragmoplast. Orange arrowheads show a cortical-telophase microtubule incorporated into the phragmoplast by parallel bundling. Bars are 5 μm , Time (s) rounded to a 10th of a second. Images were acquired using a Zeiss LSM 880 equipped with Airyscan with a 100 \times (NA = 1.46) lens.

Cortical telophase microtubules, when present, were also added into *tan1* mutant phragmoplasts. Similar to wild-type microtubules, *tan1* cortical telophase microtubules were incorporated into the phragmoplast, although relatively more microtubules interacted with the lagging edge of the phragmoplast (Table 2.1). Proportionally more of the microtubules that interacted with the phragmoplast were eventually incorporated in *tan1* phragmoplasts (90% n = 147/163 versus 78% in wild-type cells n = 197/252 Table 2.1). These data indicate that cortical telophase microtubules in close contact with the phragmoplast were primarily added into the leading edge in both wild-type and *tan1* cells. Although cortical-telophase microtubules interacted similarly with the phragmoplast in wild-type and *tan1* cells, the abundance, orientation, and relative accumulation of cortical-telophase microtubules were more variable in *tan1* cells (Figure 2.2A, D).

Effects of cortical-telophase microtubule accumulation on the trajectory of phragmoplast expansion

We hypothesized that the addition of microtubules from the cortex into the phragmoplast would alter the direction of phragmoplast expansion. Using timelapse imaging, we measured the movement of the phragmoplast over time and measured the corresponding cortical telophase microtubule array. If more cortical telophase microtubules accumulated on one side of the phragmoplast, the phragmoplast moved towards the same direction within ~15 minutes (960 s, n = 6 cells). Terms describing phragmoplasts are defined in the model (Supplemental Figure S2.5, Figure 2.5J).

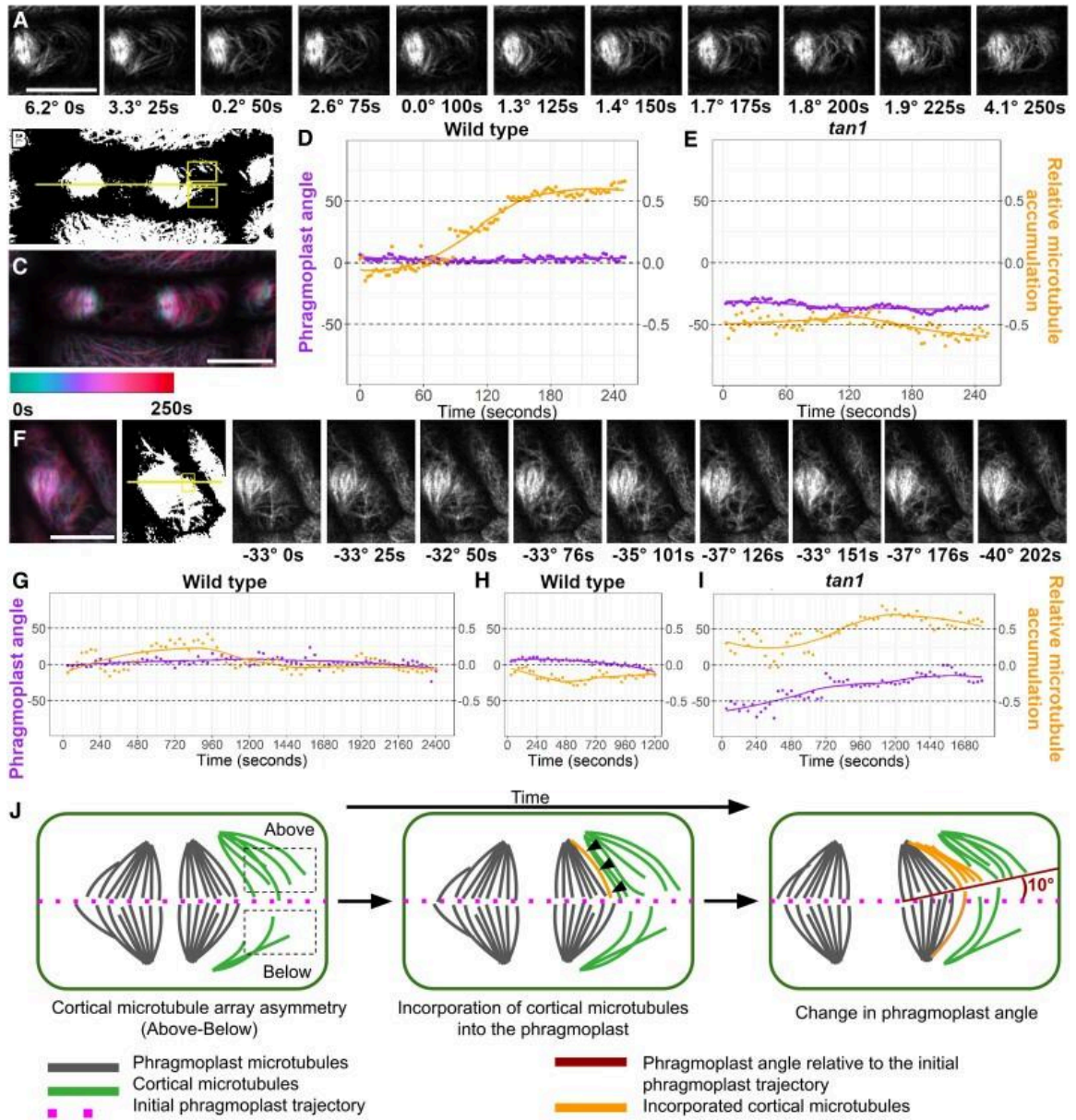
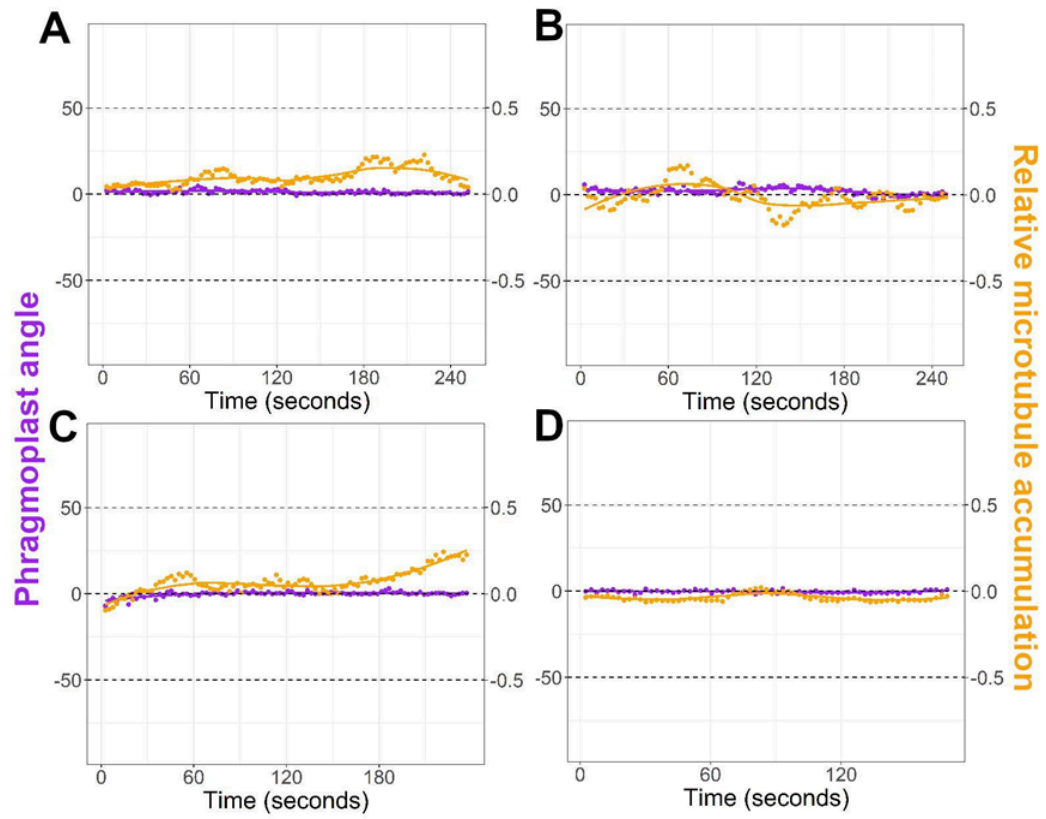


Figure 2.5. Long-term uneven accumulation of cortical-telophase microtubules is correlated with changes in phragmoplast direction.

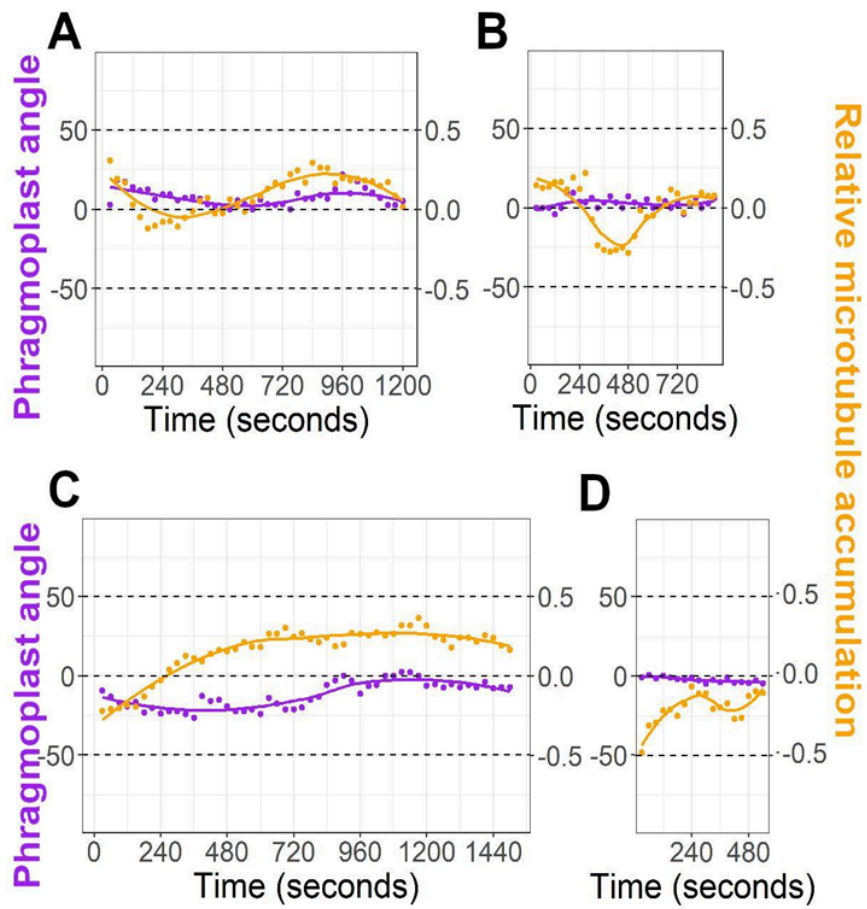
A) to D) A wild-type phragmoplast: A) Time-lapse imaging with phragmoplast angle relative to the division site and time (s) indicated below. Time-lapse images were acquired using a Zeiss LSM 880 with Airyscan (100×, NA = 1.46) or a Yokogawa spinning disk with a Nikon stand (100×, NA 1.45). B) Thresholded image with ROI (yellow rectangles) selected to measure relative cortical-telophase microtubule accumulation above and below the phragmoplast. The phragmoplast trajectory is indicated by a yellow line. C) Time projection with time-color legend. D) Graph comparing changes in phragmoplast angle over time (purple) and relative cortical-telophase microtubule accumulation (orange) above or below the phragmoplast. E) and F) A *tan1* phragmoplast E) Graph of changes in phragmoplast angle and cortical-telophase microtubule accumulation in *tan1* over time. F) Time-lapse imaging of *tan1*; phragmoplast angle and time are shown below. G-I) Longer time lapses: G) A wild-type cell with little overall phragmoplast movement. H) Wild-type cell with consistent cortical-telophase microtubule accumulation below the phragmoplast and downward phragmoplast angle movement. I) *tan1* cell with consistent cortical-telophase microtubule accumulation above the phragmoplast with phragmoplast angle movement towards the top. Bars = 10 μm. J) Model of the cell cortex of maize epidermal cells showing cortical-telophase microtubule accumulation, incorporation into the phragmoplast, and changes in the trajectory of the phragmoplast over time.

We compared the phragmoplast trajectory with the relative accumulation of cortical-telophase microtubules “above” and “below” the division plane (Figure 2.5A-C). The phragmoplast trajectory was measured as an angle parallel to the division site, defined in Figure 2.5A: if the angle is positive, it indicates that the phragmoplast angle moved above the division plane. If the angle is negative, the phragmoplast angle moved down below the division plane. We selected two equally sized region-of-interest boxes (Figure 2.5B) above and below the phragmoplast to measure the relative cortical-telophase microtubule accumulation in front of the expanding phragmoplast. Relative cortical-telophase microtubule accumulation was measured by subtracting the microtubule coverage below from above. Positive values indicate that more microtubules accumulate above the phragmoplast.

The direction of phragmoplast expansion in wild-type cells typically followed a flat trajectory within 5 minutes, with < 10 degrees overall change (n= 5, Figure 2.5D, Supplemental Figure S2.6). During longer timeframes (18-30 minutes), wild-type phragmoplast trajectories were more variable, but overall, they did not persistently change direction (n = 2/4, Supplemental Figure S2.7), which is consistent with previous time-lapse observations (Martinez et al., 2017). In wild-type cells with little overall phragmoplast angle displacement, cortical-telophase microtubule accumulation varied over time but did not maintain uneven accumulation (Figure 2.5G, Supplemental Figure S2.7B, S2.6D). By contrast, sustained accumulation of cortical telophase microtubules either above or below was correlated with phragmoplast movement in the same direction (Figure 2.5H, Supplemental Figure S2.7A and S2.7C).

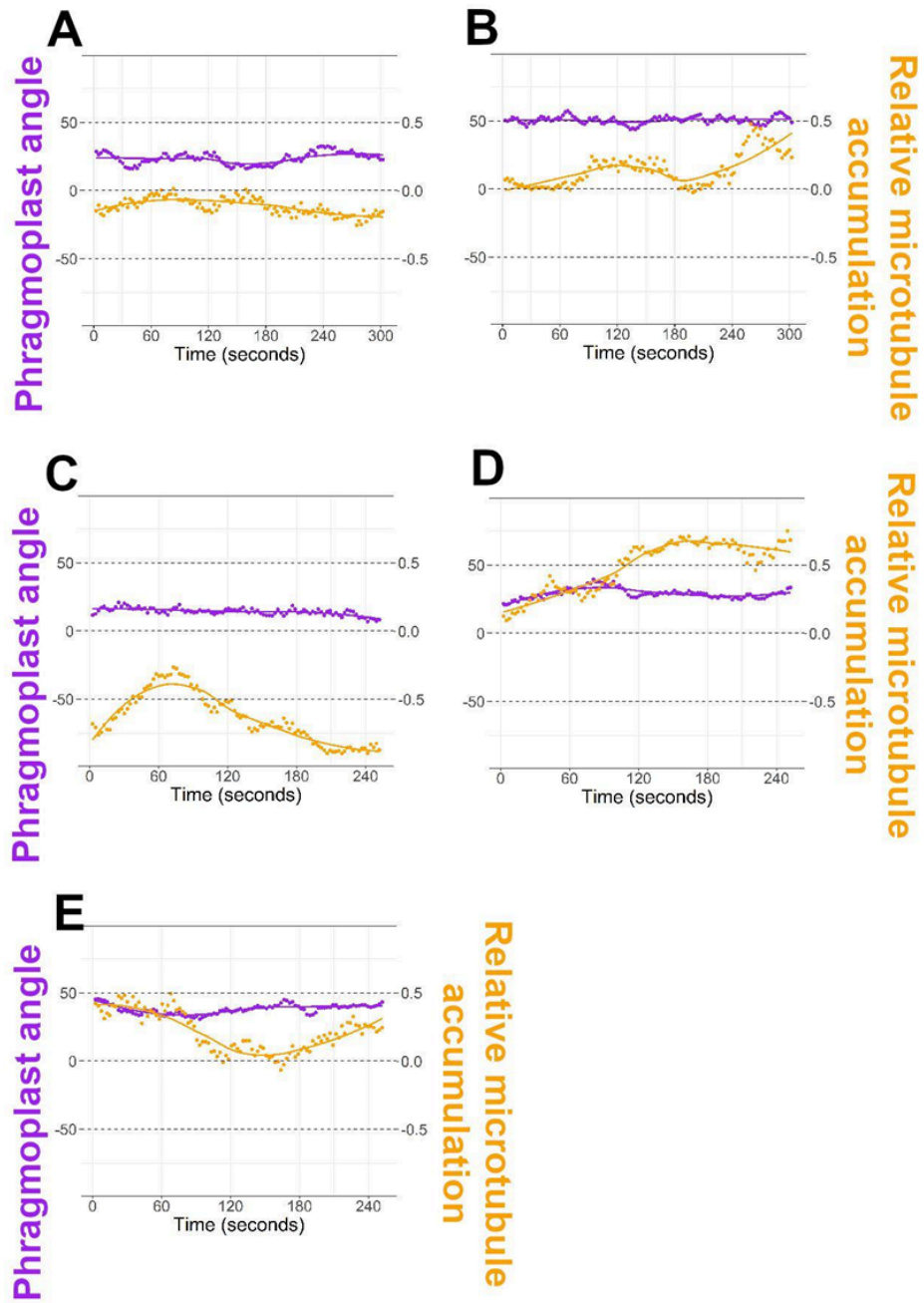


Supplemental Figure S2.6. Short time-lapses (<5 minutes) of four different wild-type phragmoplasts showing little change in direction. Supports Figure 2.5. Purple dots indicate measured phragmoplast angle compared to predicted division site.

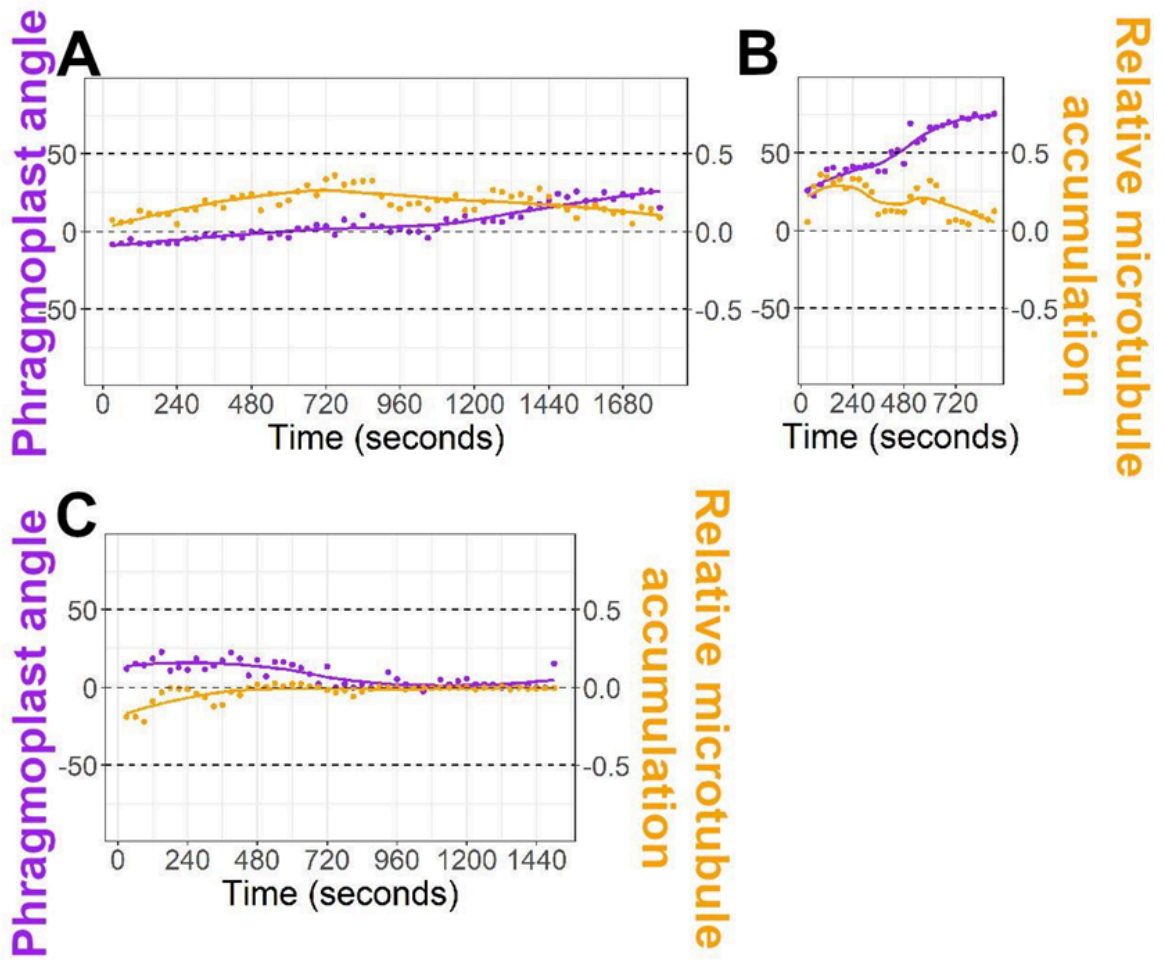


Supplemental Figure S2.7. Longer timelapses (>8 minutes) of wild-type phragmoplasts with >10 degree changes in the direction of movement. (A, C) and (B, D) with < 10 degree changes in the direction of movement. Supports Figure 2.5

In *tangled1* mutants, both phragmoplast expansion direction and cortical-telophase microtubule array accumulation were more variable than in wild-type plants, but the relationship between asymmetric cortical telophase microtubule accumulation and changes in phragmoplast direction was the same (Supplemental Figure S2.8). Over longer timeframes, sustained asymmetric cortical-telophase microtubule accumulation in *tan1* mutants also correlated with changes in phragmoplast trajectories in the same direction (Figure 2.5I, Supplemental Figure S2.9). Therefore, in both wild-type and *tan1* mutants, cortical-telophase microtubule accumulation preceded changes in the direction of the phragmoplast. Cortical-telophase microtubules interacted less with the division site in *tan1* mutants, often passing through without any pause or change in trajectory. We speculate that this in turn leads to disorganized and asymmetric cortical-telophase microtubule arrays (Figure 2.2). These asymmetric cortical-telophase arrays are then added into the phragmoplast (Figure 2.4), leading to defects in phragmoplast guidance observed as changes in phragmoplast direction over time in the *tan1* mutant (Figure 2.5). Changes in phragmoplast direction mediated by cortical-telophase also occurred in wild-type cells, albeit at lower frequency.



Supplemental Figure S2.8. Short timelapses (5 minutes or less) of five different *tan1* phragmoplasts showing little change in direction, but frequently unevenly distributed cortical-telophase array. Supports Figure 2.5.



Supplemental Figure S2.9. Longer timelapses (>12 minutes) of *tan1* phragmoplast angle measurements compared to relative cortical microtubule accumulation. Supports Figure 2.5.

DISCUSSION

We showed that cortical-telophase microtubule arrays accumulate and interact with the division site in maize during telophase before the phragmoplast reaches the cell cortex. Cortical-telophase microtubules that nucleated directly at the cortex were our focus, although some cortical-telophase microtubules may also come from the nucleus. Cortical-telophase microtubule nucleation is reminiscent of branching clusters of newly regenerating interphase cortical microtubules that form after the removal of microtubule-depolymerizing drugs (Wasteneys and Williamson, 1989). Previous reports of microtubules stabilized with Taxol showed that cortical-telophase microtubules nucleated directly on the cell cortex in the monocot durum wheat (*Triticum durum*) (Panteris et al., 1995), while they may have originated from the nuclear envelope in tobacco (*Nicotiana tabacum*) cultured cells (Van Damme and Geelen, 2008). Both cortical-telophase microtubules and nuclear envelope nucleated microtubules accumulate at the cortex in *Arabidopsis* cotyledon cells (Lucas, 2021). Whether cortical-telophase microtubules primarily originate at the cortex or the nucleus may depend on the species.

We showed that cortical-telophase microtubules often orient towards the division site due to increased microtubule plus-end pausing or capture at the division site (Figure 2.3) and that cortical-telophase microtubules are most often added into the phragmoplast by parallel bundling at low contact angles (Table 2.1). Cortical-telophase microtubules are bundled into the phragmoplast leading edge, perhaps similar to previously described “mini-phragmoplasts”, which are preassembled phragmoplast modules that are added to

the phragmoplast by parallel bundling during endosperm cellularization (Otegui and Staehelin, 2000; Lee and Liu, 2013).

Uneven or asymmetric cortical-telophase microtubule accumulation was correlated with changes in phragmoplast trajectories over time (Figure 2.5J). While it is possible that asymmetric accumulation of cortical-telophase microtubules and changes in phragmoplast angles over time both respond independently to some yet unknown cue, we propose that telophase microtubules, which are incorporated into the phragmoplast by parallel bundling, fine-tune the positioning of the phragmoplast so it reaches the exact division site at the cell cortex. The localized addition of pre-loaded and properly oriented microtubules also provides a plausible mechanism to achieve phragmoplast insertion at the cell cortex in cells with polarized cytokinesis. In maize, as well as other model systems, most divisions are polarized: the phragmoplast contacts the cortex at one location, then expands outward at the cortex to complete division. Highly polarized cytokinesis occurs during periclinal cambial divisions, in which phragmoplasts traverse tens to hundreds of microns to complete division (Kajala et al., 2014; Fischer et al., 2019). Other examples include *Arabidopsis* epidermal cells (Cutler and Ehrhardt, 2002; Lucas and Sack, 2012), cultured cells (Chan et al., 2005), and vacuolated *Nautilocalyx* cells (Venverloo and Libbenga, 1987). A guiding mechanism provided by local cortical microtubules, directly incorporated into the phragmoplast as it expands at the cell cortex, would provide the necessary specificity in targeting. The direct addition of cortical-telophase microtubules into the phragmoplast to alter its local position occurs when the phragmoplast is within micron range to the cell cortex. We suspect that this phragmoplast zippering event occurs when the addition of vesicles to the cell plate becomes slow and variable (van Oostende-Triplet et al., 2017).

We showed that cortical telophase microtubule plus ends are stabilized at the division site near TAN1 puncta. In vitro, when TAN1 is added to microtubule dynamic assays, it both decreases shrinkage rates and slows microtubule growth compared to microtubules without TAN1 addition (Martinez et al., 2020). This is consistent with the notion that TAN1 potentially stabilizes microtubules. However, in vivo, *tan1* mutants also have slower microtubule growth and shrinkage rates than WT. It is still unclear whether TAN1 could also play a role in nucleating microtubules or other functions. Given the intriguing contact angle-independent in vitro microtubule interactions observed during co-incubation with HIS-TAN1 (Martinez et al., 2020), we speculate that in vivo, TAN1 may block microtubules from passing through the division site by capturing the microtubule plus ends. Our hypothesis is that high contact angle microtubule interactions with TAN1 stabilize their plus ends to increase microtubule pause or capture times at the division site. An alternate hypothesis is that other division site-localized proteins in close proximity to TAN1 may mediate this activity. However, no other end-on microtubule-interacting proteins in plants have yet been shown to localize to the division site (Livanos and Müller, 2019; Rasmussen and Bellinger, 2018).

In addition to TAN1, other candidate MAPs might also contribute to the stabilization of cortical microtubules at the division site during telophase. The Kinesin-like Calmodulin Binding Protein (KCBP), a processive minus-end directed kinesin-14 that localizes to the division site in moss and Arabidopsis, is a highly plausible candidate (Yamada et al., 2017; Miki et al., 2014; Buschmann et al., 2015). Analogous minus-end directed motor proteins in animals and yeast (*Saccharomyces cerevisiae*), dyneins, capture and stabilize microtubule plus ends at the cell cortex during division. Dyneins play a critical role in division plane positioning by pulling on astral spindle microtubules at the cell

cortex to adjust the position of the spindle (Hendricks et al., 2012; Busson et al., 1998; Laan et al., 2012). In *Arabidopsis*, *kcbp* mutants do not have defects in division plane positioning, possibly due to a redundant function of a yet unknown minus-end directed kinesin at the division site. Whether KCBP puncta localized at the division site interact directly with microtubules is also unknown (Buschmann et al., 2015).

KCBP interacts with a transiently division site-localized protein called AUXIN INDUCED IN ROOT CULTURES9 (AIR9) (Buschmann et al., 2015). AIR9 localizes to the division site as the phragmoplast reaches the cortex but is not at the division site from metaphase until the end of telophase in tobacco cultured cells. Therefore, AIR9 is not at the division site when the cortical-telophase microtubules originate, or when interactions between cortical-telophase microtubules and division site localized proteins begin (Buschmann et al., 2006). The lack of localization of AIR9 during the majority of telophase suggests that it is unlikely to be a major player in plus-end cortical-telophase microtubule stabilization at the division site. Another candidate is the antiparallel microtubule bundling protein MAP65-4, which localizes to the division site (Li et al., 2017). However, since most cortical-telophase microtubules are not bundled into antiparallel microtubule arrays, but instead interact directly with the division site, it is more likely that cortical telophase microtubules interact with other classes of microtubule-binding proteins.

POK1 and POK2, which are plus-end directed kinesin-12 motor proteins that localize to the division site (Lipka et al., 2014; Herrmann et al., 2018; Chugh et al., 2018), might stabilize cortical-telophase microtubules. Since POK1 and POK2 directly interact with

TAN1 (Müller et al., 2006; Rasmussen et al., 2011; Mills et al., 2022; Lipka et al., 2014), they might also function together with TAN1 at the division site to capture microtubules. POK1 and POK2 may capture cortical-telophase microtubules at the division site just behind their plus-ends and then move towards the plus ends, effectively pushing the minus-ends away from the division site. This idea is consistent with microtubule buckling observed following contact with the division site.

Interactions of microtubules and microfilaments with division-site-localized proteins such as MYOSIN VIII are likely broadly conserved features of division plane positioning in plants. MYOSIN VIII interacts with both actin and microtubules: their combined interaction, which is mediated by MYOSIN VIII, guides the phragmoplast towards the proper division site (Wu and Bezanilla, 2014). Fascinatingly, both actin and MYOSIN VIII participate in incorporating peripheral microtubules, defined as microtubules that nucleate from the phragmoplast and grow outwards towards the cortex, back into the phragmoplast. Drug treatments that block myosin activity cause defects in phragmoplast guidance towards the cortex (Molchan et al., 2002), as do drugs that disrupt actin filaments (Wu and Bezanilla, 2014; Yoneda et al., 2004). MYOSIN XI also promotes proper division plane positioning in both maize and Arabidopsis (Abu-Abied et al., 2018; Nan et al., 2021). Cytoskeleton-mediated (actin-based) division-plane corrections also occur during telophase in mouse (*Mus musculus*) epithelial cells, suggesting that analogous mechanisms occur in other eukaryotes (Lough et al., 2019).

MATERIALS AND METHODS

Plant growth and imaging conditions

Maize (*Zea mays*) plants were grown in 1L pots in standard greenhouse conditions, with the temperature setpoint ~32 °C with a photoperiod of 14 hours of light (~400 $\mu\text{E}\cdot\text{m}^{-2}\cdot\text{s}^{-1}$)/10 h of dark. Supplemental lighting was provided by 1000w high pressure sodium bulbs (Gravita Pro Plus 1000W EL). Plants were grown in soil containing 20% peat, 50% bark, 10% perlite, 20% medium vermiculite with Calcium Nitrate (90ppm CA 75ppm N), Magnesium Nitrate (45ppm Mg, 50ppm N), and further supplemented with Osmocote (NPK 14-14-14). Maize plants between 3 and 5 weeks old containing YFP-TUBULIN, CFP-TUBULIN, TANGLED1-YFP (Mohanty et al., 2009; Wu et al., 2013) or the *tangled1* mutant were used for imaging and identified by microscopy or by genotyping as previously described (Martinez et al., 2017). The primers used for genotyping were as follows: for *TANGLED1-YFP* (TAN LSP1 5' ACGACCGTTAGCACAGAACC and GFP5REV 5' CTGAACTTGTGGCCGTTTACGTCGC); for *YFP-TUBULIN* (TubAlpha Rp1 5' GGTTTCGGGTGATCCCTATT and TubalphaFp1 5' GCAAGGTTTCGATTTCCGTA); and for *CFP-TUBULIN* (BTUBR3187 5' GACAGGCGGGCATAAGATCC and TUBbeta FP 5' CGAATTTTCGAATCCTCAGC). Leaves were removed from plants until the ligule height was <2 mm. Abaxially symmetrically dividing leaf blade samples were mounted in water between cover glass and glass slides (Fisherbrand) or in a Rose chamber, as previously described (Rasmussen, 2016). For FM4-64 staining, leaf samples were mounted in 50 μM FM-464 and placed in a Rose chamber for imaging. Three or more plants per genotype were analyzed. Room temperatures during imaging were between 21 and 24 °C.

Arabidopsis thaliana seedlings were grown on ½ strength Murashige and Skoog (MS) medium solidified with 0.8% agar. Plates were sealed with surgical tape (3M) and grown vertically in a growth chamber (Percival) with 16-h white light $\sim 111 \mu\text{E}\cdot\text{m}^{-2}\cdot\text{s}^{-1}$ (F17T8/TL741 Fluorescent Tube (Philips))/8-h dark cycles with a 22°C temperature set point. Arabidopsis plants containing CFP-TUBULIN (identified by microscopy) were imaged between 3 and 5 days after germination. Seedlings were mounted in water and covered with a cover slip. Root epidermal cells from the meristematic zone were imaged at 23 °C.

Confocal microscopy

Micrographs and short timelapse images were taken with a Zeiss LSM 880 confocal laser scanning microscope equipped with Airyscan with a 100X, NA = 1.46, oil immersion objective lens. A 514-excitation laser with bandpass (BP) filters 465-505 with longpass (LP) 525 filter was used with Airyscan super resolution mode. Images captured using the Zeiss LSM 880 were processed using default Airyscan settings with ZEN software (Zeiss). For longer time lapse imaging, 30 second intervals were used to capture images of microtubules at the cortex to measure both cortical-telophase microtubule accumulation and the orientation of the phragmoplast (data used in Figure 2.5G-I) with a Yokogawa W1 spinning disk microscope with an EM-CCD camera (Hamamatsu 9100c) and Nikon Eclipse TE inverted stand with a 100x, NA 1.45, oil immersion objective lens controlled with Micromanager-1.4 with an ASI Piezo Z stage and a 3 axis DC servo motor controller. Solid-state lasers (Obis) between 40 to 100 mW were used with standard emission filters from Chroma Technology. For YFP-TUBULIN or TANGLED1-YFP, a 514 laser with emission filter 540/30 was used. For CFP-TUBULIN, a

445 laser with emission filter 480/40 was used. For the membrane dye FM4-64, a 516 nm laser with emission filter 620/60 was used.

Telophase cells were identified by the presence of a phragmoplast, and cortical telophase microtubules were imaged on the cortical edges of epidermal cells.

Two-dimensional projections, time projections, and three-dimensional reconstructions of Z stacks and time-lapse images were generated in FIJI (ImageJ, <http://rsb.info.nih.gov/ij/>). Image brightness and contrast were altered using the linear levels option, and figures were assembled with FIJI and Gnu Image Manipulation Program (GIMP <https://www.gimp.org/downloads/>). Drift during timelapse imaging was corrected with StackReg <https://imagej.net/StackReg> using the translation option (Thévenaz, 1998).

Quantification of microtubule array organization and coverage

Maize lines expressing YFP-TUBULIN were used to examine the microtubule cytoskeleton. To measure anisotropy (Figure 2.2B) and orientation (Figure 2.2D), TIFF image files were converted to PNG files using Fiji software and processed with the FibrilTool plugin (Boudaoud et al., 2014). For wild-type plants, 38 arrays from 19 transverse cell divisions during telophase were measured from 5 plants with median anisotropy 0.11 +/- 0.01 A.U. For *tan1* mutants, 50 arrays from 25 transverse cell divisions during telophase were measured from 9 plants (0.07 +/- 0.01 A.U.).

To measure percent microtubule coverage in Figure 2.2C, image files were made binary and thresholded using mean fluorescence and processed using the Area/Volume fraction function in the BoneJ plugin (<https://imagej.net/BoneJ>, (Doube et al., 2010)). The median value for wild-type cells (n = 38 arrays, coverage fraction 0.33 +/- 0.02) is

significantly different from median value for *tan1* mutant cells (n = 54 arrays, coverage fraction 0.20 +/- 0.01, Mann-Whitney test, P < 0.0001.)

Measuring microtubule dynamics

Timelapse imaging was used to measure microtubule interactions at the division site, near TAN1 puncta, and with the phragmoplast. The division site was defined as a location typically parallel or perpendicular to the long axis of the cell and corresponding to the position of the phragmoplast midplane or based on the accumulation of the membrane dye FM4-64 at the cell plate. In *tan1* mutants, the “division site” was defined the same way unless the phragmoplast was misoriented, in which case the “division site” was defined as the midplane of the phragmoplast or the cell plate location defined using the membrane dye FM4-64. Individual microtubule movements were measured using the Dynamic Kymograph plugin (<https://imagej.net/plugins/dynamic-kymograph>) in Fiji and binned into categories (for phragmoplast interactions). Growth, pause, and shrinkage rates were measured by tracing the outlines of dynamic kymographs using regions of interest (ROIs) in Fiji. Pauses were defined as the presence of a microtubule plus end in a region ± 3 pixels.

Timelapse imaging was used to compare the abundance of cortical-telophase microtubules and the phragmoplast angle over time. The phragmoplast angle at each timepoint was measured in FIJI and saved in Google sheets or Excel (Microsoft Office). Timelapse image files were first processed to remove drift using the transformation selection within StackReg, (Thévenaz, 1998) and to correct for photobleaching using bleach correction (exponential fit) in FIJI. Next, images were made binary and thresholded using mean fluorescence and processed using the Area/Volume fraction

function in the BoneJ plugin (Doubé et al., 2010). Two equally-sized ROIs were selected above and below the phragmoplast, such that the ROIs captured cortical-telophase microtubule accumulation near the phragmoplast but not touching the phragmoplast at any time frame. The bottom ROI was subtracted from the top ROI. A positive value indicated more microtubule density or accumulation on the top half of the cell. Both phragmoplast angle and relative cortical-telophase microtubule accumulation were graphed together by time using R, RStudio (Version 1.3.1093) and ggplot2 (Computing and Others, 2013; Wickham et al., 2008). Figures were made using the Gnu Image Manipulation Program (Gimp, versions 2.10.22-2.10.32) with no interpolation during scaling and linear adjustments to levels.

Statistical analysis

Microtubule anisotropy measurements were made for wild-type and *tan1* mutant plants described above. Differences in anisotropy were analyzed with GraphPad Prism, and statistical significance was determined with a Mann-Whitney *U*-test, $P = 0.0054$.

Microtubule coverage of the cortex during telophase was measured in wild-type and *tan1* mutant plants. Differences in coverage were analyzed with GraphPad Prism, and significance was determined with a Mann-Whitney *U*-test, $P < 0.0001$. Microtubule dynamics data were graphed in GraphPad Prism and statistically analyzed with R using the Kruskal-Wallis test followed by Dunn's test (p -values adjusted with Bonferroni correction).

Accession numbers

Sequence data from this article can be found in the GenBank/EMBL libraries under the following accession numbers: TANGLED1: NP_001105636.1

Maize lines are available at the Maize Cooperative (<http://maizecoop.cropsci.uiuc.edu/>) or upon request.

AUTHOR CONTRIBUTIONS

MAB: Formal Analysis, Investigation, Writing – Original Draft, Visualization, Funding acquisition. ANU: Formal analysis, Investigation, Writing – Original Draft Writing – Review and Editing, Visualization, Funding acquisition. PM: Investigation, Writing – Review and Editing, Funding acquisition. MM: Resources, Visualization. LAA: Investigation, Visualization. CGR: Formal analysis, Investigation, Writing – Original Draft, Writing - Review and Editing, Visualization, Supervision, Project administration, Funding acquisition.

Competing interests: Authors declare no competing interests.

REFERENCES

- Abu-Abied, M., Belausov, E., Hagay, S., Peremyslov, V., Dolja, V., and Sadot, E. (2018). Myosin XI-K is involved in root organogenesis, polar auxin transport, and cell division. *J. Exp. Bot.* 69: 2869–2881.
- Boruc, J. et al. (2016). Phosphorylation of MAP65-1 by Arabidopsis Aurora kinases is required for efficient cell cycle progression. *Plant Physiol.*: 01602.2016.
- Boudaoud, A., Burian, A., Borowska-Wykręć, D., Uyttewaal, M., Wrzalik, R., Kwiatkowska, D., and Hamant, O. (2014). FibrilTool, an ImageJ plug-in to quantify fibrillar structures in raw microscopy images. *Nat. Protoc.* 9: 457–463.
- Buschmann, H., Chan, J., Sanchez-Pulido, L., Andrade-Navarro, M.A., Doonan, J.H., and Lloyd, C.W. (2006). Microtubule-associated AIR9 recognizes the cortical division site at preprophase and cell-plate insertion. *Curr. Biol.* 16: 1938–1943.
- Buschmann, H., Dols, J., Kopischke, S., Peña, E.J., Andrade-Navarro, M.A., Heinlein, M., Szymanski, D.B., Zachgo, S., Doonan, J.H., and Lloyd, C.W. (2015). Arabidopsis KCBP interacts with AIR9 but stays in the cortical division zone throughout mitosis via its MyTH4-FERM domain. *J. Cell Sci.* 128: 2033–2046.
- Busson, S., Dujardin, D., Moreau, A., Dompierre, J., and De Mey, J.R. (1998). Dynein and dynactin are localized to astral microtubules and at cortical sites in mitotic epithelial cells. *Curr. Biol.* 8: 541–544.
- Chan, J., Calder, G., Fox, S., and Lloyd, C. (2005). Localization of the microtubule end binding protein EB1 reveals alternative pathways of spindle development in Arabidopsis suspension cells. *Plant Cell* 17: 1737–1748.
- Chugh, M., Reißner, M., Bugiel, M., Lipka, E., Herrmann, A., Roy, B., Müller, S., and Schäffer, E. (2018). Phragmoplast Orienting Kinesin 2 Is a Weak Motor Switching between Processive and Diffusive Modes. *Biophys. J.* 115: 375–385.
- Cleary, A.L. and Smith, L.G. (1998). The Tangled1 gene is required for spatial control of cytoskeletal arrays associated with cell division during maize leaf development. *Plant Cell* 10: 1875–1888.
- Computing, R. and Others (2013). R: A language and environment for statistical computing. Vienna: R Core Team.

- Cutler, S.R. and Ehrhardt, D.W. (2002). Polarized cytokinesis in vacuolate cells of *Arabidopsis*. *Proc. Natl. Acad. Sci. U. S. A.* 99: 2812–2817.
- Doube, M., Kłosowski, M.M., Arganda-Carreras, I., Cordelières, F.P., Dougherty, R.P., Jackson, J.S., Schmid, B., Hutchinson, J.R., and Shefelbine, S.J. (2010). BoneJ: Free and extensible bone image analysis in ImageJ. *Bone* 47: 1076–1079.
- Fischer, U., Kucukoglu, M., Helariutta, Y., and Bhalerao, R.P. (2019). The Dynamics of Cambial Stem Cell Activity. *Annu. Rev. Plant Biol.*
- Flanders, D.J., Rawlins, D.J., Shaw, P.J., and Lloyd, C.W. (1990). Re-establishment of the interphase microtubule array in vacuolated plant cells, studied by confocal microscopy and 3-D imaging. *Development.*
- Gunning, B.E., Hardham, A.R., and Hughes, J.E. (1978). Evidence for initiation of microtubules in discrete regions of the cell cortex in *Azolla* root-tip cells, and an hypothesis on the development of cortical arrays of microtubules. *Planta* 143: 161–179.
- Hamada, T., Igarashi, H., Itoh, T.J., Shimmen, T., and Sonobe, S. (2004). Characterization of a 200 kDa microtubule-associated protein of tobacco BY-2 cells, a member of the XMAP215/MOR1 family. *Plant Cell Physiol.* 45: 1233–1242.
- Hendricks, A.G., Lazarus, J.E., Perlson, E., Gardner, M.K., Odde, D.J., Goldman, Y.E., and Holzbaur, E.L.F. (2012). Dynein tethers and stabilizes dynamic microtubule plus ends. *Curr. Biol.* 22: 632–637.
- Herrmann, A., Livanos, P., Lipka, E., Gadeyne, A., Hauser, M.-T., Van Damme, D., and Müller, S. (2018). Dual localized kinesin-12 POK2 plays multiple roles during cell division and interacts with MAP65-3. *EMBO Rep.* 19: e46085.
- Hotta, T., Kong, Z., Ho, C.-M.K., Zeng, C.J.T., Horio, T., Fong, S., Vuong, T., Lee, Y.-R.J., and Liu, B. (2012). Characterization of the *Arabidopsis* augmin complex uncovers its critical function in the assembly of the acentrosomal spindle and phragmoplast microtubule arrays. *Plant Cell* 24: 1494–1509.
- Kajala, K., Ramakrishna, P., Fisher, A., Bergmann, D.C., De Smet, I., Sozzani, R., Weijers, D., and Brady, S.M. (2014). Omics and modelling approaches for understanding regulation of asymmetric cell divisions in *Arabidopsis* and other angiosperm plants. *Ann. Bot.* 113: 1083–1105.

- Kawamura, E., Himmelspach, R., Rashbrooke, M.C., Whittington, A.T., Gale, K.R., Collings, D.A., and Wasteneys, G.O. (2006). MICROTUBULE ORGANIZATION 1 Regulates Structure and Function of Microtubule Arrays during Mitosis and Cytokinesis in the Arabidopsis Root. *Plant Physiol.* 140: 102–114.
- Kong, Z., Hotta, T., Lee, Y.R., Horio, T., and Liu, B. (2010). The γ -tubulin complex protein GCP4 is required for organizing functional microtubule arrays in Arabidopsis thaliana. *Plant Cell* 22 | 1: 191–204.
- Laan, L., Pavin, N., Husson, J., Romet-Lemonne, G., van Duijn, M., López, M.P., Vale, R.D., Jülicher, F., Reck-Peterson, S.L., and Dogterom, M. (2012). Cortical dynein controls microtubule dynamics to generate pulling forces that position microtubule asters. *Cell* 148: 502–514.
- Lee, Y.-R.J., Hiwatashi, Y., Hotta, T., Xie, T., Doonan, J.H., and Liu, B. (2017). The Mitotic Function of Augmin Is Dependent on Its Microtubule-Associated Protein Subunit EDE1 in Arabidopsis thaliana. *Curr. Biol.* 27: 3891–3897.e4.
- Lee, Y.-R.J. and Liu, B. (2019). Microtubule nucleation for the assembly of acentrosomal microtubule arrays in plant cells. *New Phytol.* 222: 1705–1718.
- Lee, Y.-R.J. and Liu, B. (2013). The rise and fall of the phragmoplast microtubule array. *Curr. Opin. Plant Biol.* 16: 757–763.
- Li, H., Sun, B., Sasabe, M., Deng, X., Machida, Y., Lin, H., Julie Lee, Y.-R., and Liu, B. (2017). Arabidopsis MAP65-4 plays a role in phragmoplast microtubule organization and marks the cortical cell division site. *New Phytol.* 215: 187–201.
- Lipka, E., Gadeyne, A., Stöckle, D., Zimmermann, S., De Jaeger, G., Ehrhardt, D.W., Kirik, V., Van Damme, D., and Müller, S. (2014). The Phragmoplast-Orienting Kinesin-12 Class Proteins Translate the Positional Information of the Preprophase Band to Establish the Cortical Division Zone in Arabidopsis thaliana. *Plant Cell* 26: 2617–2632.
- Liu, B., Joshi, H.C., and Palevitz, B.A. (1995). Experimental manipulation of γ -tubulin distribution in Arabidopsis using anti-microtubule drugs. *Cell Motil. Cytoskeleton* 31: 113–129.
- Livanos, P. and Müller, S. (2019). Division Plane Establishment and Cytokinesis. *Annu. Rev. Plant Biol.*

- Lough, K.J., Byrd, K.M., Descovich, C.P., Spitzer, D.C., Bergman, A.J., Beaudoin, G.M., Reichardt, L.F., and Williams, S.E. (2019). Telophase correction refines division orientation in stratified epithelia. *Elife* 8.
- Lucas, J.R. (2021). Appearance of microtubules at the cytokinesis to interphase transition in *Arabidopsis thaliana*. *Cytoskeleton* 78: 361–371.
- Lucas, J.R. and Sack, F.D. (2012). Polar development of preprophase bands and cell plates in the *Arabidopsis* leaf epidermis. *Plant J.* 69: 501–509.
- Martinez, P., Dixit, R., Balkunde, R.S., Zhang, A., O’Leary, S.E., Brakke, K.A., and Rasmussen, C.G. (2020). TANGLED1 mediates microtubule interactions that may promote division plane positioning in maize. *J. Cell Biol.* 219.
- Martinez, P., Luo, A., Sylvester, A., and Rasmussen, C.G. (2017). Proper division plane orientation and mitotic progression together allow normal growth of maize. *Proc. Natl. Acad. Sci. U. S. A.* 114: 2759–2764.
- Miki, T., Naito, H., Nishina, M., and Goshima, G. (2014). Endogenous localizome identifies 43 mitotic kinesins in a plant cell. *Proc. Natl. Acad. Sci. U. S. A.* 111: E1053–E1061.
- Mills, A.M., Morris, V.H., and Rasmussen, C.G. (2022). Localization of PHRAGMOPLAST ORIENTING KINESIN1 at the division site depends on the microtubule binding proteins TANGLED1 and AUXIN-INDUCED IN ROOT CULTURES9 in *Arabidopsis*. *Plant Cell*.
- Mohanty, A., Luo, A., DeBlasio, S., Ling, X., Yang, Y., Tuthill, D.E., Williams, K.E., Hill, D., Zadrozny, T., Chan, A., Sylvester, A.W., and Jackson, D. (2009). Advancing cell biology and functional genomics in maize using fluorescent protein-tagged lines. *Plant Physiol.* 149: 601–605.
- Molchan, T.M., Valster, A.H., and Hepler, P.K. (2002). Actomyosin promotes cell plate alignment and late lateral expansion in *Tradescantia* stamen hair cells. *Planta* 214: 683–693.
- Müller, S., Han, S., and Smith, L.G. (2006). Two kinesins are involved in the spatial control of cytokinesis in *Arabidopsis thaliana*. *Curr. Biol.* 16: 888–894.
- Murata, T., Sano, T., Sasabe, M., Nonaka, S., Higashiyama, T., Hasezawa, S., Machida, Y., and Hasebe, M. (2013). Mechanism of microtubule array expansion in the cytokinetic phragmoplast. *Nat. Commun.* 4: 1967.

- Nakamura, M., Ehrhardt, D.W., and Hashimoto, T. (2010). Microtubule and katanin-dependent dynamics of microtubule nucleation complexes in the acentrosomal Arabidopsis cortical array. *Nat. Cell Biol.* 12: 1064–1070.
- Nakaoka, Y., Miki, T., Fujioka, R., Uehara, R., Tomioka, A., Obuse, C., Kubo, M., Hiwatashi, Y., and Goshima, G. (2012). An inducible RNA interference system in *Physcomitrella patens* reveals a dominant role of augmin in phragmoplast microtubule generation. *Plant Cell* 24: 1478–1493.
- Nan, Q., Liang, H., Mendoza, J., Liu, L., Fulzele, A., Wright, A., Bennett, E.J., Rasmussen, C.G., and Facette, M.R. (2021). The OPAQUE1/DISCORDIA2 myosin XI is required for phragmoplast guidance during asymmetric cell division in maize. *bioRxiv*: 2021.08.29.458084.
- van Oostende-Triplet, C., Guillet, D., Triplet, T., Pandzic, E., Wiseman, P.W., and Geitmann, A. (2017). Vesicle Dynamics during Plant Cell Cytokinesis Reveals Distinct Developmental Phases. *Plant Physiol.* 174: 1544–1558.
- Otegui, M. and Staehelin, L.A. (2000). Cytokinesis in flowering plants: more than one way to divide a cell. *Curr. Opin. Plant Biol.* 3: 493–502.
- Panteris, E., Adamakis, I.-D.S., Voulgari, G., and Papadopoulou, G. (2011). A role for katanin in plant cell division: microtubule organization in dividing root cells of *fra2* and *lue1* Arabidopsis thaliana mutants. *Cytoskeleton* 68: 401–413.
- Panteris, E., Apostolakos, P., and Galatis, B. (1995). Telophase-interphase transition in taxol-treated Triticum root cells: cortical microtubules appear without the prior presence of a radial perinuclear array. *Protoplasma* 188: 78–84.
- Rasmussen, C.G. (2016). Using Live-Cell Markers in Maize to Analyze Cell Division Orientation and Timing. *Methods Mol. Biol.* 1370: 209–225.
- Rasmussen, C.G. and Bellinger, M. (2018). An overview of plant division-plane orientation. *New Phytol.*
- Rasmussen, C.G., Sun, B., and Smith, L.G. (2011). Tangled localization at the cortical division site of plant cells occurs by several mechanisms. *J. Cell Sci.* 124: 270–279.
- Sasabe, M. and Machida, Y. (2012). Regulation of organization and function of microtubules by the mitogen-activated protein kinase cascade during plant cytokinesis. *Cytoskeleton* 69: 913–918.

- Sasabe, M., Soyano, T., Takahashi, Y., Sonobe, S., Igarashi, H., Itoh, T.J., Hidaka, M., and Machida, Y. (2006). Phosphorylation of NtMAP65-1 by a MAP kinase down-regulates its activity of microtubule bundling and stimulates progression of cytokinesis of tobacco cells. *Genes Dev.* 20: 1004–1014.
- Sasaki, T., Tsutsumi, M., Otomo, K., Murata, T., Yagi, N., Nakamura, M., Nemoto, T., Hasebe, M., and Oda, Y. (2019). A Novel Katanin-Tethering Machinery Accelerates Cytokinesis. *Curr. Biol.* 29: 4060–4070.e3.
- Schmidt, S. and Smertenko, A. (2019). Identification and characterization of the land-plant-specific microtubule nucleation factor MACET4. *J. Cell Sci.* 132.
- Smertenko, A. et al. (2017). Plant Cytokinesis: Terminology for Structures and Processes. *Trends Cell Biol.* 27: 885–894.
- Stöckle, D., Herrmann, A., Lipka, E., Lauster, T., Gavidia, R., Zimmermann, S., and Müller, S. (2016). Putative RopGAPs impact division plane selection and interact with kinesin-12 POK1. *Nat Plants* 2: 16120.
- Thévenaz, P. (1998). StackReg: an ImageJ plugin for the recursive alignment of a stack of images. Biomedical Imaging Group, Swiss Federal Institute of Technology Lausanne 2012.
- Van Damme, D. and Geelen, D. (2008). Demarcation of the cortical division zone in dividing plant cells. *Cell Biol. Int.* 32: 178–187.
- Vavrdová, T., Šamajová, O., Křenek, P., Ovečka, M., Floková, P., Šnaurová, R., Šamaj, J., and Komis, G. (2019). Multicolour three dimensional structured illumination microscopy of immunolabeled plant microtubules and associated proteins. *Plant Methods* 15: 22.
- Venverloo, C.J. and Libbenga, K.R. (1987). Regulation of the Plane of Cell Division in Vacuolated Cells I. The Function of Nuclear Positioning and Phragmosome Formation. *J. Plant Physiol.* 131: 267–284.
- Walker, K.L., Müller, S., Moss, D., Ehrhardt, D.W., and Smith, L.G. (2007). Arabidopsis TANGLED Identifies the Division Plane throughout Mitosis and Cytokinesis. *Curr. Biol.* 17: 1827–1836.
- Wasteneys, G.O. and Williamson, R.E. (1989). Reassembly of microtubules in *Nitella tasmanica*: assembly of cortical microtubules in branching clusters and its relevance to steady-state microtubule assembly. *J. Cell Sci.* 93: 705–714.

- Wickham, H., Chang, W., and Others (2008). ggplot2: An implementation of the Grammar of Graphics. R package version 0. 7, URL: <http://CRAN.R-project.org/package=ggplot2> 3.
- Wick, S.M. (1985). Immunofluorescence microscopy of tubulin and microtubule arrays in plant cells. III. Transition between mitotic/cytokinetic and interphase microtubule arrays. *Cell Biol. Int. Rep.* 9: 357–371.
- Wu, Q., Luo, A., Zadrozny, T., Sylvester, A., and Jackson, D. (2013). Fluorescent protein marker lines in maize: generation and applications. *Int. J. Dev. Biol.* 57: 535–543.
- Wu, S.-Z. and Bezanilla, M. (2014). Myosin VIII associates with microtubule ends and together with actin plays a role in guiding plant cell division. *Elife* 3.
- Yamada, M., Tanaka-Takiguchi, Y., Hayashi, M., Nishina, M., and Goshima, G. (2017). Multiple kinesin-14 family members drive microtubule minus end-directed transport in plant cells. *J. Cell Biol.* 216: 1705–1714.
- Yasuhara, H., Muraoka, M., Shogaki, H., Mori, H., and Sonobe, S. (2002). TMBP200, a microtubule bundling polypeptide isolated from telophase tobacco BY-2 cells is a MOR1 homologue. *Plant Cell Physiol.* 43: 595–603.
- Yoneda, A., Akatsuka, M., Kumagai, F., and Hasezawa, S. (2004). Disruption of Actin Microfilaments Causes Cortical Microtubule Disorganization and Extra-Phragmoplast Formation at M/G1 Interface in Synchronized Tobacco Cells. *Plant Cell Physiol.* 45: 761–769.
- Young, D.H. and Lewandowski, V.T. (2000). Covalent binding of the benzamide RH-4032 to tubulin in suspension-cultured tobacco cells and its application in a cell-based competitive-binding assay. *Plant Physiol.* 124: 115–124.
- Zhou, R., Liu, H., Ju, T., and Dixit, R. (2020). Quantifying the polymerization dynamics of plant cortical microtubules using kymograph analysis. *Methods Cell Biol.* 160: 281–293.

CHAPTER 3:
DE NOVO TANGLED1 RECRUITMENT FROM THE PHRAGMOPLAST TO ABERRANT
CELL PLATE FUSION SITES IN MAIZE

Aimee N. Uyehara¹, Beatrice N. Diep^{1,2}, Lindy A. Allsman¹, Sarah G. Gayer¹, Stephanie E. Martinez¹, Janice J. Kim¹, Shreya Agarwal¹, Carolyn G. Rasmussen^{1*}

¹Department of Botany and Plant Sciences, Center for Plant Cell Biology, University of California, Riverside, CA, USA 92521

² Current address: Cellular and Molecular Biology Graduate Program, University of Wisconsin, Madison, WI, USA 53706

* Corresponding author: crasmu@ucr.edu

ORCID:

CGR 0000-0002-4354-6295

ANU 0000-0003-4010-4771

BND 0009-0004-0199-9976

LAA 0000-0002-0190-9086

SGG 0000-0002-1032-5971

SEM 0000-0002-7008-5164

JJK 0009-0000-2138-8823

Keywords: Preprophase band, division, phragmoplast, mitosis, cytoskeleton, maize

SUMMARY STATEMENT

The plant division site protein TANGLED1 is recruited to de novo cell plate insertion sites independently of the preprophase band.

ABSTRACT

Division plane positioning is critical for proper growth and development in many organisms. In plants, the division plane is established before mitosis, by accumulation of a cytoskeletal structure called the preprophase band (PPB). The PPB is thought to be essential for recruitment of division site localized proteins, which remain at the division site after the PPB disassembles. Here, we show that a division site localized protein, TANGLED1 (TAN1), is recruited independently of the PPB to the cell cortex by the plant cytokinetic machinery, the phragmoplast, using the PPB-defective mutant *discordia1* and chemical treatments that disrupt the phragmoplast. TAN1 recruitment to de novo sites on the cortex is partially dependent on intact actin filaments and the myosin XI motor protein OPAQUE1 (O1). These data imply a yet unknown role for TAN1 and possibly other division site localized proteins during the last stages of cell division when the phragmoplast touches the cell cortex to complete cytokinesis.

INTRODUCTION

In typical land plant cell divisions, two cytoskeletal structures participate in division plane positioning: the PPB, which assembles during late G2, and the phragmoplast, which assembles during telophase and expands to complete cytokinesis. The PPB is a transient cortical ring of microtubules and actin that is an early indicator of the cell division plane (Pickett-Heaps and Northcote, 1966; Kakimoto and Shibaoka, 1987; Mineyuki, 1999; Smertenko *et al.*, 2017). Following chromosome and organelle redistribution in metaphase and anaphase, the phragmoplast forms to facilitate cell plate formation which divides the two daughter cells (Gunning, 1982; Samuels, Giddings and Staehelin, 1995; Müller and Jürgens, 2016). The location where cytokinesis is completed is the cell-plate fusion site, and if the cell plate fuses at the location previously marked by the PPB, that location is called the division site (Smertenko *et al.*, 2017).

Genetic disruption of PPB formation often leads to significantly stunted growth, division plane positioning defects, and disrupted cortical microtubule organization which may impede cell expansion (Whittington *et al.*, 2001; Torres-Ruiz and Jürgens, 1994; Camilleri *et al.*, 2002; Kawamura *et al.*, 2006; Azimzadeh *et al.*, 2008; Wright, Gallagher and Smith, 2009; Drevensek *et al.*, 2012; Kirik, Ehrhardt and Kirik, 2012; Spinner *et al.*, 2013; Kumari *et al.*, 2021; Muroyama *et al.*, 2023). However, absence of >80% of PPBs generates macroscopically normal plants with minor division plane orientation defects that were attributed to spindle positioning defects (Ambrose and Cyr, 2008; Shaefer *et al.* 2017).

PPB formation requires the PROTEIN PHOSPHATASE TYPE 2A (PP2A) B” regulatory subunit encoded by two related genes in maize called *discordia1* (*dcd1*) and *alternative discordia1* (*add1*) (Gallagher and Smith, 1999; Wright, Gallagher and Smith,

2009), homologs to *fass/ton2* in *Arabidopsis* (Torres-Ruiz and Jürgens, 1994; Camilleri *et al.*, 2002). In *A. thaliana* FASS/DCD1/ADD1 forms a complex with microtubule-binding proteins including TONNEAU1, TONNEAU1-RECRUITING-MOTIF proteins, and other PP2A subunits that disrupt cortical microtubule organization and PPB formation (Wright, Gallagher and Smith, 2009; Spinner *et al.*, 2013). While *dcd1 add1* is seedling lethal and never forms PPBs, single *dcd1* mutants grow well and do not have PPB formation defects in symmetrically dividing cells (Wright *et al.* 2009). Instead, *dcd1* single mutants produce defective PPBs in several asymmetrically dividing cells such as the grass-specific stomatal complex subsidiary cells, leading to division positioning defects. Subsidiary cells, generated from an asymmetric division, serve as an excellent model to analyze division-plane orientation due to consistently positioned divisions and well-characterized signaling pathways (Gray *et al.* 2020; Spiegelhalder and Raissig 2021; Ashraf *et al.* 2023).

The PPB serves as a hub to recruit multiple proteins, including a small subset that remains at the division site after PPB disassembly. One division-site localized protein, TANGLED1 (TAN1), binds microtubules and is required for properly oriented divisions (Smith *et al.* 1996; Smith *et al.* 2001, Martinez *et al.* 2017, Martinez *et al.* 2020). TAN1 localization to the division site requires an intact PPB, where it is maintained until cytokinesis is completed (Walker *et al.* 2007; Rasmussen *et al.* 2011; Martinez *et al.* 2017). In maize, TAN1 also colocalizes with the phragmoplast midline (Martinez *et al.* 2017). The maize *tan1* mutant has mostly normally placed PPBs, but phragmoplast guidance defects lead to misoriented symmetric and asymmetric divisions (Smith *et al.* 1996; Martinez *et al.* 2017; Martinez *et al.* 2020). TAN1 promotes contact angle

independent microtubule interactions which guide the phragmoplast to the division site (Bellinger et al. 2023; Martinez et al. 2020).

Here, we use the partially defective PPBs in *dcd1* mutants to measure the contribution of PPB formation to division plane positioning. To our surprise, and contrary to previous reports, the *dcd1* mutant revealed an unexpected de novo recruitment of TANGLED1 from the phragmoplast to misoriented cell plate fusion sites. We demonstrate that de novo TAN1 accumulation occurs in multiple mutants and chemically treated cells that have division plane positioning defects. Further, TAN1 accumulation is partially dependent on actin and a myosin XI OPAQUE1 (O1).

RESULTS AND DISCUSSION

Defects in *dcd1* PPB formation reduce TAN1-YFP accumulation

To determine whether partially defective PPBs affect TAN1 recruitment to the division site, we observed TAN1-YFP in *dcd1* and wild-type siblings with the microtubule marker CFP-TUBULIN (Martinez *et al.*, 2017). Wild-type subsidiary cells had no defects in PPB formation or TAN1-YFP accumulation (n = 0/112 cells from 19 plants, Figure 3.1A, Supplemental Figure S3.1A). In contrast, *dcd1* cells often had defective PPBs that incompletely encircled the cell, similar to previous results (~40%, Wright, Gallagher and Smith, 2009) (38%, n = 42/110 cells from 7 plants). Defective PPBs had uneven microtubule accumulation, including one-sided accumulation (“singular”, Figure 3.1B, Supplemental Figure S3.1B). Correspondingly, uneven or singular TAN1-YFP accumulation at the division site was observed in preprophase/prophase (35% n = 38/110 from 7 *dcd1* plants) in metaphase and anaphase (35%, n = 16/46), and in telophase (41%, n = 65/157, Figure 3.1C), suggesting that PPB establishment is required for TAN1 recruitment to the division site.

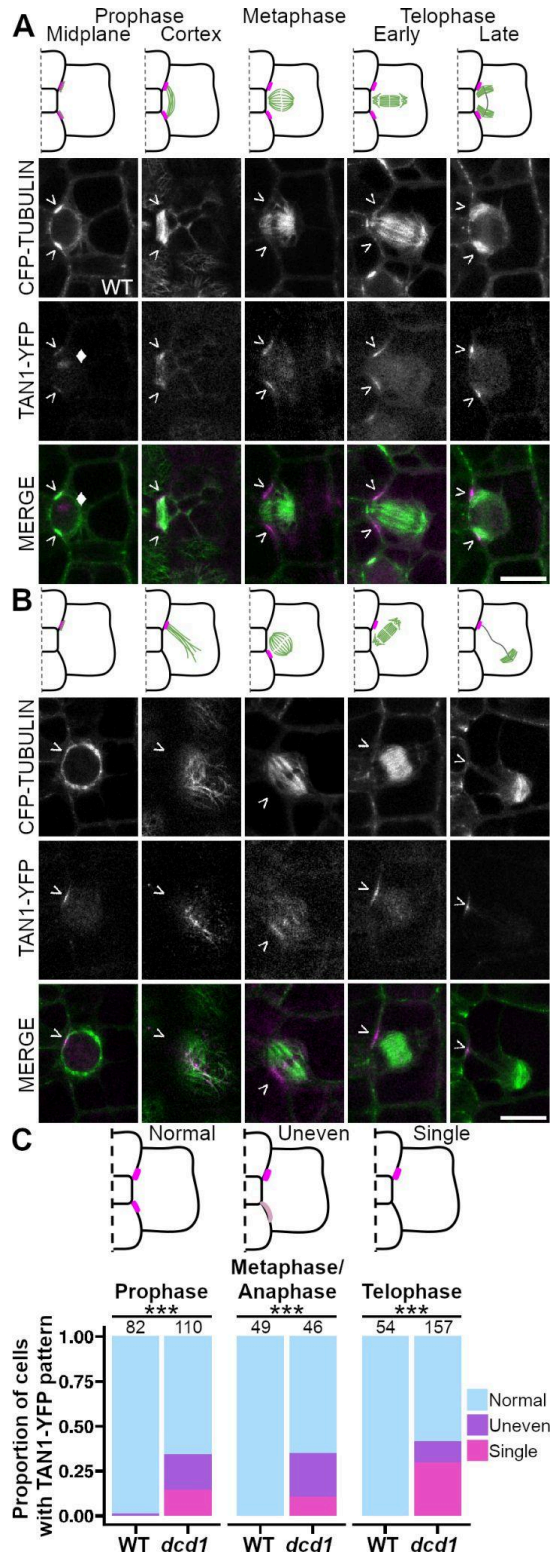
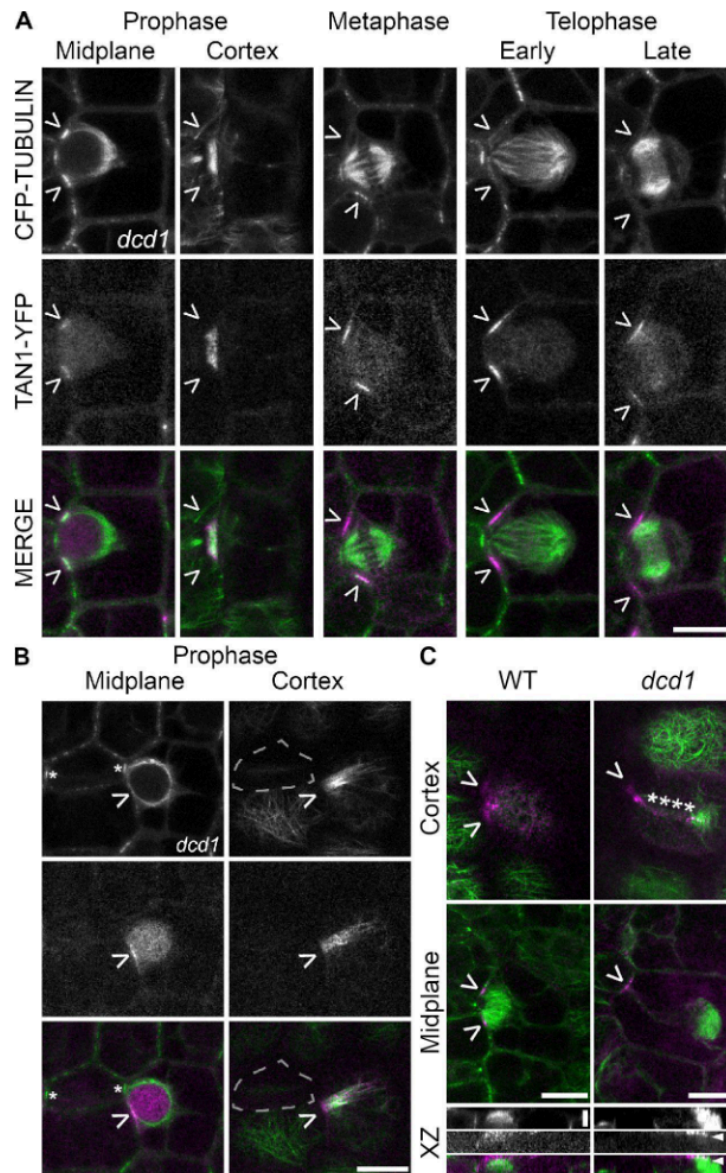


Figure 3.1. PPB formation and TAN1-YFP recruitment is defective in *dcd1*.

(A-B) Model of (A) wild-type or (B) *dcd1* subsidiary cell divisions. Cell walls (black), microtubule structures (green), and TAN1-YFP (magenta) are shown. Below are representative images with CFP-TUBULIN labeling microtubules (green) and TAN1-YFP (magenta) labeling the division site (>) and sometimes the nucleolus indicated with a diamond (◆). (C) Observed TAN1-YFP accumulation patterns. Darker and lighter shades of magenta represent higher and lower TAN1-YFP intensities reflecting greater or less accumulation, respectively. Below, stacked bar plot comparing wild-type and *dcd1* cells that exhibit various TAN1-YFP patterns represented by the schematic models above. Numbers above bars represent cells examined. Asterisks (***) mark significant difference, $P < 0.001$, Fisher's Exact Test. $N = 19$ wild-type plants and 7 *dcd1* plants. Scale bars = 10 μm .



Supplemental Figure S3.1. Confocal micrographs of divisions in wild type (WT) and *dcd1* plants.

(A) Representative images of correctly oriented *dcd1* divisions expressing CFP-TUBULIN (green) and TAN1-YFP (magenta) with typical microtubule structures and TAN1-YFP localization. (B) An additional example of a defective preprophase band in *dcd1* with CFP-TUBULIN and TAN1-YFP accumulation on one division site and missing from the other. Asterisks mark the typical interphase microtubule accumulation in the neighboring guard mother cell. Dotted lines outline the guard mother cell. Carets point to the division site. (C) Micrographs of wild type (left) and *dcd1* (right) cells in telophase at the cell cortex and midplane expressing CFP-TUBULIN (microtubules, green) and TAN1-YFP (magenta). Below, the CFP-TUBULIN, TAN1-YFP, and merged channels of XZ-projections showing the side view of the cell. Z-slices were taken at 0.25 μm intervals. Scale bars for A-C cortex and midplane view are 10 μm , and 3.4 μm for the XZ projections in C.

Defective PPBs in *dcd1* mutants cause division plane positioning defects

Like many studies that have examined the role of the PPB in division plane positioning (Camilleri *et al.*, 2002; Azimzadeh *et al.*, 2008; Drevensek *et al.*, 2012; Schaefer *et al.*, 2017; W. Wang *et al.*, 2019; Kumari *et al.*, 2021), our initial analysis of *dcd1* was performed using static images. This data generated strong correlative support for the role of the PPB in division plane positioning, but cell division trajectories were not analyzed. To directly assess the relationship between PPB formation, TAN1 accumulation, and final division positioning, 12-minute time intervals were used to track divisions, capitalizing both on the invariant positions of subsidiary cell divisions and the *dcd1* partial PPB formation defects (Figure 3.2A-D). At *dcd1* subsidiary cell division sites (n = 374 division sites total from 4 plants), we measured the TAN1-YFP and/or CFP-TUBULIN fluorescence intensities and classed final divisions as ‘oriented’ or ‘misoriented’ dependent upon whether the phragmoplast returned to the division site. Robust PPB microtubule accumulation strongly predicts correctly oriented cell divisions. Division sites with undetectable TAN1-YFP tended to be misoriented (79%, n = 26/33 cells with TAN1-YFP fluorescence intensity at background levels, Figure 3.2E). For cell divisions captured in later stages, 94% (metaphase, anaphase, or telophase, n = 50/53) of misoriented final divisions were associated with undetectable TAN1-YFP intensity at the time lapse onset (Figure 3.2F, n = 112 cells). These data show that the PPB is essential for division plane positioning in subsidiary mother cell divisions and that TAN1-YFP localization at the division site is a reasonable proxy for previous preprophase band formation.

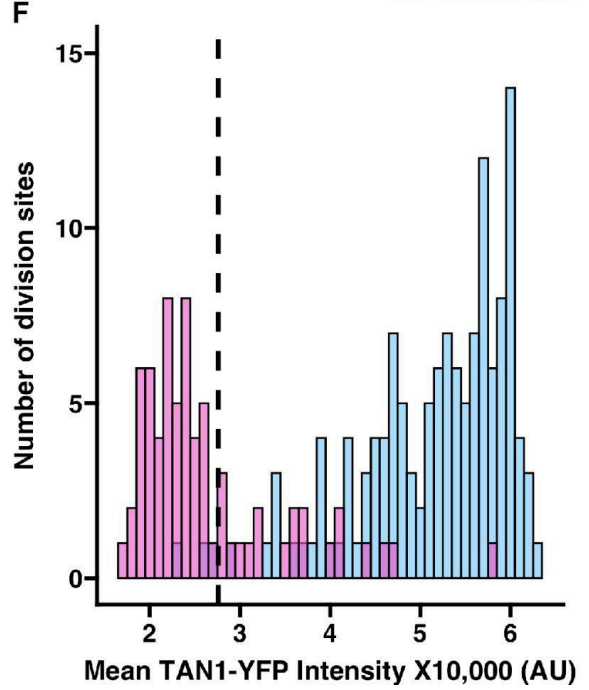
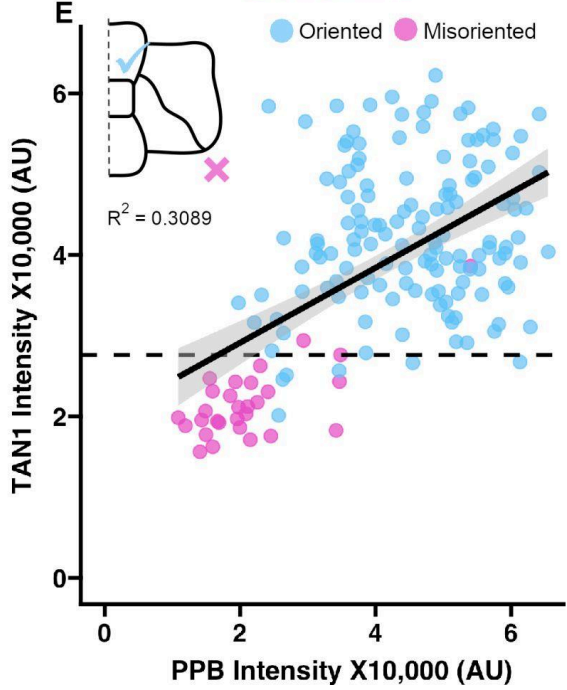
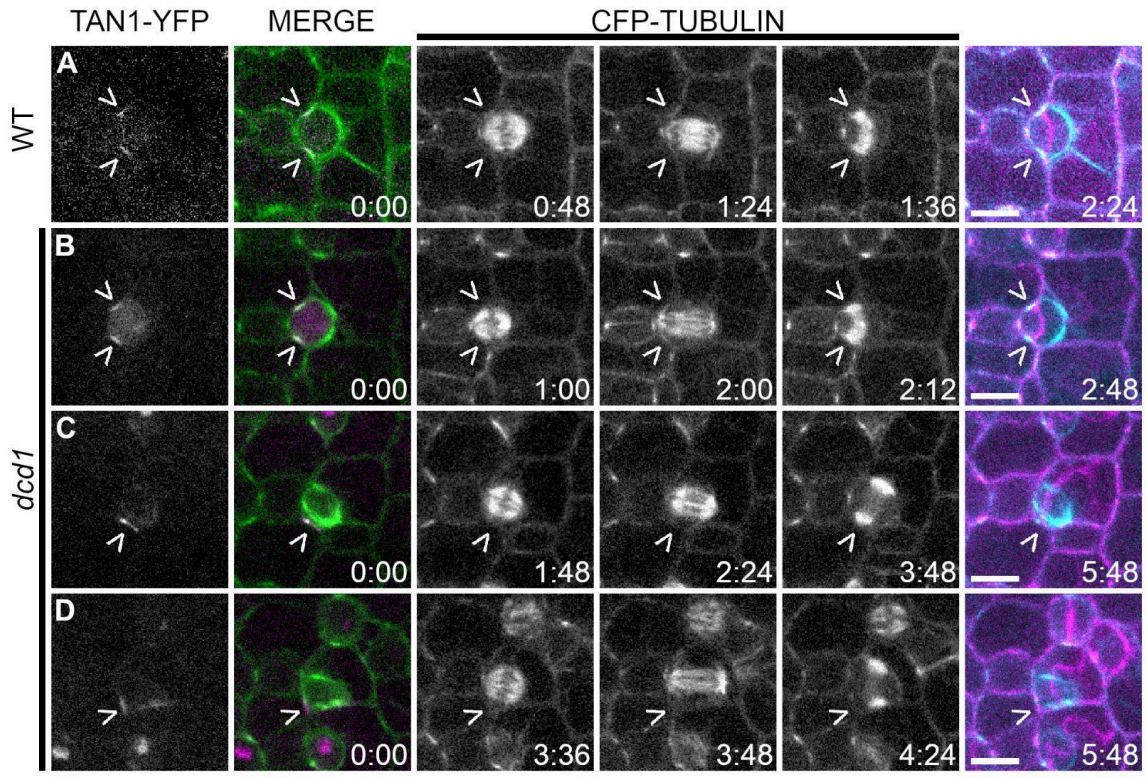


Figure 3.2. Defective preprophase bands and TAN1 localization result in misoriented divisions.

Time lapses of subsidiary cell divisions expressing *CFP-TUBULIN* and *TAN1-YFP* in (A) wild-type cells and (B-D) *dcd1* cells. Left-most columns show TAN1-YFP localization at $t = 0$ (Merge shows both TAN1-YFP (magenta) and microtubules (green)). The last column overlays the PPB in the first frame (cyan) and final division frame (magenta). Carets (>) mark the division site. Scale bars are 10 μm . (E) Comparative TAN1-YFP and PPB intensity from time lapses of *dcd1* cells. "Oriented" describes phragmoplasts that return to the division site and "misoriented" describes cell plate insertion at atypical locations. $n = 85$ cells, $N = 4$ plants. (F) Histogram displaying the mean TAN1-YFP fluorescence intensity of cell division sites in *dcd1* colored by division orientation at the first timepoint for time lapses that start after prophase. For E and F, blue = oriented, magenta = misoriented. Dotted line represents the visible detection limit or the point at which TAN1-YFP fluorescence is distinguishable over background. $n = 112$ cells. $N = 4$ plants.

TAN1-YFP accumulates at misoriented cell plate insertion sites.

dcd1 cytokinesis often completes in aberrant locations. Surprisingly, TAN1-YFP accumulated at de novo cell plate fusion sites (n = 21 misoriented phragmoplasts, N = 3 plants) (Figure 3.3A, B, E). Time-lapse imaging revealed that de novo TAN1-YFP accumulation trails behind the phragmoplast after it touches the cortex (Figure 3.3B, n = 22/22 cells from 3 plants, Supplemental Figure S3.1C). TAN1-YFP has been previously shown to accumulate near the phragmoplast midline (Martinez *et al.*, 2017). This suggests that TAN1-YFP may be transported from the phragmoplast to the cell cortex, independently from the PPB.

TAN1-YFP accumulated at the cell cortex in the *dcd1 add1* double mutant cells that never make PPBs (Figure 3.3C, Supplemental Figure S3.2) (Wright, Gallagher and Smith, 2009). *dcd1 add1* mutants are seedling lethal, so embryos were imaged 21 days after pollination. Wild-type cells showed normal TAN1-YFP division site accumulation at all stages (100%, n = 304 cells, n = 24 kernels, Supplemental Figure S3.2A). In *fass/tonneau2* mutants and in cells treated with microtubule depolymerizing drugs, AtTAN::YFP was not observed at the cortex (Walker *et al.*, 2007; Rasmussen, Sun and Smith, 2011). Similarly, in the *dcd1 add1* mutant, TAN1-YFP was not observed at the cortex in preprophase/prophase to anaphase cells (0%, n = 0/71 cells, n = 9 kernels, Supplemental Figure S3.2B). However, TAN1-YFP often accumulated at the cell cortex in telophase (72%, n = 36/50 cells from 9 kernels). Higher resolution imaging revealed that TAN1-YFP accumulated only after the phragmoplast touched the cortex (100%, n = 53/53 cells, N = 4 kernels), not before (n = 11/11 cells from 4 kernels) (Figure 3.3C, Supplemental Figure S3.2). TAN1-YFP rarely accumulated at the cortex ahead of the

phragmoplast (4%, n = 2/53, Supplemental Figure S3.3). These data further indicate that TAN1-YFP can be recruited to the cell cortex independently of the PPB.

When additional or misoriented phragmoplast arms were generated in wild-type cells using the herbicide chlorpropham (CIPC), TAN1-YFP was recruited to de novo cell plate fusion sites (Figure 3.3D). CIPC generates branched phragmoplasts through its tubulin binding activity but does not affect PPB formation (Liu, Joshi and Palevitz, 1995; Eleftheriou and Bekiari, 2000; Buschmann *et al.*, 2006). Wild-type cells expressing *TAN1-YFP* and *CFP-TUBULIN* were treated for two hours with 0.7 μ M or 1 μ M CIPC or the respective DMSO controls and imaged. De novo TAN1-YFP was observed after additional or misoriented phragmoplast arms contacted the cortex (Figure 3.3E, 67%, n = 31/46 cells from 3 plants).

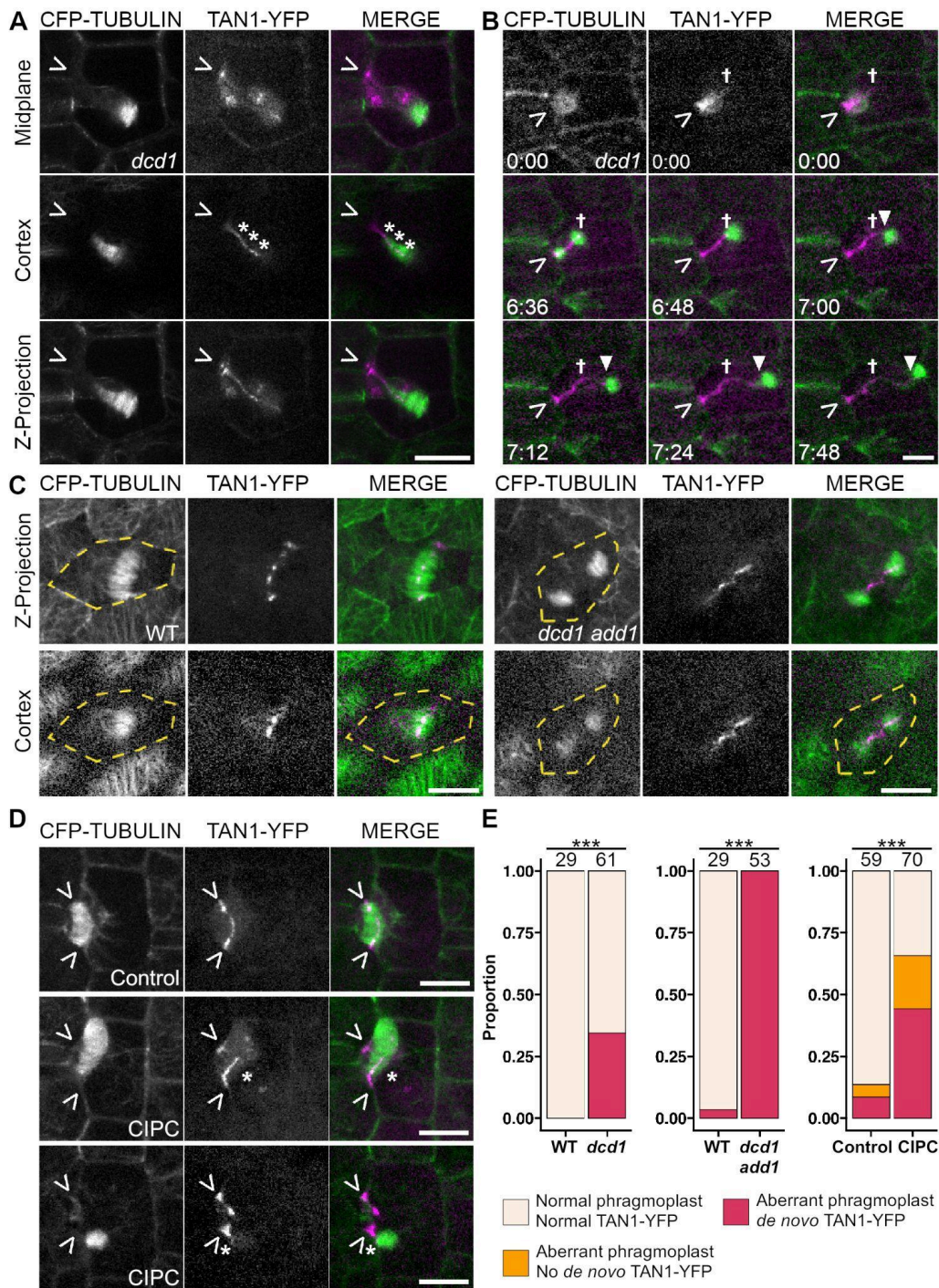
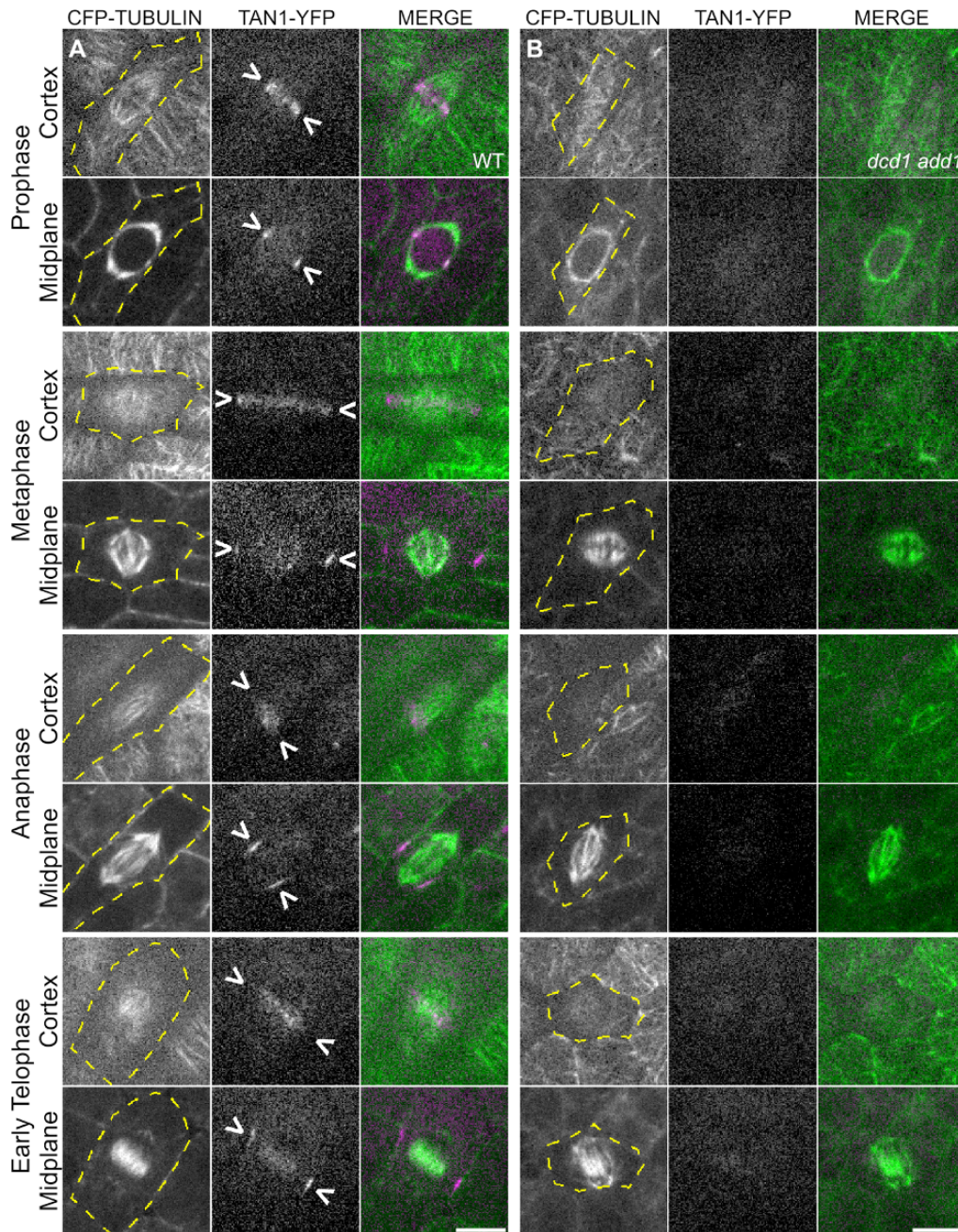


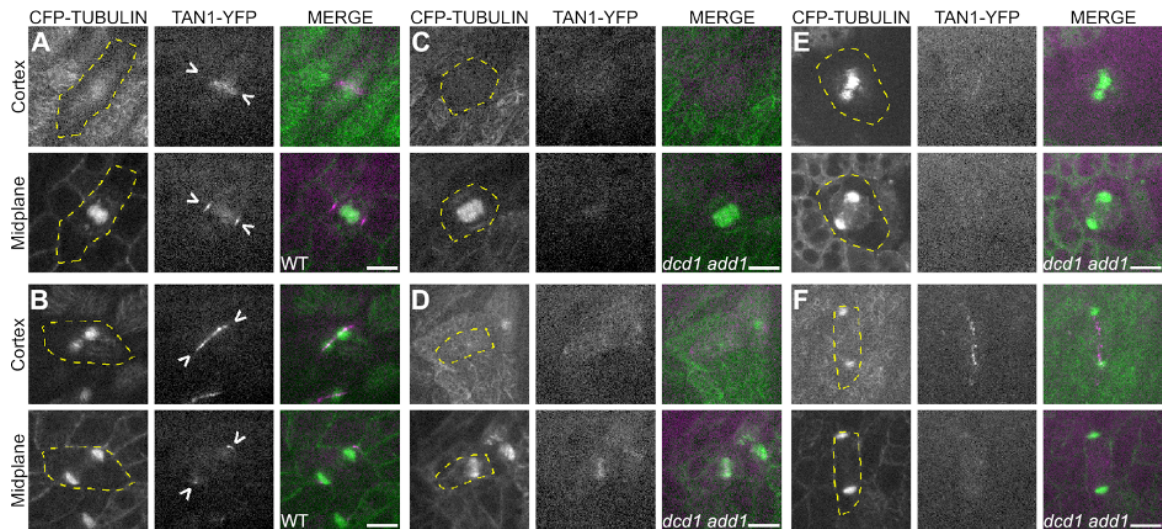
Figure 3.3. Cell plate insertion sites accumulate de novo TAN1-YFP. (A-D) CFP-TUBULIN (green) and TAN1-YFP (magenta) in various dividing cells. Carets (>) mark the division site and asterisks (*) mark de novo TAN1-YFP.

(A) *dcd1* subsidiary mother cell with **de novo** cortex-localized TAN1-YFP indicated with asterisks. (B) Time lapse of a *dcd1* cell cortex during phragmoplast expansion. Dagger (†) marks the edge of TAN1-YFP previously recruited in prophase and the triangle (▼) marks movement of the phragmoplast. Time stamps are in Hours:Minutes. (C) Z-projection and cortex views of wild type and *dcd1 add1* mutant embryos in telophase. Yellow dotted lines outline the cell. (D) Representative Z-projections of subsidiary mother cell phragmoplasts from CIPC and DMSO control treated samples. Asterisks mark **de novo** TAN1-YFP while carets mark the expected division site. (E) Bar plots of **de novo** TAN1-YFP cell cortex accumulation in *dcd1*, *dcd1 add1*, or DMSO and CIPC treated wild-type plants. Numbers above bars represent total cell numbers. $N \geq 3$ plants or kernels of each genotype or treatment. Asterisks indicate significant differences by Fisher's Exact Test, $P < 0.001$. Scale bars = 10 μm .



Supplemental Figure S3.2. TAN1-YFP localization in wild type and the *dcd1 add1* double mutant from prophase to early telophase.

Micrographs of cortex and midplane views of (A) wild-type embryos and (B) *dcd1 add1* embryos expressing CFP-TUBULIN (microtubules, green) and TAN1-YFP (magenta). Arrowheads point to TAN1-YFP localization to the division site and a yellow dotted line marks the cell outline. Scale bars are 10 μ m, all images in the two panels are the same magnification.



Supplemental Figure S3.3. TAN1-YFP localization patterns in *dcd1 add1* embryos.

(A-B) TAN1-YFP localizes to the division site (>) in wild-type embryos (A) before and (B) after the phragmoplast has reached the cell cortex. (C-D) In early telophase cells in *dcd1 add1*, TAN1-YFP is (C) absent from or (D) diffuse at the cell cortex before the phragmoplast has fully expanded. TAN1-YFP is also visible in the phragmoplast midline. (E-F) In late telophase cells in *dcd1 add1*, (E) TAN1-YFP localizes to the cell cortex as a narrow band once the phragmoplast reaches the cortex and (F) rarely localizes ahead of phragmoplast expansion. Scale bar is 10 μm .

Actin and myosin XI OPAQUE1 (O1) facilitate TAN1-YFP accumulation at de novo cell plate insertion sites

Accumulation of TAN1-YFP at de novo cell plate insertion sites is partially dependent on O1. Since TAN1 interacts with PHRAGMOPLAST ORIENTING KINESIN1 (POK1) and POK2 (Müller, Han and Smith, 2006; Rasmussen, Sun and Smith, 2011; Mills, Morris and Rasmussen, 2022), and related kinesin 12s interact with myosin XI motor proteins (Huang *et al.*, 2022; Nan, Liang, *et al.*, 2023), we hypothesized that O1 might be necessary for TAN1-YFP accumulation. TAN1-YFP fluorescence intensity during telophase was reduced but not absent in both correctly oriented and de novo cell plate fusion sites in *o1* compared to wild-type siblings (Figure 3.4A-B, $p = 1.02\text{e-}12$, One-way ANOVA followed by Tukey's HSD). Therefore, O1 facilitates TAN1-YFP accumulation during telophase.

Actin filament disruption also reduced TAN1-YFP accumulation at de novo cell plate fusion sites. Actin filament formation was inhibited with latrunculin B (Lat B) treatment in *dcd1* cells. 10-minute treatments with 25 μ M Lat B inhibited actin polymerization (Supplemental Figure S3.4). Lat B treatment reduced TAN1-YFP accumulation at de novo cell plate fusion sites (Figure 3.4C-E, $P = 0.0417$, Wilcoxon rank sum test). To determine whether de novo TAN1-YFP recruitment or maintenance depends on actin filaments, 10-minute time points were taken after treating *dcd1* cells with control or 25 μ M Lat B (Figure 3.4E). We defined recruitment as accumulation of TAN1-YFP at de novo division sites, and maintenance as the persistence of TAN1-YFP accumulation once the phragmoplast disassembled in that location. In control-treated *dcd1* cells, TAN1-YFP accumulated and remained at the cell cortex as a narrow line following the phragmoplast trajectory ($n = 15/17$ cells, $n = 4$ plants, Figure 3.4E i-ii). Rarely, TAN1-YFP accumulation was reduced ($n = 1/17$) or not maintained at the cell cortex ($n = 1/17$). In Lat B treatments, TAN1 accumulation was often reduced ($n = 13/18$, e.g., Figure 3.4 iii-iv) or not maintained after treatment ($n = 5/18$, e.g., Figure 3.4E v-vi). Therefore, both TAN1-YFP recruitment and maintenance at de novo sites are reduced when actin filaments were disrupted.

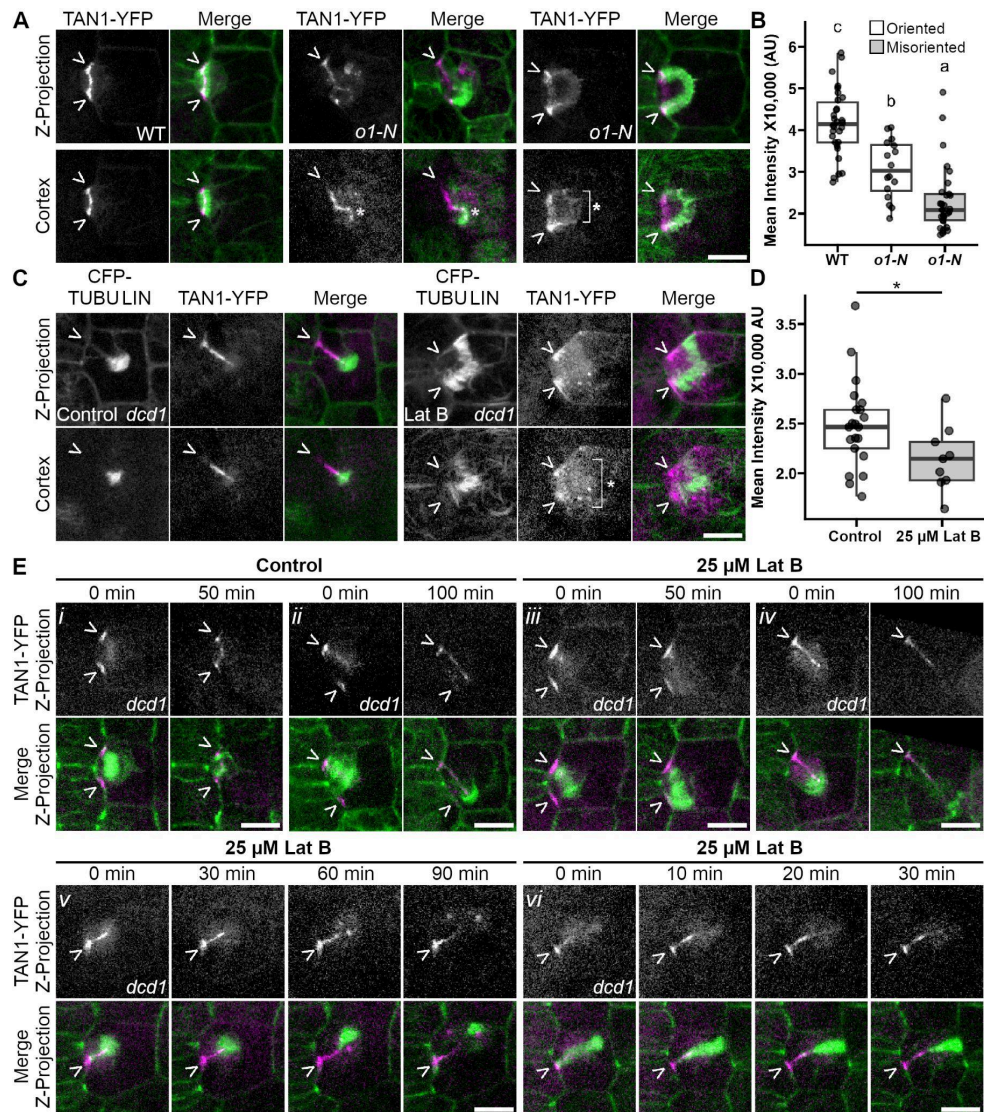
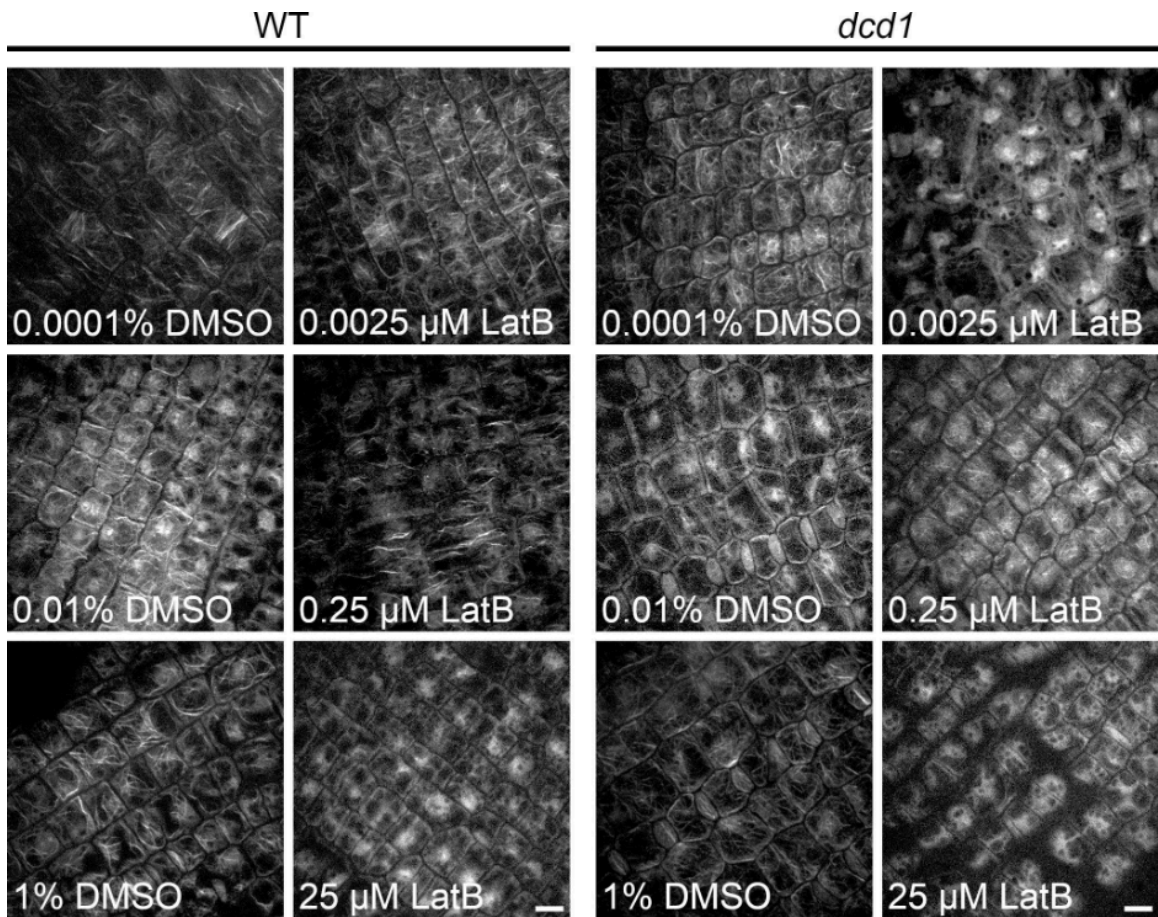


Figure 3.4. Actin and myosin XI motor protein OPAQUE1 increase TAN1 accumulation at de novo cell plate insertion sites.

A) Subsidiary cell divisions in the *opaque1* (*o1-n*) mutant and wild-type siblings. B) Boxplot of TAN1-YFP intensities at telophase in oriented and misoriented divisions in wild type and *o1-n* mutant cells. $P = 1.02e-12$, One-way ANOVA followed by Tukey's HSD, letters mark significant differences between groups. (C) TAN1-YFP accumulation in control and 25 μ M Lat B treated *dcd1* cells. Bracket and asterisk indicate diffuse TAN1-YFP observed in Lat B treatments. (D) Boxplot of TAN1-YFP intensity at misoriented divisions of *dcd1* in DMSO control ($n = 23$ cells, $N = 2$ plants) and 25 μ M Lat B ($n = 9$ cells, $N = 2$ plants) treatments. $P = 0.0417$, Wilcoxon rank sum test. (E) Timelapse of *dcd1* cells in control and Lat B treatments. Panels display two examples each of cells at the beginning and end of control or Lat B treatment: (i-ii) Sharp TAN1 accumulation in control treatment, (iii-iv) reduced TAN1 accumulation in Lat B treatment, and (v-vi) lack of TAN1 maintenance with Lat B treatment. Carets (>) mark the division site and asterisks (*) mark de novo TAN1-YFP. Boxplot horizontal lines represent the quartiles and median. Whiskers are $1.5 \times$ IQR.



Supplemental Figure S3.4. Optimization of latrunculin B treatment for *dcd1* and its wild-type sibling.

Micrographs of actin filaments immunostained with Alex fluor 488-phalloidin. Scale bar is 10 μm.

In the absence of PPB-mediated recruitment, we observe TAN1-YFP accumulation at aberrant cell-plate-fusion sites that is partially dependent on actin filaments and O1. Consistently, when actin is disrupted in *Arabidopsis* root cells, TAN1, POK1 and Myosin XI division-site localization becomes diffuse (Huang *et al.*, 2022). Actin connects the leading edge of the phragmoplast with the division site through the action of myosin VIII in *Physcomitrium patens* (Wu and Bezanilla, 2014) and is required for division plane positioning (Mineyuki and Palevitz, 1990; Gallagher and Smith, 1999; Frank, Cartwright and Smith, 2003; Gilliland *et al.*, 2003; Galatis and Apostolakos, 2004; Facette and Smith, 2012; Vaškebová, Šamaj and Ovecka, 2017). During the late stages of phragmoplast expansion, actin facilitates completion of cell plate fusion (van Oostende-Triplet *et al.*, 2017), a process potentially dependent on recruitment of TAN1 and other division site proteins. Recruitment of other division site proteins (e.g. POK1) to de novo cell plate fusion sites have also been observed in mutants which generate additional ectopic cell plates, suggesting that de novo localization may be a common feature during cytokinesis (Lebecq *et al.*, 2023).

We hypothesize that TAN1-YFP accumulation may reflect the assembly of entire “division-site modules”, which may accelerate completion of cytokinesis. In the *tan1* mutant, phragmoplast disassembly at the cell cortex is significantly delayed, taking twice as long as wild-type phragmoplasts (Martinez *et al.* 2017). Additionally, aberrantly targeted cell plates generated by CIPC treatment retain the cell-plate-specific callose polymer long after properly oriented cell plates replace callose with cellulose, indicating delays in completing cytokinesis (Buschmann *et al.* 2006). We hypothesize that division site proteins facilitate the rapid completion of cytokinesis, and determining how this is accomplished is a fascinating question for future research.

Author Contributions

ANU: Conceptualization, Investigation, Formal Analysis, Visualization, Writing - Original Draft, Writing - Review & Editing, Project administration, Funding acquisition; **BND**: Methodology, Investigation, Formal Analysis, Visualization, Funding acquisition; **LAA**: Methodology, Project administration; **SGG**: Methodology, Investigation, Formal Analysis; **SM**: Investigation, Formal Analysis, Funding acquisition; **JJK**: Formal Analysis; **SA**: Formal Analysis, Funding acquisition; **CGR**: Conceptualization, Resources, Supervision, Funding acquisition, Writing - Original Draft, Writing - Review & Editing, Project administration, Funding acquisition.

Competing Interests

No competing interests declared.

Funding

Funding from NSF-CAREER#1942734, NSF-MCB#1852923 to CGR, from NSF-NRT DBI#1922642 to ANU and SEM, from NSF-DBI#1461297 to SGG, from UCR Chancellor's Fellowship to BND and from UCR RISE Fellowship to SA and BND.

Data availability

All relevant data can be found in the article and its supplementary information.

MATERIALS AND METHODS

RESOURCE AVAILABILITY

Lead contact

Further information and requests for resources and reagents should be directed to and will be fulfilled by Carolyn Rasmussen (crasmu@ucr.edu).

Materials availability

This study did not generate new unique reagents.

Data and code availability

- All data reported in this paper will be shared by the lead contact upon request.
- This paper does not report original code.
- Any additional information required to reanalyze the data reported in this paper is available from the lead contact upon request.

EXPERIMENTAL MODEL DETAILS

Maize (*Zea mays*) plants were grown in standard greenhouse conditions (31-33°C temperature setpoints with supplementary lighting from 5-9 PM at $\sim 400 \mu \text{E m}^{-2} \text{s}^{-1}$) in 1 L pots with soil (20% peat, 50% bark, 10% perlite, and 20% medium vermiculite) supplemented with additional magnesium nitrate (50 ppm N and 45 ppm Mg) and calcium nitrate (75 ppm N and 90 ppm CA) and Osmocote Classic 3-4M (NPK 14-14-14%, AICL SKU#E90550). Alternatively, plants were grown in the field (Agricultural Operations <https://agops.ucr.edu/>, Riverside, CA, USA) to generate maize embryos, which were hand harvested from ears 21-23 days after pollination.

METHOD DETAILS

Plant material and genotyping/phenotyping:

Plants expressing CFP- β -TUBULIN and/or TAN1-YFP (Mohanty *et al.*, 2009; Wu *et al.*, 2013) were genotyped with CFP-TUBULIN forward primer GFP5FOR (5'-GCGACGTAAACGGCCACAAGTTCAG-3') and the reverse primer TubB3433R (5'-CGGAAGCAGATGTCGTAGAGC-3') and the TAN1-YFP forward primer TAN LSP1 (5'-ACGACCGTTAGCACAGAACC-3') and the reverse primer GFP5Rev (5'-CTGAACTTGTGGCCGTTTACGTGCGC-3') or identified by painting leaves with 4 g/L glufosinate (Finale, Bayer) in 0.1% Tween 20 (Sigma). Resistance to glufosinate was assessed after 2–5 d.

The *dcd1 add1* and *dcd1* mutants were a kind gift from Dr. Amanda Wright. The *dcd1-mu1* and *add1* alleles were genotyped according to Wright *et al.* 2009 (Wright, Gallagher and Smith, 2009) using the forward MuE2 (5'-TCCATAATGGCAATTATCTC-3') and the reverse 55862nrev (5'-GGTGCTACATATACGCTAAAG-3') for *dcd1-mu1* and the forward 3dCAPbfor (5'-GTTGTTTTCCCCCTTGGATT-3') and the reverse 3dCAPbrev (5'-CTTGAGTTCTTGTGTTGCTCAG-3') for *add1*. To distinguish between wild type and *add1* mutant alleles, PCR products were digested with the restriction enzyme KpnI overnight and then run on a 4% agarose gel for 90 minutes at 110V. *dcd1* mutant plants were also identified by phenotype using glue impressions of epidermal leaf cells (Allsman, Dieffenbacher and Rasmussen, 2019). The *opaque1/dcd2* mutants were a kind gift from Dr. Michelle Facette. *o1-N1242A* mutants were identified by phenotype using a lightbox and/or glue impressions.

Leaves were dissected for imaging after 3-5 weeks of growth from the whorl until the ligule was 2 mm from the base and the abaxial epidermal cells were placed into a Rose chamber as described (Rasmussen, 2016) to observe dividing cells. For live imaging of wild-type and *dcd1 add1* double mutant embryos, maize plants were grown in the greenhouse or in the field under standard conditions. Ears were harvested 21-23 days after pollination. Embryos were dissected from kernels and loaded onto a Rose chamber with the flat plumule face down (Kiesselbach, 1949).

Chemical treatments

1 M CIPC (CAS 101-21-3 from TCI, #C2555) was dissolved in DMSO. Leaf samples were loaded in 0.7 μ M or 1 μ M CIPC or the respective 0.07% or 0.1% DMSO control in a rose chamber and imaged after 1 to 2 hours of treatment. Samples were loaded into 25 μ M Lat B (Fisher Scientific, #2182-1) or the respective DMSO control. Z stacks were acquired 2 hours after treatment. For time lapse imaging, samples were loaded directly into 40 μ l of 25 μ M Lat B and a time lapse was started with 10-minute time points. To identify what concentration of Lat B was required to depolymerize actin filaments, leaf tissue samples were treated with 0.0025 μ M, 0.25 μ M, or 25 μ M Lat B for 1 hour, fixed, and stained with Alexa Fluor 488 Phalloidin (Fisher Scientific, #A12379) following Nan *et al.* 2019 (Nan, Mendoza and Facette, 2019).

Confocal Microscopy:

Micrographs and time-lapse data were acquired using a Yokogawa W1 spinning disk microscope with an EM-CCD camera (Hamamatsu 9100c) on a Nikon Eclipse TE inverted stand. Solid-state Obis lasers with power ranging from 40 to 100 mW were used in combination with standard emission filters (Chroma Technology). For

TANGLED1-YFP, a 514 nm laser with emission filter 540/30 nm was used. For CFP-TUBULIN, a 445 nm laser with emission filter 480/40 nm was used. Oil or water immersion objectives (60X/1.2 NA, 100X/1.45 NA) were used. Images and time-lapses were taken with Micromanager-1.4 using a 3-axis DC servo motor controller and ASI Piezo Z stage. For time-lapse, 10 or 12 minute time intervals were used as specified with Z-intervals ranging from 3 to 5 μm . For Z-stacks acquired with no timelapse, 0.5 μm steps were used.

Images were also acquired using a Zeiss LSM 880 confocal laser scanning microscope (100X oil objective immersion lens, NA = 1.46) with Airyscan super resolution mode and Z-intervals of 0.25 μm or 3 μm . The 0.25 μm Z-intervals were used to generate the X-Z projection in Supplemental Figure S3.1C. A 514 nm-excitation laser with bandpass filters 465-505 with long-pass 525 filter was used. Images were processed using default Airyscan settings with Zen software (Zeiss).

Figure Preparation

Figures were made using Gnu Image Manipulation Program (Gimp, version 2.10.32, <https://www.gimp.org/>). Image levels were only adjusted linearly and images were enlarged or rotated with no interpolation.

Accessions

CFP-TUBULIN and TAN1-YFP lines were generated by the Maize Cell Genomics Group (Mohanty *et al.*, 2009). Gene sequences can be found at MaizeGDB (<https://www.maizegdb.org/gbrowse>) using the following accession numbers (B73, v4): *DISCORDIA 1* (Zm00001d024857), *ALTERNATIVE DISCORDIA 1* (Zm00001d010862), and *TANGLED 1* (Zm00001d038060).

QUANTIFICATION AND STATISTICAL ANALYSIS

Time lapse images, X-Z projections, and Z-projections were generated using Fiji (ImageJ, <http://rsb.info.nih.gov/ij/>, RRID:SCR_003070). Mean fluorescence intensity was measured using the “straight” or “oval” tool. X-Y drift in time lapses was corrected using the translation function in the StackReg plug-in in ImageJ (Thévenaz, 1998) or the Fast4DReg plugin (Laine *et al.*, 2019). Analysis of TAN1-YFP localization and/or intensity measurements was done by separating the CFP-TUBULIN channel from the TAN1-YFP channel and using the CFP-TUBULIN channel to identify the stage of cell division and location at the midplane or the cell cortex.

For Figure 3.1, TAN1-YFP localization to the division site was described as “Normal”, “Faint”, “Uneven”, or “Single” based on the presence or absence of localization and TAN1-YFP intensity at the cell midplane. “Normal” intensity describes wild type TAN1-YFP localization– two bright accumulations in the subsidiary mother cell that flank the guard mother cell. “Faint” describes two accumulations that are less intense than “normal”. “Uneven” describes two accumulations, one that is more intense than the other. Finally, “Single” describes cells with TAN1-YFP accumulation at one division site and absence from the other. Because there was no statistical difference between the proportion of faint classes between WT and *dcd1*, “Faint” was merged with the “Normal” class.

In Figure 3.2E and F, the fluorescence intensity of TAN1-YFP was measured using a line ROI at the cell midplane, bisecting the region of TAN1-YFP accumulation at the division site. The number of division sites is always twice the number of cells, as at the midplane, the division sites of the subsidiary mother cell flank the guard mother cell. For cells in prophase, the same ROI was used to measure CFP-TUBULIN accumulation

in the preprophase band at the division site (Figure 3.2E). When TAN1-YFP or CFP-TUBULIN accumulation was below detection as frequently observed in *dcd1* subsidiary mother cell divisions, the ROI was selected at the expected division site location for a subsidiary mother cell division.

When analyzing de novo TAN1-YFP localization in *dcd1*, *dcd1 add1*, or the CIPC treated cells in Figure 3E, phragmoplasts were categorized as normal or aberrant, where aberrant includes misoriented phragmoplasts and split phragmoplasts in the CIPC treatments (Figure 3E). TAN1-YFP localization was determined to be “normal” if TAN1-YFP was only observed to localize to the division site, and “de novo” if TAN1-YFP was observed to accumulate at de novo cell plate fusion sites, which were identified by observing the phragmoplast and the cell cortex.

For cortical TAN1-YFP intensity measurements in Figure 3.4B and D, mean intensity was measured using a 2 μm line ROI. For misoriented phragmoplasts, ROIs were drawn starting from the leading edge of the phragmoplast along the phragmoplast midline.

Graphs, tables, and statistics were generated using R(R Core Team, 2023) and Rstudio (Posit team, 2023) using the following packages: tidy, ggplot2, ggprism, ggpubr (Wickham, 2016; Dawson, 2022; Kassambara, 2023; Wickham *et al.*, 2023; Wickham, Vaughan and Girlich, 2023). Statistical details of experiments can be found in the main text and/or figure legends. Significance was defined as $P < 0.05$ and parametric tests were used unless data distribution was non-normal, whereupon an equivalent non-parametric test was used instead. In Figure 3.4B, the One-way ANOVA was followed by a Tukey’s HSD multiple comparison test. For the comparison of categorical variables in Figure 3.1C and Figure 3E, a Fisher’s Exact Test was used.

RESOURCES TABLE

REAGENT or RESOURCE	SOURCE	IDENTIFIER
Chemicals, peptides, and recombinant proteins		
Chlorpropham (CIPC);	TCI	Cat#C2555; CAS:101-21-3
Latrunculin B (Lat B)	Fisher Scientific	Cat#2182-1; CAS: 76343-94-7
Dimethyl sulfoxide (DMSO)	Fisher Scientific	Cat#D128-4; CAS: 67-68-5
Alexa Fluor 488 Phalloidin	Fisher Scientific	Cat#A12379
KpnI	New England Biolabs	Cat#R3142S
Glufosinate (Finale)	Bayer	Cat#4193473
Tween 20	Fisher Scientific	Cat#BP337-500; CAS: 9005-64-5
Experimental models: Organisms/strains		
CFP-TUBULIN maize fluorescent protein tagged line	Maize Cell Genomics Group(Mohanty <i>et al.</i> , 2009); Maize Genetics Cooperation Stock Center (http://maizecoop.cropsci.uiuc.edu)	Stock #UWYO-FP019
TAN1-YFP maize fluorescent protein tagged line	Maize Cell Genomics Group(Mohanty <i>et al.</i> , 2009); Maize Genetics Cooperation Stock Center (http://maizecoop.cropsci.uiuc.edu)	Zm00001d038060 (Zm-B73 REFERENCE-GRAMENE-4.0) or Zm00001eb286860 (Zm-B73-REFERENCE-NAM-5.0); Stock #UWYO-FP017
<i>discordia 1</i>	Gallagher and Smith; Wright et al. 2009 (Gallagher and Smith, 1999; Wright, Gallagher and Smith, 2009)	Zm00001d024857 (Zm-B73 REFERENCE-GRAMENE-4.0) or Zm00001eb418170 (Zm-B73-REFERENCE-NAM-5.0)
<i>alternative discordia 1</i>	Wright et al. 2009 (Wright, Gallagher and Smith, 2009)	Zm00001d010862 (Zm-B73 REFERENCE-GRAMENE-4.0) or Zm00001eb354190 (Zm-B73-REFERENCE-NAM-5.0)
<i>opaque 1</i>	Nan et al. 2023 (Nan, Liang, <i>et al.</i> , 2023)	Zm00001d052110 (Zm-B73 REFERENCE-GRAMENE-4.0) or Zm00001eb193160 (Zm-B73-REFERENCE-NAM-5.0)
Oligonucleotides		
Primer: CFP-TUBULIN Forward Primer (GFP5FOR)	Integrated DNA Technologies	N/A

5'-GCGACGTAAACGGCCACAAG TTCAG-3'		
Primer: CFP-TUBULIN Reverse Primer (TubB3433R) 5'-CGGAAGCAGATGTCGTAGAG C-3'	Integrated DNA Technologies	N/A
Primer: TAN1-YFP Forward Primer (TAN LSP1) 5'-ACGACCGTTAGCACAGAACC- 3'	Integrated DNA Technologies	N/A
Primer: TAN1-YFP Reverse Primer (GFP5Rev) 5'-CTGAACTTGTGGCCGTTTACG TCGC-3'	Integrated DNA Technologies	N/A
Primer: <i>dcd1-mu1</i> Forward Primer (muE2) 5'-TCCATAATGGCAATTATCTC-3'	Integrated DNA Technologies	N/A
Primer: <i>dcd1-mu1</i> Reverse Primer (55862nrev) 5'-GGTGCTACATATACGCTAAAG- 3'	Integrated DNA Technologies	N/A
Primer: <i>add1</i> Forward Primer (3dCAPbfor) 5'-GTTGTTTTCCCCCTTGGATT-3'	Integrated DNA Technologies	N/A
Primer: <i>add1</i> Reverse Primer (3dCAPbrev) 5'-CTTGAGTTCTTGTGTTGCTCAG- 3	Integrated DNA Technologies	N/A
Software and algorithms		
Fiji	Schindelin et al. 2012 (Schindelin <i>et al.</i> , 2012)	https://fiji.sc/
GNU Image Manipulation Program (GIMP)		https://www.gimp.org/
R	R Core Team 2023 (R Core Team, 2023)	https://www.r-project.org/
RStudio	Posit Team 2023 (Posit team, 2023)	https://posit.co/products/op en-source/rstudio/

REFERENCES

- Allsman, L.A., Dieffenbacher, R.N. and Rasmussen, C.G. (2019) 'Glue Impressions of Maize Leaves and Their Use in Classifying Mutants', *Bio-protocol*, 9(7), p. e3209.
- Ambrose, J.C. and Cyr, R. (2008) 'Mitotic spindle organization by the preprophase band', *Molecular plant*, 1(6), pp. 950–960.
- Ashraf, M. A., Liu, L. and Facette, M. R. (2023). A polarized nuclear position specifies the correct division plane during maize stomatal development. *Plant Physiol.*
- Azimzadeh, J. *et al.* (2008) 'Arabidopsis TONNEAU1 proteins are essential for preprophase band formation and interact with centrin', *The Plant cell*, 20(8), pp. 2146–2159.
- Bellinger, M. A., Uyehara, A. N., Allsman, L., Martinez, P., McCarthy, M. C. and Rasmussen, C. G. (2023). Cortical microtubules contribute to division plane positioning during telophase in maize. *Plant Cell* 35, 1496–1512.
- Buschmann, H. *et al.* (2006) 'Microtubule-associated AIR9 recognizes the cortical division site at preprophase and cell-plate insertion', *Current biology: CB*, 16(19), pp. 1938–1943.
- Camilleri, C. *et al.* (2002) 'The Arabidopsis TONNEAU2 gene encodes a putative novel protein phosphatase 2A regulatory subunit essential for the control of the cortical cytoskeleton', *The Plant cell*, 14(4), pp. 833–845.
- Dawson, C. (2022) 'ggprism: A "ggplot2" Extension Inspired by "GraphPad Prism"'. Available at: <https://CRAN.R-project.org/package=ggprism>.
- Drevensek, S. *et al.* (2012) 'The Arabidopsis TRM1--TON1 interaction reveals a recruitment network common to plant cortical microtubule arrays and eukaryotic centrosomes', *The Plant cell*, 24(1), pp. 178–191.
- Eleftheriou, E.P. and Bekiari, E. (2000) 'Ultrastructural effects of the herbicide chlorpropham (CIPC) in root tip cells of wheat', *Plant and soil*, 226(1), pp. 11–19.
- Facette, M.R. and Smith, L.G. (2012) 'Division polarity in developing stomata', *Current opinion in plant biology*, 15(6), pp. 585–592.
- Frank, M.J., Cartwright, H.N. and Smith, L.G. (2003) 'Three Brick genes have distinct functions in a common pathway promoting polarized cell division and cell morphogenesis in the maize leaf epidermis', *Development*, 130(4), pp. 753–762.
- Galatis, B. and Apostolakos, P. (2004) 'The role of the cytoskeleton in the morphogenesis and function of stomatal complexes', *The New phytologist*, 161(3), pp. 613–639.
- Gallagher, K. and Smith, L.G. (1999) 'discordia mutations specifically misorient asymmetric cell divisions during development of the maize leaf epidermis',

- Development*, 126(20), pp. 4623–4633.
- Gilliland, L.U. *et al.* (2003) 'Arabidopsis actin gene ACT7 plays an essential role in germination and root growth', *The Plant journal: for cell and molecular biology*, 33(2), pp. 319–328.
- Gray, A., Liu, L. and Facette, M. (2020) 'Flanking Support: How Subsidiary Cells Contribute to Stomatal Form and Function', *Frontiers in plant science*, 11, p. 881.
- Gunning, B.E.S. (1982) 'The Cytokinetic Apparatus: Its Development and Spatial Regulation', in C.W. Lloyd (ed.) *The Cytoskeleton in plant growth and development*. Academic Press, pp. 230–292.
- Huang, C.H. *et al.* (2022) 'The microtubular preprophase band recruits Myosin XI to the division site for plant cytokinesis', *bioRxiv*. Available at: <https://doi.org/10.1101/2022.11.08.515512>.
- Kakimoto, T. and Shibaoka, H. (1987) 'Actin filaments and microtubules in the preprophase band and phragmoplast of tobacco cells', *Protoplasma*, 140(2), pp. 151–156.
- Kassambara, A. (2023) 'ggpubr: "ggplot2" Based Publication Ready Plots'. Available at: <https://CRAN.R-project.org/package=ggpubr>.
- Kawamura, E. *et al.* (2006) 'MICROTUBULE ORGANIZATION 1 Regulates Structure and Function of Microtubule Arrays during Mitosis and Cytokinesis in the Arabidopsis Root', *Plant physiology*, 140(1), pp. 102–114.
- Kiesselbach, T.A. (1949) 'The Structure and Reproduction of Corn'. Available at: <http://digitalcommons.unl.edu/ardhistrb/284> (Accessed: 30 March 2023).
- Kirik, A., Ehrhardt, D.W. and Kirik, V. (2012) 'TONNEAU2/FASS regulates the geometry of microtubule nucleation and cortical array organization in interphase Arabidopsis cells', *The Plant cell*, 24(3), pp. 1158–1170.
- Kumari, P. *et al.* (2021) 'IQ67 DOMAIN proteins facilitate preprophase band formation and division-plane orientation', *Nature plants*, 7(6), pp. 739–747.
- Laine, R.F. *et al.* (2019) 'NanoJ: a high-performance open-source super-resolution microscopy toolbox', *Journal of physics D: Applied physics*, 52(16), p. 163001.
- Lebecq, A. *et al.* (2023) 'The phosphoinositide signature guides the final step of plant cytokinesis', *Science advances*, 9(29), p. eadf7532.
- Liu, B., Joshi, H.C. and Palevitz, B.A. (1995) 'Experimental manipulation of gamma-tubulin distribution in Arabidopsis using anti-microtubule drugs', *Cell motility and the cytoskeleton*, 31(2), pp. 113–129.
- Martinez, P. *et al.* (2017) 'Proper division plane orientation and mitotic progression together allow normal growth of maize', *Proceedings of the National Academy of Sciences of the United States of America*, 114(10), pp. 2759–2764.

- Martinez, P., Dixit, R., Balkunde, R. S., Zhang, A., O'Leary, S. E., Brakke, K. A. and Rasmussen, C. G. (2020). TANGLED1 mediates microtubule interactions that may promote division plane positioning in maize. *J. Cell Biol.* 219.
- Mills, A. M., Morris, V. H. and Rasmussen, C. G. (2022). Localization of PHRAGMOPLAST ORIENTING KINESIN1 at the division site depends on the microtubule binding proteins TANGLED1 and AUXIN-INDUCED IN ROOT CULTURES9 in Arabidopsis. *Plant Cell*.
- Mineyuki, Y. (1999) 'The Preprophase Band of Microtubules: Its Function as a Cytokinetic Apparatus in Higher Plants', in K.W. Jeon (ed.) *International Review of Cytology*. Academic Press, pp. 1–49.
- Mineyuki, Y. and Palevitz, B.A. (1990) 'Relationship between preprophase band organization, F-actin and the division site in Allium', *Journal of cell science*, 97(2), pp. 283–295.
- Mohanty, A. *et al.* (2009) 'Advancing cell biology and functional genomics in maize using fluorescent protein-tagged lines', *Plant physiology*, 149(2), pp. 601–605.
- Müller, S., Han, S. and Smith, L.G. (2006) 'Two kinesins are involved in the spatial control of cytokinesis in Arabidopsis thaliana', *Current biology: CB*, 16(9), pp. 888–894.
- Müller, S. and Jürgens, G. (2016) 'Plant cytokinesis—No ring, no constriction but centrifugal construction of the partitioning membrane', *Seminars in cell & developmental biology*, 53, pp. 10–18.
- Muroyama, A. *et al.* (2023) 'Cortical polarity ensures its own asymmetric inheritance in the stomatal lineage to pattern the leaf surface', *Science*, 381(6653), pp. 54–59.
- Nan, Q., Liang, H., *et al.* (2023) 'The OPAQUE1/DISCORDIA2 myosin XI is required for phragmoplast guidance during asymmetric cell division in maize', *The Plant cell*, 35(7), pp. 2678–2693.
- Nan, Q., Mendoza, J. and Facette, M. (2019) 'Double labeling of microtubules and actin filaments in maize leaf division zone', *Bio-protocol*, 9(12). Available at: <https://doi.org/10.21769/bioprotoc.3262>.
- van Oostende-Triplet, C. *et al.* (2017) 'Vesicle Dynamics during Plant Cell Cytokinesis Reveals Distinct Developmental Phases', *Plant physiology*, 174(3), pp. 1544–1558.
- Pickett-Heaps, J.D. and Northcote, D.H. (1966) 'Organization of microtubules and endoplasmic reticulum during mitosis and cytokinesis in wheat meristems', *Journal of cell science*, 1(1), pp. 109–120.
- Posit team (2023) 'RStudio: Integrated Development Environment for R'. Boston, MA: Posit Software, PBC. Available at: <http://www.posit.co/>.
- Rasmussen, C.G. (2016) 'Using Live-Cell Markers in Maize to Analyze Cell Division

- Orientation and Timing', in M.-C. Caillaud (ed.) *Plant Cell Division: Methods and Protocols*. New York, NY: Springer New York (Methods in Molecular Biology, 1370), pp. 209–225.
- Rasmussen, C.G., Sun, B. and Smith, L.G. (2011) 'Tangled localization at the cortical division site of plant cells occurs by several mechanisms', *Journal of cell science*, 124(Pt 2), pp. 270–279.
- R Core Team (2023) 'R: A Language and Environment for Statistical Computing'. Vienna, Austria: R Foundation for Statistical Computing. Available at: <https://www.R-project.org/>.
- Samuels, A.L., Giddings, T.H., Jr and Staehelin, L.A. (1995) 'Cytokinesis in tobacco BY-2 and root tip cells: a new model of cell plate formation in higher plants', *The Journal of cell biology*, 130(6), pp. 1345–1357.
- Schaefer, E. *et al.* (2017) 'The preprophase band of microtubules controls the robustness of division orientation in plants', *Science*, 356(6334), pp. 186–189.
- Schindelin, J. *et al.* (2012) 'Fiji: an open-source platform for biological-image analysis', *Nature methods*, 9(7), pp. 676–682.
- Smertenko, A. *et al.* (2017) 'Plant Cytokinesis: Terminology for Structures and Processes', *Trends in cell biology*, 27(12), pp. 885–894.
- Smith, L. G., Hake, S. and Sylvester, A. W. (1996). The tangled-1 mutation alters cell division orientations throughout maize leaf development without altering leaf shape. *Development* 122, 481–489.
- Smith, L. G., Gerttula, S. M., Han, S. and Levy, J. (2001). Tangled1: a microtubule binding protein required for the spatial control of cytokinesis in maize. *J. Cell Biol.* 152, 231–236.
- Spiegelhalder, R. P. and Raissig, M. T. (2021). Morphology made for movement: formation of diverse stomatal guard cells. *Curr. Opin. Plant Biol.* 63, 102090.
- Spinner, L. *et al.* (2013) 'A protein phosphatase 2A complex spatially controls plant cell division', *Nature communications*, 4, p. 1863.
- Thévenaz, P. (1998) 'StackReg: an ImageJ plugin for the recursive alignment of a stack of images', *Biomedical Imaging Group, Swiss Federal Institute of Technology Lausanne*, 2012.
- Torres-Ruiz, R.A. and Jürgens, G. (1994) 'Mutations in the FASS gene uncouple pattern formation and morphogenesis in Arabidopsis development', *Development*, 120(10), pp. 2967–2978.
- Vaškebová, L., Šamaj, J. and Ovecka, M. (2018). Single-point ACT2 gene mutation in the Arabidopsis root hair mutant der1-3 affects overall actin organization, root growth and plant development. *Ann. Bot.* 122, 889–901.

- Walker, K.L. *et al.* (2007) 'Arabidopsis TANGLED identifies the division plane throughout mitosis and cytokinesis', *Current biology: CB*, 17(21), pp. 1827–1836.
- Wang, W. *et al.* (2019) 'Gene editing of the wheat homologs of TONNEAU1-recruiting motif encoding gene affects grain shape and weight in wheat', *The Plant journal: for cell and molecular biology*, 100(2), pp. 251–264.
- Whittington, A.T. *et al.* (2001) 'MOR1 is essential for organizing cortical microtubules in plants', *Nature*, 411(6837), pp. 610–613.
- Wickham, H. (2016) 'ggplot2: Elegant Graphics for Data Analysis'. Springer-Verlag New York. Available at: <https://ggplot2.tidyverse.org>.
- Wickham, H. *et al.* (2023) 'dplyr: A Grammar of Data Manipulation'. Available at: <https://CRAN.R-project.org/package=dplyr>.
- Wickham, H., Vaughan, D. and Girlich, M. (2023) 'tidyr: Tidy Messy Data'. Available at: <https://CRAN.R-project.org/package=tidyr>.
- Wright, A.J., Gallagher, K. and Smith, L.G. (2009) 'discordia1 and alternative discordia1 function redundantly at the cortical division site to promote preprophase band formation and orient division planes in maize', *The Plant cell*, 21(1), pp. 234–247.
- Wu, Q. *et al.* (2013) 'Fluorescent protein marker lines in maize: generation and applications', *The International journal of developmental biology*, 57(6-8), pp. 535–543.
- Wu, S.-Z. and Bezanilla, M. (2014) 'Myosin VIII associates with microtubule ends and together with actin plays a role in guiding plant cell division', *eLife*, 3. Available at: <https://doi.org/10.7554/eLife.03498>.

CHAPTER 4:
OTHER MOLECULAR PLAYERS INVOLVED WITH MAIZE DIVISION PLANE
ORIENTATION AND CYTOKINESIS

Keywords: bulked segregant analysis, maize, cytokinesis

ABSTRACT

Cell division is key to proper growth and development in multicellular organisms. In plants, the division plane is established early in the cell cycle and is marked by proteins that remain at the division site until the new cell wall is built. The final steps of cell division are executed in cytokinesis by the phragmoplast, a cytoskeletal and vesicular structure, that lays down the new cell wall. While key players important to cytokinesis have been reported, many more remain to be identified. Severe defects in cytokinesis often result in embryo lethality, making this a difficult process to study. Here, I describe *cytokinesis3 (cyto3)*, a recessive cytokinesis maize mutant generated through an ethyl methanesulfonate (EMS) mutagenesis forward genetics screen. *cyto3* is a mutant with minor cytokinesis defects characterized by incomplete cell walls and no misoriented divisions. I used whole genome resequencing and bulked segregant analysis to identify a 2 Mb region on Chromosome 9 that likely contains the causative variant. To validate our candidate, new alleles generated through pollen EMS mutagenesis will be Sanger sequenced. Additionally, the bioinformatics pipeline will be applied to additional mutants that were generated through this screen.

INTRODUCTION

While much progress has been made towards understanding the mechanisms controlling plant division plane orientation, many unanswered questions remain regarding the interactions between division site proteins and their functions in the stages of division. Experiments in *Arabidopsis* examining the redundant functions of the proteins TANGLED1 and AUXIN INDUCED IN ROOT CULTURES 9 (AIR9) in maintaining division plane orientation suggest that an additional protein is important for mediating interactions that promote TANGLED1 maintenance at the division site (Mills et al., 2022). Mutants identified can be divided into classes that describe the section of division plane orientation that is affected: division plane establishment, division plane maintenance, phragmoplast guidance, and cytokinesis (Müller et al., 2016; Rasmussen et al., 2018; Uyehara et al., 2023). These mutants are involved in processes such as cytoskeletal organization and dynamics, membrane trafficking, and cell signaling, and have proven to be useful genetic tools to investigate cell division (Uyehara et al., 2023).

To identify new molecular players involved with controlling division plane orientation or cytokinesis in maize, a forward genetics ethyl methanesulfonate (EMS) screen was done in maize. EMS induces GC→AT transition mutations randomly across the genome which will lead to occasional changes in phenotype. Previously, EMS-treated B73 was planted, open pollinated, and screened for cellular phenotypes by glue impression (Figure 4.1) (Allsman et al., 2019). Mutants with clear recessive division plane orientation or cytokinesis phenotypes were further backcrossed into the inbred B73. The first mutant chosen for sequencing was *cytokinesis 3 (cyto3)*, a mutant with mild, but obvious epidermal cytokinesis defects such as incomplete cell walls, otherwise called cell wall stubs, and enlarged nuclei (Figure 4.2). Plant cytokinesis begins at the

center of the cell with the formation of the phragmoplast, a microtubule and actin structure that facilitates the formation of the cell plate (Müller et al., 2016; Smertenko et al., 2017). Vesicles containing cell plate materials accumulate at the phragmoplast midline as the phragmoplast expands, eventually reaching the mother cell plasma membrane where the cell plate fuses (Müller et al., 2016; Murata et al., 2005, 2013; Smertenko, 2018). Failures in cytokinesis result when defects occur in the processes regulating phragmoplast reorganization (Hiwatashi et al., 2008; Kosetsu et al., 2013; Li et al., 2017; Sasabe et al., 2011), or tethering and fusion of the cell plate (Assaad et al., 1996; Lukowitz et al., 1996; Söllner et al., 2002; Waizenegger et al., 2000).

Maize has an extensive amount of sequenced genetic resources that make it an ideal model crop system to use in genetic screens (Cannon et al., 2024). The maize haploid genome size is 2.2 Gb with a haploid chromosome number of 10 (Hufford et al., 2021; Schnable et al., 2009). B73 was the first sequenced maize inbred line and is used as a standard genetic background (Schnable et al., 2009). We used bulked segregant analysis (BSA)-seq to identify candidate genes for our mutants. BSA was developed to identify genomic markers in linkage disequilibrium with genes of interest through genotypic analysis of individuals pooled by a phenotype (Michelmore et al. 1991). BSA is now coupled with whole genome sequencing to generate thousands of genetic markers from pools of recombinants to map mutations (Michelmore et al., 1991; Schneeberger et al., 2009). In maize, BSA-seq has been used to clone genes from mutant populations with 101 or as little as 9 mutant individuals (Klein et al., 2018).

Here we describe the initial characterization and sequencing of a maize cytokinesis mutant, *cyto3*.

METHODS

EMS seed treatment

About 7000 B73 maize inbred seeds were treated with 25 mM EMS in 10 mM KH_2PO_4 (pH 7.0) and incubated for about 6 hours with manual stirring (Cliff Weil, personal communication and (Gnanamurthy et al., 2011)). Seeds were rinsed 10X with water with at least 2X changes in volume and planted the next morning.

Plant Cultivation

All plants were grown at Agricultural Operations (<https://agops.ucr.edu/>, Riverside, CA, USA) at the University of California, Riverside using standard field conditions during the summer (April - July) or the fall (August - December) field seasons.

Bulked Segregant Analysis (BSA) Material

The first bulked segregant analysis experiment sent for sequencing was a population segregating for *cytokinesis3* (Figure 4.2) that had been backcrossed once into B73. Due to the complex nature of the *cyto3*, B73(1) background, *cyto3* was outcrossed to the maize inbred W22 (seeds courtesy of Patricia Springer) and the resulting F_1 population was selfed and crossed to W22 two additional times to create a BC_3F_2 population. Two sibling packets (K573-5 and K573-10) were planted to reach the desired number of mutants for the experiment.

The second mutant used for bulked segregant analysis was the mutant *tangled64* (*tan64*) which was backcrossed into B73 twice. *tan64* was planted and collected for bulked segregant analysis during the Summer of 2020.

DNA Extractions and Whole Genome Resequencing

Populations segregating for the mutant and wild type phenotype were planted in the field and screened by glue impression. Tissue was collected and bulked by phenotype and stored in the -80°C. DNA was extracted in 2% cetyltrimethylammonium bromide (CTAB) and washed with 24:1 chloroform:iso amyl alcohol, followed by isopropanol, 95% ethanol, and 75% ethanol, then resuspended in water with RNase (protocol courtesy of Daniel Koenig). Libraries were made in collaboration with Keely Brown (Koenig Lab) or the UCR Genomics Core (see Table 4.1). Libraries were sent for 150 bp paired end whole genome resequencing on the NovaSeq 6000 at the University of California, Berkeley with a target coverage of 20X.

Table 4.1. Overview of sequencing experiments for cyto3 and tan64.

	Number of individuals (WT, mutant)	Year	Library	Sequencing
cyto3, B73	(49, 49)	2019	SeqOnce Kit	Illumina NovaSeq 6000 2 X 150 PE at UCSF
cyto3, B73	Same DNA	May 2019	Neb Ultrall Kit	Illumina NovaSeq 6000 2 X 150 PE at UCSF
cyto3, W22	(228, 66)	2023	NEBNext® Ultra™ II FS DNA Library Prep Kit for Illumina	Illumina NovaSeq 6000 2 X 150 PE at UCB
tan64, B73	(106, 106)	2020	IlluminaNextEra	Illumina NovaSeq 6000 2 X 150 PE at UCSF
tan64, B73	Same DNA	2023	NEBNext® Ultra™ II FS DNA Library Prep Kit for Illumina	Illumina NovaSeq 6000 2 X 150 PE at UCB

Bulked segregant analysis bioinformatics pipeline for *cyto3*

Sequencing data was analyzed with a custom pipeline adapted from Klein et al. 2018 (Klein et al., 2018)) on UCR's HPCC. Initial sequence quality was assessed using FastQC version 0.11.9 (Andrews, 2010). Because some sequences had 5% adapter content, sequences were trimmed using Trimmomatic (Bolger et al., 2014). After trimming, 93%-94% of read pairs remained and were mapped to either the B73 v5 or the W reference genome using BWA-MEM (Vasimuddin et al., 2019). For all sequences, about 99% of reads mapped to the W22 v2 genome (Table 4.2). Mean coverage was 15.4X for the wild-type pool and 20.3X for the *cyto3* pool. Variants were called using VarScan2 with the settings `-min-coverage 2 \ -min-reads2 2 \ -min-avg-qual 15 \ -min-var-freq 0.01 \ -minfreq-for-hom 0.99` (Koboldt et al., 2013). Allele frequencies were plotted in R using `windowscanR` (Tavares, 2024) to identify a region of fixed variants unique to the mutant pool. Once the region was identified, variant effects were predicted using variant effect predictor. Reads were viewed using the Integrative Genomics Viewer(IGV) (Robinson et al., 2011) to confirm mutation against the genome.

In parallel, Easymap2 (Lup et al., 2023) was also used to identify candidate genes using the experimental design arguments `--ed ref_bc_f2wt` and `--ed noref_bc_f2wt`.

Table 4.2. Percent mapping and mean coverage of bulked segregant analysis populations.

	% Mapped	Mean coverage
WT-c3_L219	99.76%	6.1X
WT-c3_L266	99.76%	9.3X
cyto3_L219	99.82%	9.9X
cyto3_L266	99.79%	10.4X

EMS pollen mutagenesis

A non-complementation screen was done using EMS to generate new alleles for *cyto3* and *tan64*. A segregating population of *cyto3* or *tan64* was grown in the field and phenotypes screened by glue impression. Wild-type plants were killed and remaining mutant individuals were detasseled to prevent recovery of the original allele. Pollen was collected from B73 individuals and about 2 ml of pollen was added to 20 ml of 5 mM EMS in paraffin oil. Pollen was incubated in EMS-paraffin mixture for 30 minutes with mixing every five minutes. 1 ml of pollen-EMS-paraffin solution was applied to mutant ears that had cut back the day before. Pollinated ears were covered with a shoot bag and a tassel bag and grown until harvest.

Toluidine Blue O Staining

Toluidine Blue O staining was done following Bellinger et al 2019 (Bellinger et al., 2019). Briefly, leaf tissue fixed in a 4% formaldehyde solution was incubated in a 0.1% pectolyase solution until the leaf epidermis could be gently peeled away with tweezers (1-3 hrs). The epidermal peel was then stained with Toluidine Blue O, rinsed with dH₂O, then imaged with a compound light microscope.

RESULTS

cytokinesis 3 (cyto3) is a maize mutant with defects in cytokinesis

The *cyto3* mutant in maize was generated through a forward genetics EMS screen and has a recessive cytokinetic defect with mendelian segregation consistent with a single locus (Figure 4.1). At the seedling stage, *cyto3* plants do not have an obvious macroscopic phenotype compared to their wild-type sibling. However, at tasseling, *cyto3* plants tend to be shorter with thinner stems. Cytokinetic defects such as incomplete cell walls (cell wall stubs) in *cyto3* can be observed using epidermal glue impressions (Figure 4.2 A-B). Cell wall stubs were observed in both transverse and longitudinal divisions (Figure 4.2). In addition to cell wall stubs, *cyto3* nuclei as visualized through TBO stains are stretched and deformed compared to wild type (Figure 4.2 C-D). This is consistent with cytokinetic defects observed in cytokinesis mutants in *Arabidopsis* (Nacry et al., 2000).

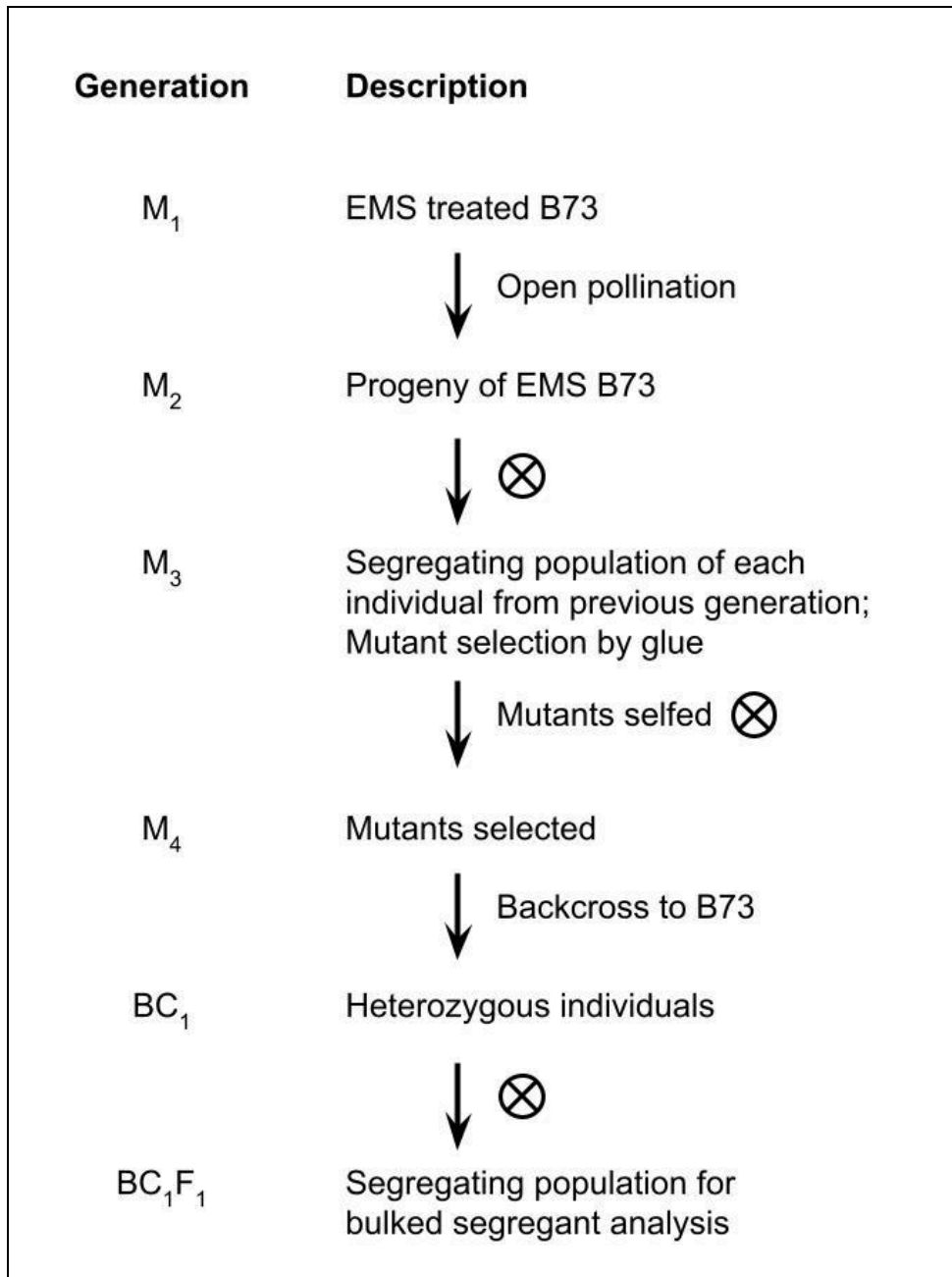


Figure 4.1. Overview of generation of EMS population.

B73 seeds were treated with EMS, open pollinated, then selfed to generate lines segregating for cellular phenotypes. Individuals with interesting phenotypes were backcrossed to B73 and selfed to generate segregating populations for analysis or for continued backcrossing.

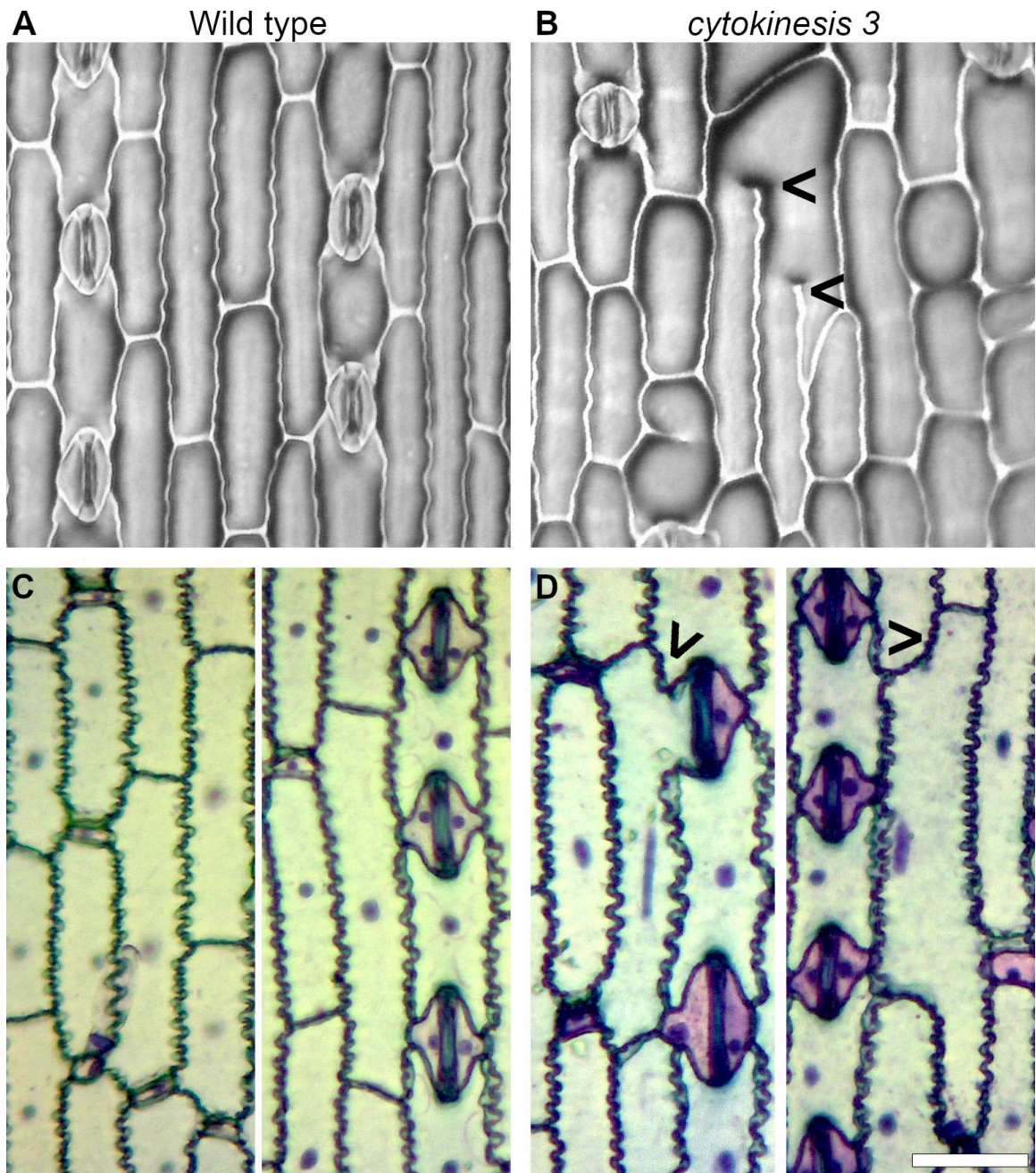


Figure 4.2. *cyto3* epidermal cells have defects in cytokinesis.

(A-B) Glue impressions of wild type (A) and *cyto3* (B) epidermal cells. (C-D) Toluidine Blue O stains of wild type (C) and *cyto3* (D) epidermal peels. Scale bar for all is 100 μm . Black carats point to incomplete cell walls.

Resequencing of *cyto3*, B73 and *cyto3*, W22(3)

Initial sequencing and mapping of *cyto3*, B73(1) and wild-type pools revealed large blocks of fixed variants across the genome that indicated the genetic background of *cyto3* was not purely B73. Because we bulked mutant phenotypes together in the mutant pool and the phenotypically wild-type siblings in the wild-type pool, we expected the allele frequency of the causative mutation to be 100% and 33% in the mutant and wild-type pools respectively. The majority of fixed alleles occurred on chromosome 9, suggesting that the candidate gene was somewhere on chromosome 9. However, the millions of fixed differences in both the wild-type and mutant pools made it impossible to identify a candidate region for *cyto3*.

To address this problem, *cyto3* was outcrossed to W22, a different inbred background. We expected that with continued backcrossing into W22 and chromosomal recombination, the *cyto3* background would become more W22-like except in the candidate region, allowing us to identify it. The new bulked segregant analysis population was backcrossed into W22 three times, bulked by phenotype, and sent for sequencing.

Mapping and candidate region identification

Wild-type and *cyto3* pools were mapped against the W22 version 2 genome using BWA-MEM2 and variants called using VarScan2. Allele frequencies were calculated by dividing the alternate allele depth (AD) by the total read depth (DP) and plotted in R using WindowscanR. In parallel, trimmed FASTQ files were also input into Easymap v.2, which takes into account the experiment design and uses linkage analysis to output a candidate region and list of candidates.

After importing the variant calls into R, it was clear that the candidate region occurred on chromosome 9 based on the elevated number of fixed variants unique to the *cyto3* pool (Table 4.3).

Table 4.3 Number of fixed variants per chromosome

Chromosome	Chromosome size (bp)	Number of Raw Homozygous Variants	Number of variants after filtering
1	310925244	2,446,783	28,086
2	244237062	1,461,261	8,442
3	241278614	1,588,040	9,803
4	254269898	1,545,755	6,370
5	222590201	1,494,894	8,605
6	171602414	1,241,427	8,792
7	181422836	1,282,899	5,749
8	182570339	1,490,140	26,501
9	163066665	1,476,105	294,424
10	149450367	997,265	8,817

To identify a narrower region, allele frequencies were averaged over chromosome 9 using a sliding window in R starting with 20 kb windows and 10 kb steps and moving up to 1 Mb windows with 0.5 Mb steps. Averaging with the sliding window revealed a peak in allele frequencies towards the beginning of chromosome 9 that neared 1 which was absent from the wild type pool (Figure 4.3). The output of Easymap v2 also identified a similar albeit larger region of 20 Mb (that contained 165 gene models with amino acid changes (Figure 4.4).

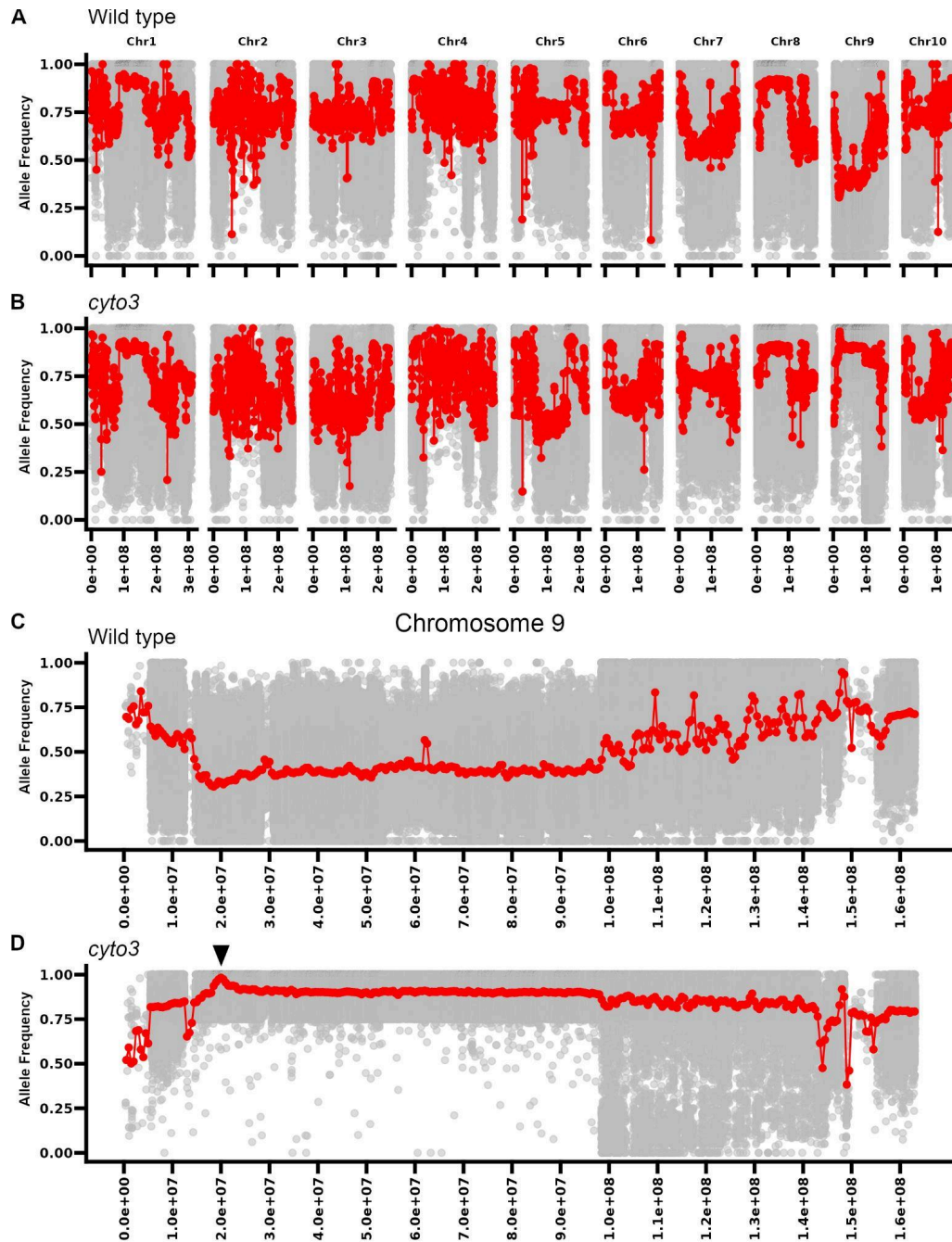


Figure 4.3. *cyto3* is on chromosome 9.

Sliding window means of wild type and *cyto3* allele frequencies. (A-B) Allele frequency means across all ten chromosomes in (A) wild type and (B) *cyto3*. (C-D) Allele frequency of chromosome 9 in (C) wild type and (D) *cyto3*. Black arrow points to the mapping region. Red lines indicate window means and gray points are raw allele frequencies. Plot generated with the R package WindowScanR.

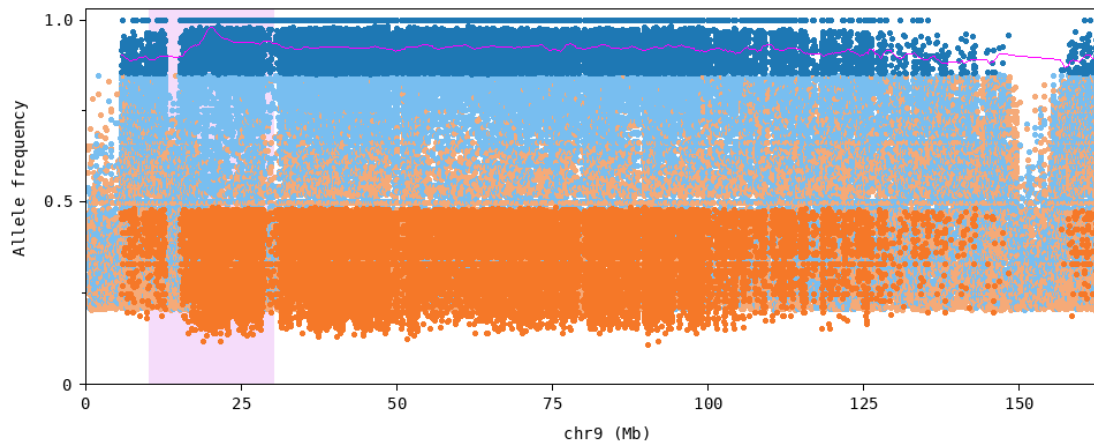


Figure 4.4. Mapping analysis overview from Easymap v2 output.

Plot shows the allele frequency of the non-reference allele on the y axis by genomic position on the x axis. The candidate region is highlighted in pink. Blue dots represent polymorphisms from the mutant pool, and orange dots represent polymorphisms from the wild-type pool.

To narrow the list of candidate genes, we mapped the original wild type and *cyto3*, B73 (1) pools to the W22 genome and called variants. Variants with an alternate allele frequency of 1 were first removed if they were shared with the wild-type pools from the B73 or W22 populations. Next, variants were removed if they were not shared between the *cyto3*, W22 (3) and the *cyto3*, B73 (1) mutant pools. These positions were then used to pull out gene models from the W22 general feature format (GFF) file, resulting in a candidate list of 18 genes (Table 4.4). In total three lists of genes were generated: (1) Gene models from within a 4.5 Mb region that includes the peak of allele frequencies, (2) Gene models that overlap with variant positions specific to the *cyto3* pools, and (3) Gene models from the Easymap output.

Table 4.4. List of candidates specific to cyto3, W22(3) and cyto3, B73(1) pools.

Gene Identifier	Predicted Function
Zm00004b031849	zmm3 - Zea mays MADS3; transcription factor; regulation of meristem development
Zm00004b031923	Predicted cellular component
Zm00004b031946	Predicted acyltransferase, lyase, and dioxygenase activity
Zm00004b031984	fat2 - fatty acyl-ACP thioesterase2; fatty acid biosynthesis
Zm00004b031986	bub3 - budding inhibited by benzimidazoles homolog3; mitotic checkpoint
Zm00004b031993	Predicted mRNA binding, nucleotidyltransferase activity, metal ion binding
Zm00004b032019	Predicted similarity to Arabidopsis ATP-dependent Clp protease
Zm00004b032064	Predicted protein peptidyl-prolyl isomerization, nucleosome, DNA binding, peptidyl-prolyl cis-trans isomerase activity, protein folding, protein heterodimerization activity
Zm00004b032065	bbr4 - BBR/BPC-transcription factor 4; transcription factor, response to ethylene
Zm00004b032104	No prediction; protein BLAST results in hypothetical or uncharacterized proteins
Zm00004b032430	Integral component of membrane
Zm00004b032459	Xax1 - xylan arabinosyl 2- O-xylosyltransferase 1; golgi membrane, integral component of membrane
Zm00004b032462	pub36 - a plant U-box type E3 ubiquitin ligase; protein ubiquitination
Zm00004b032483	Uncharacterized protein
Zm00004b032659	Putative glucuronosyltransferase (by BLAST)
Zm00004b032675	mads71 - MADS-transcription factor 71
Zm00004b032770	Uncharacterized protein
Zm00004b032791	3-hydroxyisobutyryl-CoA hydrolase activity; valine catabolic process, plastid

In R, these three lists were compared and a Venn diagram was used to find gene model(s) in common (Figure 4.5, Table 4.5-4.7). Only one gene model was shared between all three lists Zm00004b031986 (W22 v2), also known as Zm00001d045389 (B73 v4) or Zm00001eb377380 (B73 v5), a putative BUDDING INHIBITED BY BENZIMIDAZOLES HOMOLOG3. Zm00004b031986 has a cytosine to thymine transition mutation in exon 7 that results in an amino acid change from a glycine to aspartate.

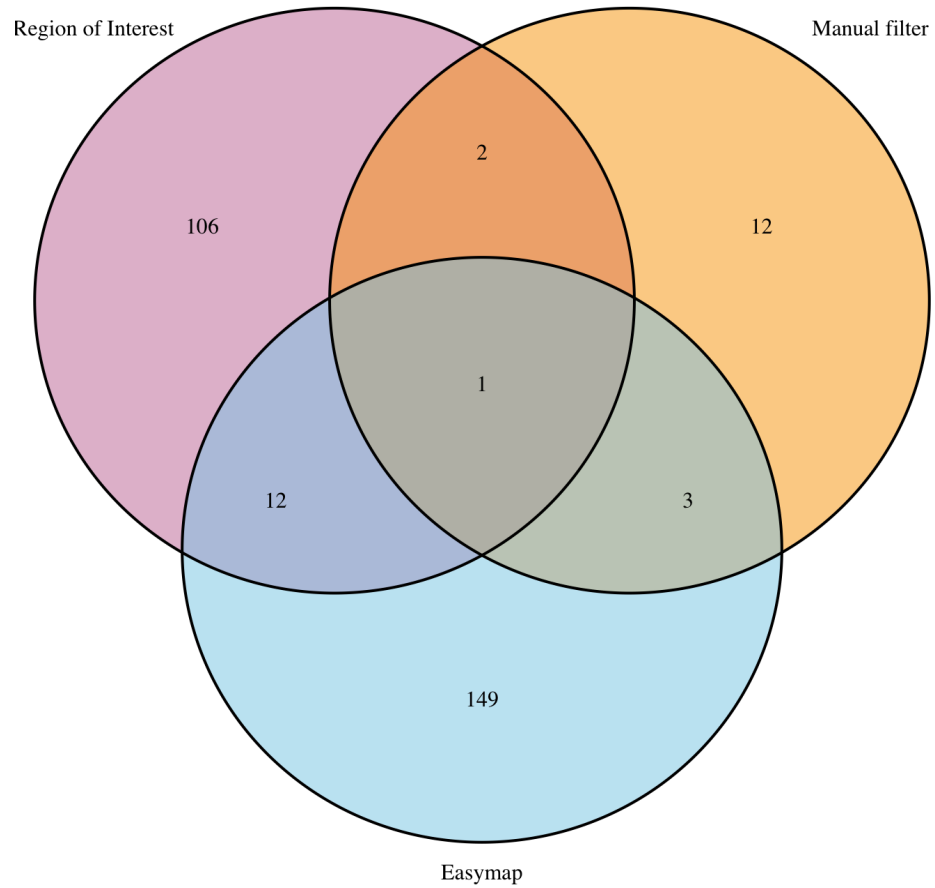


Figure 4.5. Venn diagram of candidate gene models generated with different methods. Region of interest (pink) represents the gene models within a 4.5 Mb region on chromosome 9 of W22. The manual filter (orange) represents gene models with variants that were shared between the cyto3, B73 and the cyto3, W22 pools. Easymap (blue) are the gene models that were output by Easymap.

Table 4.5 Gene candidates shared between Easymap and Region of Interest

Gene Identifier	Predicted Function
Zm00004b031969	No prediction; protein BLAST results in hAT transposon superfamily protein
Zm00004b031951	DNA replication checkpoint, DNA binding, nucleus
Zm00004b031973	Helicase activity
Zm00004b031974	No information; BLAST results in TORTIFOLIA1-like protein 3-like
Zm00004b031978	Golgi membrane, structural molecular activity, intracellular protein transport, vesicle-mediated transport, membrane coat, COP1-coated vesicle membrane
Zm00004b031979	Single strand break repair, damaged DNA binding
Zm00004b031980	mRNA splicing, response to salt stress, response to lithium ion, precatalytic spliceosome
Zm00004b031981	NADH dehydrogenase activity, electron transport chain, carbohydrate biosynthetic process
Zm00004b031982	sod16- superoxide dismutase16; superoxide dismutase activity, removal of superoxide radicals, chloroplast nucleoid, metal ion binding
Zm00004b031996	pub76 - plant U-box type E3 ubiquitin ligase76; acid phosphatase activity, protein kinase activity, protein ubiquitination
Zm00004b032001	Threonine-type endopeptidase activity, nucleus, cytoplasm, proteasome core complex, response to zinc ion, regulation of plant-type hypersensitive response, proteolysis of cellular protein catabolic process
Zm00004b032004	Cytoplasm, methyltransferase activity, membrane, methylation, intracellular membrane-bounded organelle

Table 4.6 Gene candidates shared between the Region of Interest and the Manual Filter

Gene Identifier	Predicted Function
Zm00004b031984	Fatty acid biosynthetic process, chloroplast, ACP phosphopantetheine attachment site binding
Zm00004b031993	mRNA binding, nucleotidyltransferase activity, metal ion binding

Table 4.7 Gene candidates shared between the Manual Filter and Easymap

Gene Identifier	Predicted Function
Zm00004b032019	ATP-dependent peptidase activity; serine-type endopeptidase activity, proteolysis, plastid envelope, chloroplast thylakoid, chloroplast organization, chloroplast endopeptidase Clp complex, integral component of membrane, cellular protein catabolic process ATPase
Zm00004b032430	Integral component of membrane
Zm00004b032462	pub36 - a plant U-box type E3 ubiquitin ligase; protein ubiquitination

Generation of new *cyto3* alleles using pollen EMS mutagenesis

To generate new alleles of *cyto3*, *cyto3* plants were pollinated with EMS mutagenized B73 pollen. Because *cyto3* is a recessive mutant, crossing with B73 should result in complementation, i.e. wild-type plants, while crossing with mutagenized B73 pollen could result in noncomplementation, i.e. the presence of cytokinetic defects in glue impressions due to an independent mutation in the same gene. A total of 58 *cyto3* ears were used for pollination with EMS treated B73. Of the resulting F₁s two plants were recovered that exhibited cytokinesis defects: H949-14 and H1016-15 (Figure 4.6). Unfortunately the H949-14 individual was not crossable and tissue was collected for DNA extraction (Figure 4.6).

The biallelic H1016-15 was backcrossed to B73 to make BC₁ plants that segregate fifty percent of the time as heterozygous for the original *cyto3* allele or heterozygous for the new *cyto3* allele, hereby referred to as *cyto3-2*. BC₁ plants were selfed to create a BC₁F₁ population. Four BC₁F₁ populations were randomly selected for planting in the greenhouse and screened for the cytokinesis phenotype. Homozygous mutants were sent for light (2-5X) whole genome resequencing and mapped to the B73

genome. Unfortunately all individuals have the C to T mutation in our top candidate Zm00004b031986/Zm00001d045389/Zm00001eb377380 suggesting that 1) Zm00004b031986 is the wrong gene, 2) there was contamination with the original allele during the pollen mutagenesis, or 3) we were unlucky in the BC₁F₁ populations we chose to sequence (Figure 4.7A). Based on the pattern of allele frequency means, it seems that three of the four individuals chosen are the original *cyto3* allele due to the blocks of high allele frequencies that indicate *cyto3*'s original mixed background (Figure 4.7B). The pattern of IGH76-1 is perplexing because of the blocks of average allele frequencies at about 0.25 and may represent a heterozygous individual. However, low sequencing coverage limits the interpretation of these plots. Additional high and moderate effect variants are listed in Tables 4.8 and 4.9 respectively.



Figure 4.6. Noncomplementation of *cyto3* resulted in the identification of two potential new alleles.

Glue impressions of (A) wild type and (B) two noncomplemented mutants generated from pollen EMS mutagenesis of *cyto3*. Scale bar is 100 μ m and black carets point to cytokinesis defects. (C) Macroscopic phenotype of the uncrossable H494-14 in the field. May it rest in peace. Scale bar is 2 cm.

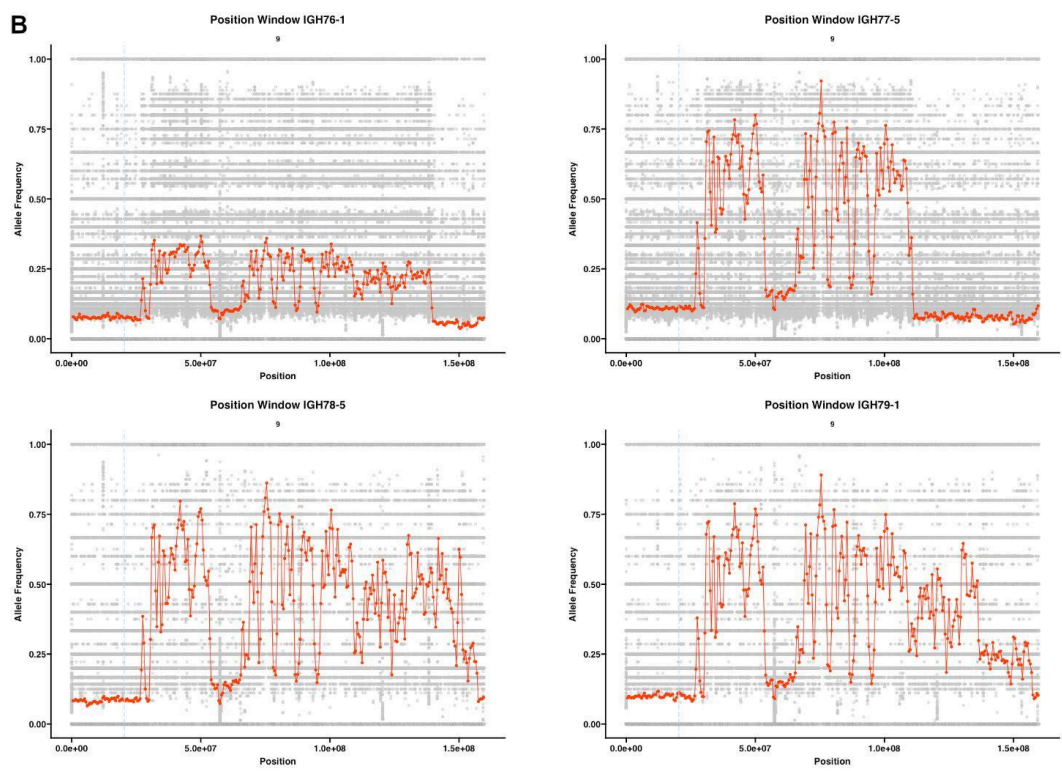


Figure 4.7. Sequencing of potential new alleles of *cyto3*.
 (A) IGV view of putative SNP position in the four BC₁F₁ individuals with cytokinesis defects. (B) Sliding window means of BC₁F₁ allele frequencies. Red lines indicate 1 Mb window means with a step of 0.5 Mb and gray points are raw allele frequencies. Plot generated with the R package WindowScanR.

Table 4.8. High effect variants as predicted by Variant Effect Predictor (VEP) for the 2 Mb candidate region spanning Chr9:19000000-21000000.

CHROM	POS	REF	ALT	Consequence	Gene model	Predicted function
chr9	19060315	C	T	3' UTR variant	Zm00004b031923	BLAST: Putative sugar phosphate/ phosphate translocator
chr9	19061588	G	A	intron variant	Zm00004b031923	BLAST: Putative sugar phosphate/ phosphate translocator
chr9	19127889	A	C	splice acceptor variant	Zm00004b031927	BLAST: Putative transcription elongation factor 1
chr9	20411336	T	G	stop gained	Zm00004b031982	sod16 - superoxide dismutase16; superoxide dismutase activity, removal of superoxide radicals, chloroplast nucleoid, metal ion binding

Table 4.9. Moderate effect variants from Chr9:1900000-2100000. For variants that had a similar predicted impact on the same gene model, the top variant was given.

CHROM	POS	REF	ALT	Consequence	Gene Model	Predicted Function
chr9	19011849	A	G	missense variant	Zm00004b031921	BLAST: F-box protein MAX2
chr9	19061074	T	C	intron_variant	Zm00004b031923	BLAST: Putative sugar phosphate/ phosphate translocator
chr9	19104343	T	C	missense variant	Zm00004b031925	BLAST: Hypothetical protein
chr9	19128068	T	C	missense variant	Zm00004b031927	BLAST: Putative transcription elongation factor 1
chr9	19143685	A	G	missense variant	Zm00004b031928	BLAST: cold-shock protein, dehydrin
chr9	19166515	T	C	upstream gene variant	Zm00004b031930	dbb11- double B-box zinc finger protein 11
chr9	19174214	T	C	upstream gene variant	Zm00004b031931	GO: protein tyrosine phosphatase
chr9	19178448	G	A	missense variant	Zm00004b031932	BLAST: 6-phosphofructokinase
chr9	19181726	G	T	downstream gene variant	Zm00004b031932	
chr9	19267146	G	A	upstream gene variant	Zm00004b031938	BLAST: PIF4
chr9	19273181	C	T	missense variant	Zm00004b031939	BLAST: hypothetical protein
chr9	19281090	C	T	upstream_gene_variant	Zm00004b031940	BLAST: putative disease resistance RPP13-like protein 1
chr9	19366895	T	C	upstream_gene_variant	Zm00004b031944	BLAST: trafficking protein particle complex subunit 4
chr9	19370699	G	T	missense variant	Zm00004b031945	cys6 - cysteine synthase6
chr9	19382481	C	T	missense variant	Zm00004b031946	BLAST: glyoxalase/bleomycin resistance protein
chr9	19524437	C	T	missense variant	Zm00004b031950	BLAST: hypothetical protein
chr9	19545461	C	G	downstream gene variant	Zm00004b031950	
chr9	19549399	G	C	downstream gene variant	Zm00004b031951	DNA replication checkpoint signaling
chr9	19605033	T	C	missense variant	Zm00004b031953	BLAST: Nuclear speckle RNA-binding protein
chr9	19610888	G	A	downstream gene variant	Zm00004b031953	
chr9	19634263	T	C	missense variant	Zm00004b031956	BLAST: hypothetical protein
chr9	19777572	G	C	missense variant	Zm00004b031959	BLAST: Putative cyclin-dependent kinase
chr9	19781200	A	G	downstream gene variant	Zm00004b031959	
chr9	19806214	G	C	missense variant	Zm00004b031961	BLAST: hypothetical protein
chr9	19876157	A	G	missense variant	Zm00004b031962	BLAST: COBRA-like protein 4 precursor
chr9	19913176	T	C	missense variant	Zm00004b031967	BLAST: anthranilate synthase alpha subunit 1, chloroplastic
chr9	20052491	T	C	missense variant	Zm00004b031969	BLAST: hAT transposon superfamily
chr9	20215969	A	G	missense variant	Zm00004b031973	BLAST: Hypothetical protein
chr9	20238059	G	A	missense variant	Zm00004b031974	BLAST: TORTIFOLIA1-like protein 3
chr9	20360692	A	C	missense variant	Zm00004b031978	COP1 coated vesicle membrane
chr9	20370669	A	G	upstream gene variant	Zm00004b031978	
chr9	20375834	G	A	missense variant	Zm00004b031979	BLAST: DNA-repair protein XRCC1
chr9	20379169	G	A	downstream gene variant	Zm00004b031979	
chr9	20391169	C	A	missense variant	Zm00004b031981	dxs3 - deoxy xylulose synthase3
chr9	20411308	G	T	missense variant	Zm00004b031982	sod16 - superoxide dismutase16
chr9	20419863	T	C	missense variant	Zm00004b031983	BLAST: LRR repeat protein
chr9	20485592	T	C	missense variant	Zm00004b031984	Fatty acid biosynthesis
chr9	20532227	T	G	missense variant	Zm00004b031985	BLAST: Putative D-mannose binding lectin receptor-like protein kinase
chr9	20538661	C	T	missense variant	Zm00004b031986	bub3 - budding inhibited by benzimidazoles homolog3
chr9	20543103	A	G	upstream gene variant	Zm00004b031986	BLAST: ankyrin repeat-containing protein
chr9	20618103	C	T	missense variant	Zm00004b031992	
chr9	20650529	C	T	downstream gene variant	Zm00004b031993	BLAST: Ran BP2/NZF zinc finger-like protein
chr9	20655580	A	G	downstream gene variant	Zm00004b031994	BLAST: hydrolase, NUDIX family protein
chr9	20725335	T	G	missense variant	Zm00004b031996	BLAST: U-box domain-containing protein 35 isoform X1
chr9	20774330	G	C	missense variant	Zm00004b031999	hb4 - homeobox-transcription factor 4
chr9	20793964	C	G	missense variant	Zm00004b032000	BLAST: L-type lectin-domain containing receptor kinase IX.1
chr9	20858008	T	G	missense variant	Zm00004b032001	BLAST: proteasome subunit beta type-6
chr9	20859892	C	T	downstream gene variant	Zm00004b032001	
chr9	20977027	A	G	missense variant	Zm00004b032004	BLAST: S-adenosyl-L-methionine-dependent methyltransferase superfamily protein

CONCLUSIONS AND FUTURE DIRECTIONS

Despite the mixed genetic background of *cyto3*, we have been able to identify a 1-2 Mb region on chromosome 9 that likely contains the causative SNP. Our top gene candidate is Zm00004b031986, a homolog of BUB3;1 and BUB3;2 in *Arabidopsis* which, in *Arabidopsis*, localize to the phragmoplast midline and have cytokinetic defects when double mutants are challenged with caffeine (Zhang et al., 2018). To validate, we will Sanger sequence the Zm00004b031986 locus from the two biallelic noncomplementation individuals in addition to developing primers for genotyping.

Additionally, light sequencing (2-5X) of other mutants identified from the EMS population suggests that the genetic background is purely B73. This will likely make cloning of additional mutants much easier. Currently, two additional mutants, *tangled64* (*tan64*) and *cytokinesis5* (*cyto5*) have been sequenced and mapped to the B73 version 5 genome. All of these mutants will provide important insight to the cellular processes important for plant growth in maize, an agriculturally significant crop plant.

REFERENCES

- Allsman, L. A., Dieffenbacher, R. N., & Rasmussen, C. G. (2019). Glue Impressions of Maize Leaves and Their Use in Classifying Mutants. *Bio-Protocol*, 9(7), e3209.
- Andrews, S. (2010). *FastQC: A Quality Control Tool for High Throughput Sequence Data*. Retrieved from <http://www.bioinformatics.babraham.ac.uk/projects/fastqc/>
- Assaad, F. F., Mayer, U., Wanner, G., & Jürgens, G. (1996). The KEULE gene is involved in cytokinesis in Arabidopsis. *Molecular & General Genetics: MGG*, 253(3), 267–277.
- Bellinger, M., Sidhu, S., & Rasmussen, C. (2019). Staining maize epidermal leaf peels with toluidine blue O. *Bio-Protocol*, 9(8). doi: 10.21769/bioprotoc.3214
- Bolger, A. M., Lohse, M., & Usadel, B. (2014). Trimmomatic: a flexible trimmer for Illumina sequence data. *Bioinformatics*, 30(15), 2114–2120.
- Cannon, E. K., Portwood, J. L., 2nd, Hayford, R. K., Haley, O. C., Gardiner, J. M., Andorf, C. M., & Woodhouse, M. R. (2024). Enhanced pan-genomic resources at the maize genetics and genomics database. *Genetics*, 227(1). doi: 10.1093/genetics/iyae036
- Gnanamurthy, S., Dhanavel, D., & Girija, M. (2011). STUDIES ON INDUCED CHEMICAL MUTAGENESIS IN MAIZE (*Zea mays* (L.)). *International Journal of Current Research and Review*, 3(11), 37–40.
- Hiwatashi, Y., Obara, M., Sato, Y., Fujita, T., Murata, T., & Hasebe, M. (2008). Kinesins are indispensable for interdigitation of phragmoplast microtubules in the moss *Physcomitrella patens*. *The Plant Cell*, 20(11), 3094–3106.
- Hufford, M. B., Seetharam, A. S., Woodhouse, M. R., Chougule, K. M., Ou, S., Liu, J., Ricci, W. A., Guo, T., Olson, A., Qiu, Y., Della Coletta, R., Tittes, S., Hudson, A. I., Marand, A. P., Wei, S., Lu, Z., Wang, B., Tello-Ruiz, M. K., Piri, R. D., ... Dawe, R. K. (2021). De novo assembly, annotation, and comparative analysis of 26 diverse maize genomes. *Science*, 373(6555), 655–662.
- Klein, H., Xiao, Y., Conklin, P. A., Govindarajulu, R., Kelly, J. A., Scanlon, M. J., Whipple, C. J., & Bartlett, M. (2018). Bulk-Segregant Analysis Coupled to Whole Genome Sequencing (BSA-Seq) for Rapid Gene Cloning in Maize. *G3*, 8(11), 3583–3592.
- Koboldt, D. C., Larson, D. E., & Wilson, R. K. (2013). Using VarScan 2 for Germline Variant Calling and Somatic Mutation Detection. *Current Protocols in Bioinformatics / Editorial Board, Andreas D. Baxevanis ... [et Al.]*, 44, 15.4.1–17.
- Kosetsu, K., de Keijzer, J., Janson, M. E., & Goshima, G. (2013). MICROTUBULE-ASSOCIATED PROTEIN65 is essential for maintenance of phragmoplast bipolarity and formation of the cell plate in *Physcomitrella patens*. *The Plant Cell*, 25(11), 4479–4492.

- Li, H., Sun, B., Sasabe, M., Deng, X., Machida, Y., Lin, H., Julie Lee, Y.-R., & Liu, B. (2017). Arabidopsis MAP65-4 plays a role in phragmoplast microtubule organization and marks the cortical cell division site. *The New Phytologist*, 215(1), 187–201.
- Lukowitz, W., Mayer, U., & Jürgens, G. (1996). Cytokinesis in the Arabidopsis embryo involves the syntaxin-related KNOLLE gene product. *Cell*, 84(1), 61–71.
- Lup, S. D., Navarro-Quiles, C., & Micol, J. L. (2023). Versatile mapping-by-sequencing with Easymap v.2. *Frontiers in Plant Science*, 14, 1042913.
- Michelmore, R. W., Paran, I., & Kesseli, R. V. (1991). Identification of markers linked to disease-resistance genes by bulked segregant analysis: a rapid method to detect markers in specific genomic regions by using segregating populations. *Proceedings of the National Academy of Sciences of the United States of America*, 88(21), 9828–9832.
- Mills, A. M., Morris, V. H., & Rasmussen, C. G. (2022). Localization of PHRAGMOPLAST ORIENTING KINESIN1 at the division site depends on the microtubule binding proteins TANGLED1 and AUXIN-INDUCED IN ROOT CULTURES9 in Arabidopsis. *The Plant Cell*. doi: 10.1093/plcell/koac266
- Müller, S., & Jürgens, G. (2016). Plant cytokinesis-No ring, no constriction but centrifugal construction of the partitioning membrane. *Seminars in Cell & Developmental Biology*, 53, 10–18.
- Murata, T., Sano, T., Sasabe, M., Nonaka, S., Higashiyama, T., Hasezawa, S., Machida, Y., & Hasebe, M. (2013). Mechanism of microtubule array expansion in the cytokinetic phragmoplast. *Nature Communications*, 4, 1967.
- Murata, T., Sonobe, S., Baskin, T. I., Hyodo, S., Hasezawa, S., Nagata, T., Horio, T., & Hasebe, M. (2005). Microtubule-dependent microtubule nucleation based on recruitment of gamma-tubulin in higher plants. *Nature Cell Biology*, 7(10), 961–968.
- Nacry, P., Mayer, U., & Jürgens, G. (2000). Genetic dissection of cytokinesis. *Plant Molecular Biology*, 43(5-6), 719–733.
- Rasmussen, C. G., & Bellinger, M. (2018). An overview of plant division-plane orientation. *The New Phytologist*, 219(2), 505–512.
- Robinson, J. T., Thorvaldsdóttir, H., Winckler, W., Guttman, M., Lander, E. S., Getz, G., & Mesirov, J. P. (2011). Integrative genomics viewer. *Nature Biotechnology*, 29(1), 24–26.
- Sasabe, M., Kosetsu, K., Hidaka, M., Murase, A., & Machida, Y. (2011). Arabidopsis thaliana MAP65-1 and MAP65-2 function redundantly with MAP65-3/PLEIADE in cytokinesis downstream of MPK4. *Plant Signaling & Behavior*, 6(5), 743–747.
- Schnable, P. S., Ware, D., Fulton, R. S., Stein, J. C., Wei, F., Pasternak, S., Liang, C., Zhang, J., Fulton, L., Graves, T. A., Minx, P., Reily, A. D., Courtney, L., Kruchowski, S. S., Tomlinson, C., Strong, C., Delehaunty, K., Fronick, C., Courtney, B., ...

- Wilson, R. K. (2009). The B73 maize genome: complexity, diversity, and dynamics. *Science*, 326(5956), 1112–1115.
- Schneeberger, K., Ossowski, S., Lanz, C., Juul, T., Petersen, A. H., Nielsen, K. L., Jørgensen, J.-E., Weigel, D., & Andersen, S. U. (2009). SHOREmap: simultaneous mapping and mutation identification by deep sequencing. *Nature Methods*, 6(8), 550–551.
- Smertenko, A. (2018). Phragmoplast expansion: the four-stroke engine that powers plant cytokinesis. *Current Opinion in Plant Biology*, 46, 130–137.
- Smertenko, A., Assaad, F., Baluška, F., Bezanilla, M., Buschmann, H., Drakakaki, G., Hauser, M.-T., Janson, M., Mineyuki, Y., Moore, I., Müller, S., Murata, T., Otegui, M. S., Panteris, E., Rasmussen, C., Schmit, A.-C., Šamaj, J., Samuels, L., Staehelin, L. A., ... Žárský, V. (2017). Plant Cytokinesis: Terminology for Structures and Processes. *Trends in Cell Biology*, 27(12), 885–894.
- Söllner, R., Glässer, G., Wanner, G., Somerville, C. R., Jürgens, G., & Assaad, F. F. (2002). Cytokinesis-defective mutants of Arabidopsis. *Plant Physiology*, 129(2), 678–690.
- Tavares, H. (2024). *windowscanr: Apply functions using sliding windows*.
- Uyehara, A. N., & Rasmussen, C. G. (2023). Redundant mechanisms in division plane positioning. *European Journal of Cell Biology*, 102(2), 151308.
- Vasimuddin, M., Misra, S., Li, H., & Aluru, S. (2019). Efficient Architecture-Aware Acceleration of BWA-MEM for Multicore Systems. *2019 IEEE International Parallel and Distributed Processing Symposium (IPDPS)*, 314–324.
- Waizenegger, I., Lukowitz, W., Assaad, F., Schwarz, H., Jürgens, G., & Mayer, U. (2000). The Arabidopsis KNOLLE and KEULE genes interact to promote vesicle fusion during cytokinesis. *Current Biology: CB*, 10(21), 1371–1374.
- Zhang, H., Deng, X., Sun, B., Lee Van, S., Kang, Z., Lin, H., Lee, Y.-R. J., & Liu, B. (2018). Role of the BUB3 protein in phragmoplast microtubule reorganization during cytokinesis. *Nature Plants*, 4(7), 485–494.